Department of Biomedical Sciences
University of Veterinary Medicine Vienna

Institute of Medical Biochemistry
(Head: Univ.-Prof. Dr.rer.nat. Florian Grebien)

Ludwig Boltzmann Institute for Traumatology
The Research Center in Cooperation with AUVA
(Head: Assoc.Prof. Dr. Johannes Grillari)

Role of heme oxygenase and nitric oxide synthase activity in hepatic stress response upon systemic inflammation

PhD thesis submitted for the fulfilment of the requirements for the degree of

DOCTOR OF PHILOSOPHY (PhD)

University of Veterinary Medicine Vienna

submitted by

Andrea Müllebner, MSc

Vienna, January 2023

PhD Committee

1st supervisor

Dipl.-Biol. Dr. rer.nat. Catharina Duvigneau

Department of Biomedical Sciences
Institute of Medical Biochemistry
University of Veterinary Medicine Vienna

2nd supervisor

Univ.Doz. Dr. Andrey Kozlov

LBI for Traumatology
The Research Center in Cooperation with AUVA

3rd supervisor

Ao.-Prof. Dr.rer.nat. Katrin STANIEK

Department of Biomedical Sciences
Institute of Pharmacology and Toxicology
University of Veterinary Medicine Vienna

Publications included in the PhD thesis

[I] **Müllebner A**, Herminghaus A, Miller I, Kames M, Luís A, Picker O, Bauer I, Kozlov AV, Duvigneau JC. 2022. Tissue Damage, Not Infection, Triggers Hepatic Unfolded Protein Response in an Experimental Rat Peritonitis Model. Frontiers in medicine, 9: 785285. DOI 10.3389/fmed.2022.785285.

Impact factor: 5,058 (2021); Citations: 0.

[II] **Müllebner A**, Moldzio R, Redl H, Kozlov AV, Duvigneau JC. 2015. Heme Degradation by Heme Oxygenase Protects Mitochondria but Induces ER Stress via Formed Bilirubin. Biomolecules, 5 (2): 679–701. DOI 10.3390/biom5020679.

Impact factor: none (first impact factor 2018: 4,694); Citations: 15.

[III] **Müllebner A**, Dorighello GG, Kozlov AV, Duvigneau JC. 2017. Interaction between Mitochondrial Reactive Oxygen Species, Heme Oxygenase, and Nitric Oxide Synthase Stimulates Phagocytosis in Macrophages. Frontiers in medicine, 4: 252. DOI 10.3389/fmed.2017.00252.

Impact factor: none (first impact factor 2018: 3,113); Citations: 20.

Impact factors released in the year of publication, listed in Web of Science™.
Number of Citations in Web of Science™ (Accessed: 19.12.2022).

Author's contributions

[I] Müllebner A, Herminghaus A, Miller I, Kames M, Luís A, Picker O, Bauer I, Kozlov AV, Duvigneau JC. 2022. Tissue Damage, Not Infection, Triggers Hepatic Unfolded Protein Response in an Experimental Rat Peritonitis Model. Frontiers in medicine, 9: 785285. DOI 10.3389/fmed.2022.785285.

Müllebner A	performed and interpreted qPCR analysis
	performed the statistical analysis and the graphical data presentation
	wrote the first draft of the manuscript
Herminghaus A	performed and supervised animal experiments
Miller I	performed and interpreted western blot analysis
Kames M	performed and interpreted qPCR analysis
Luís A	provided critical feedback
	revised the manuscript
Picker O	performed and supervised animal experiments
Bauer I	designed and supervised the study
Kozlov AV	designed and supervised the study
	provided critical feedback
	wrote the final version of the manuscript
Duvigneau JC	designed and supervised the study
	provided critical feedback
	wrote the final version of the manuscript

All authors gave intellectual input and approved the final version of the manuscript.

[II] Müllebner A, Moldzio R, Redl H, Kozlov AV, Duvigneau JC. 2015. Heme Degradation by Heme Oxygenase Protects Mitochondria but Induces ER Stress via Formed Bilirubin. Biomolecules, 5 (2): 679–701. DOI 10.3390/biom5020679.

Müllebner A	planned the experiments
	performed and interpreted qPCR experiments
	wrote the first draft and revised the manuscript

Moldzio R	performed and interpreted viability assays
Redl H	designed a part of the study
	supervised the animal experiments
Kozlov AV	designed and supervised the study
	performed and interpreted experiments with mitochondria
	optimized the assay for the determination of the heme oxygenase activity
	contributed to the writing and editing of the manuscript
Duvigneau JC	designed and supervised the study
	performed and interpreted experiments with mitochondria
	optimized the assay for the determination of the heme oxygenase activity
	contributed to the writing and editing of the manuscript

All authors gave intellectual input and approved the final version of the manuscript.

[III] Müllebner A, Dorighello GG, Kozlov AV, Duvigneau JC. 2017. Interaction between Mitochondrial Reactive Oxygen Species, Heme Oxygenase, and Nitric Oxide Synthase Stimulates Phagocytosis in Macrophages. Frontiers in medicine, 4: 252. DOI 10.3389/fmed.2017.00252.

Müllebner A	designed the study
	performed and interpreted Phagotest experiments
	performed and interpreted ESR experiments
	wrote the first draft and revised the manuscript
Dorighello GG	performed and interpreted Amplex Red experiments
Kozlov AV	designed and supervised the study
	interpreted data
	wrote the final version of the manuscript
Duvigneau JC	designed and supervised the study
	interpreted data
	wrote the final version of the manuscript

All authors gave intellectual input and approved the final version of the manuscript.

Declaration

I hereby declare that I have followed the rules of good Scientific Practice in all aspects.

Vienna, January 2023 _____

Andrea Müllebner, MSc

Acknowledgements

I would like to express my sincere gratitude to all the people that supported me during my PhD. Without all of you this would not have been accomplished.

First of all I want to thank my supervisors Catharina Duvigneau and Andrey Kozlov for their guidance, scientific support and for giving me the opportunity to carry out my PhD studies in their groups.

I am grateful to my third thesis committee member Katrin Staniek for her suggestions and constant support.

Thanks to Heinz Redl (LBI for Traumatology) and Florian Grebien (Institute for Medical Biochemistry, University of Veterinary Medicine) who made it possible for me to conduct this research project at their institutions.

I want to express my gratitude to Anna Herminghaus and Inge Bauer for their support, objectivity and challenging discussion and to Anne Rupprecht and Gabriel Dorighello for helpful comments and methodical input.

Special thanks go to all my colleagues, previous and present ones, for a great working atmosphere. For helpful discussions and comments, as well as mental support, I am grateful to Ingrid Miller, Rudolf Moldzio and Adelheid Weidinger. Thanks to Sergiu Dumitrescu, Andras Meszaros, Andreia Luis and Julia Jilge for a remarkable time.

Special thanks to Stefan Puchner, Marcus Schefzig, Hans Peter Satzer, Jamile Paier-Pourani, Ingeborg Kehrer, Annika Cronstedt-Fell, Jasmin Weeger, Carmen Konzett and Susanne Haindl for technical support. Further, I want to thank Martina Kames, Helene Michenthaler, Licha Wortha, Johanna Piringer, and all the other students who temporary supported our working group. They diversified the life in the lab.

Finally, I would like to thank my family and friends for their love and support and for providing distraction whenever needed. Special thanks goes to Mathias for his patience and support.

Table of contents

1 Introduction

1.1 Sepsis, systemic inflammatory response syndrome and multiple organ dysfunction syndrome

With an estimated incidence of 48.9 million cases and 11.0 million sepsis-related deaths representing 19.7% of all global deaths, sepsis is considered a major health concern (Rudd et al. 2020). Sepsis is a “life-threatening organ dysfunction caused by a dysregulated host response to infection” (Singer et al. 2016). This response clinically manifests as systemic inflammatory response syndrome (SIRS) that is defined by the presence of two or more of the following symptoms (Bone et al. 1992): (1) body temperature > 38 °C or < 36 °C; (2) heart rate > 90 beats/min; (3) respiratory rate > 20 breaths/min or a $PaCO_2$ of < 32 mm Hg; and (4) white blood cell counts > 12,000 /mm^3 or < 4,000 /mm^3, or the presence of more than 10 % immature neutrophils. The clinical picture of SIRS can also be triggered by sterile inflammation as a consequence of ischemia, multiple trauma, tissue injury, and hemorrhagic shock, but also by exogenous administration of pro-inflammatory cytokines, such as tumor necrosis factor alpha (TNF-α) (Bone et al. 1992).

SIRS culminates in the development of multiple organ dysfunction syndrome (MODS). MODS is a leading cause of death of critically ill patients in intensive care units, with an increasing risk with the number of organs failing (Sakr et al. 2012). Organs sensitive to MODS are lung, liver, intestinal tract, and kidney. Ultimately failure of the hematologic system occurs, which also affects the heart. Of affected organ systems, liver dysfunction has an exceptional prognostic value for the progression of sepsis and is associated with a poor prognosis (Dizier et al. 2015, Koch et al. 2011).

1.2 Liver in systemic inflammation

The liver is the largest gland of the body with over 200 functions including detoxification, nutrient conversion, storage, energy production, protein synthesis, regulation of coagulation, iron recycling and immune surveillance. Thus, it plays a central role in metabolic and immunologic homeostasis. Owing to these important physiological functions, liver dysfunction and failure constitute a particularly serious complication in sepsis directly contributing to disease progression and death (Dizier et al. 2015, Koch et al. 2011).

The liver provides the first line of defense against blood borne infections. Clearance of particulates and other immunoreactive material from the blood is carried out by Kupffer cells, tissue resident macrophages, which make up 80-90% of the tissue macrophages of the entire body. Located in the liver sinusoids, where they are attached to the liver sinusoidal endothelial cells, Kupffer cells are directly exposed to the blood stream and clear gut derived bacteria, but also senescent erythrocytes (reviewed in Bilzer et al. 2006) and stay immunological tolerant under physiological conditions (reviewed in Jenne and Kubes 2013).

However, during systemic inflammation the liver is the major site of the inflammatory response to bacterial endotoxins (Siore et al. 2005). Kupffer cells in response to endotoxin release early pro-inflammatory cytokines TNF-α and interleukin (IL)-1β, which can be envisioned as signal amplifiers causing release of further inflammatory signals **i**ncluding cytokines (e.g. IL-6), chemokines (e.g. IL-8) and reactive oxygen (ROS) and nitrogen species (RONS) (reviewed in Kozlov et al. 2017).

In the hepatocytes, the major parenchymal cell type in the liver TNF-α directly stimulates IL-6 production. IL-6 together with TNF-α and IL-1β activates the acute phase reaction (Castell et al. 1989), an adaptation of the synthesis of plasma proteins towards acute phase reactants that support the immune response and promote the defense against pathogens. Among those are complement factors that act as opsonins and pore forming proteins (reviewed in Kozlov and Grillari 2022), pro-coagulant factors that shift the balance towards pro-coagulant activity (reviewed in Dhainaut et al. 2001) and iron sequestration molecules (Nemeth et al. 2004). Concomitantly the hepatocyte's metabolism is significantly altered (Mainali et al. 2021).

The inflammatory response is counteracted by a compensatory anti-inflammatory response that is mediated by release of interleukins IL-4 and IL-10 to inhibit the production of TNF-α, IL-1, IL-6, and IL-8. A complex molecular and cellular network regulates the anti-inflammatory response by silencing pro-inflammatory genes, while simultaneously maintaining anti-infectious processes (reviewed in Perl et al. 2006). However, the factors that disturb the balance of pro- and anti-inflammatory reaction resulting in organ dysfunction are still not completely determined.

Overwhelming inflammatory response and resulting tissue hypoperfusion and hypoxia are important drivers, but cannot sufficiently explain development of liver failure. Generally, failing organs show minimal signs of cell death (Nürnberger et al. 2012, Watanabe et al. 2009), even

in patients who deceased from unresolved MODS (Takasu et al. 2013). Further, organs in patients that recovered from critical illness quickly regain function. Both, the reversibility of organ dysfunction and the structural integrity of the affected organs, point towards a functional, and potentially transient, impairment at (sub-) cellular level (Singer et al. 2004).

Besides the nutrient conversion and provision of energy production, hepatocytes play a fundamental role for plasma protein synthesis. In the endoplasmic reticulum (ER) synthesis and quality control of secretory and membrane proteins takes place. A dysfunctional ER with reduced protein folding capacity has recently been emphasized as a key mechanism of numerous diseases including MODS (reviewed in Almanza et al. 2019). The unfolded protein response (UPR) is a stress response mechanism, which enables the cell to restore and maintain the capacity for folding proteins correctly even under stressful conditions. However, failure to adapt the protein processing capacity to a changed demand may explain a dysfunctional cell state.

1.3 Unfolded protein response

Perturbations impacting the ER homeostasis like elevated protein traffic, expression of folding-defective proteins, nutrient deprivation, infections, altered redox status, hypoxia, intraluminal calcium and altered post-translational modifications, are characterized by the accumulation of unfolded/misfolded protein in the ER, a condition known as ER stress (reviewed in Pahl 1999). Misfolded proteins disturb the balance between protein folding capacity of ER and cellular demand. To overcome stress and restore ER homeostasis cells activate the UPR.

The UPR restores ER homeostasis by attenuating protein synthesis, clearance of unfolded/misfolded proteins and increasing protein folding capacity. The UPR signaling cascade is initiated by three ER membrane proteins, the protein kinases protein kinase RNA-activated (PKR)-like ER kinase (PERK) and inositol requiring enzyme 1 (IRE1α) and the transcription factor activating transcription factor (ATF) 6. Glucose regulated protein 78 (GRP78) is a major ER chaperone and acts as primary sensor of ER stress by activating canonical UPR, upon dissociation from transmembrane sensors (Bertolotti et al. 2000, Kopp et al. 2019).

PERK dimerization and subsequent trans-autophosphorylation leads to the activation of its eukaryotic translation initiation factor 2 alpha subunit (eIF2α) kinase function. Phosphorylation

of eIF2α causes a transient attenuation of protein translation, the most immediate response to ER stress. Despite general translational attenuation eIF2α-phosphorylation activates selective translation of selected mRNAs via up-regulation of ATF 4. Among these UPR-targets are genes encoding proteins functioning in amino acid biosynthesis and transport, anti-oxidative stress response, and apoptosis, such as CAAT/Enhancer binding protein (C/EBP) homologous protein (CHOP) (reviewed in Ron 2002) (**Figure 1**).

IRE1 release from GRP78 leads to homodimerization and activation of its cytosolic RNase domain by autophosphorylation. The RNase-function of IRE1 removes a 26 nucleotide intron from its substrate X-box binding protein (XBP1) mRNA in a process known as unconventional splicing (Uemura et al. 2009). The protein derived from spliced XBP1 (XBP1s) is a potent transcription factor that triggers transcription of ER chaperones, foldases and components of the ER associated protein degradation pathway (Travers et al. 2000) (**Figure 1**).

ATF6 is exported to the Golgi-apparatus where it is cleaved by proteases site-1 protease (S1P) and site-2 protease (S2P) releasing the cytosolic domain that contains a bZIP transcription factor (ATF6p50) (Ye et al. 2000). ATF6p50 induces transcription of genes involved in protein folding and ER associated protein degradation. Additionally ATF6p50 also regulates the transcription of XBP1 (Yoshida et al. 2001) (**Figure 1**).

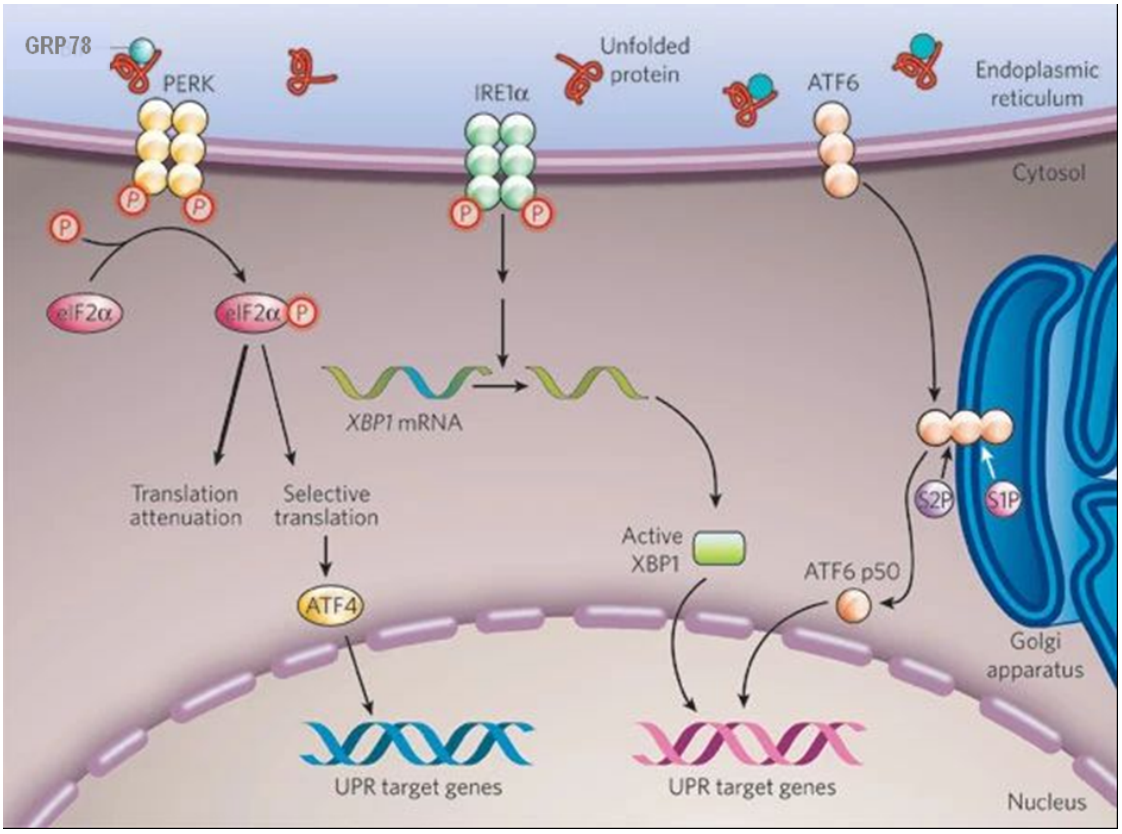

Figure 1: The unfolded protein response (UPR) pathways. In unstressed cells the chaperon glucose regulated protein 78 (GRP78) is bound to ER stress sensors protein kinase RNA-activated (PKR)-like ER kinase (PERK), inositol requiring enzyme 1 (IRE1α) and activating transcription factor 6 (ATF6). Upon ER stress GRP78 preferentially binds to unfolded proteins and thereby releases ER stress sensors. This leads to the initiation of the UPR signaling cascades. PERK is activated by homodimerization and transautophosphorylation. Activated PERK phosphorylates eukaryotic translation initiation factor 2 alpha subunit (eIF2α), which reduces overall translational initiation. However, selected mRNAs, like ATF4 mRNA are preferably translated. ATF4 initiates the expression of UPR target genes encoding proteins involved in amino-acid biosynthesis, antioxidative-stress response and apoptosis. Free IRE1α forms dimers, activating its protein-kinase and its endoribonuclease activity. Active IRE1α cleaves a 26-base intron from X-box binding protein 1 (XBP1) mRNA. The spliced XBP1 mRNA encodes a potent transcription factor that activates UPR target gene expression. Unbound ATF6 is exported to the Golgi-apparatus, and cleaved by the proteases site-1 protease (S1P) and site-2 protease (S2P). The cytosolic ATF6 fragment (ATF6 p50) activates the transcription of UPR target genes. Figure is adapted from (Zhang and Kaufman 2008)

An increased upregulation of chaperons, including GRP78, in response to ER stress occurs predominantly via IRE1α and ATF6 and aims at restoring the protein folding capacity of the ER. Besides its function as chaperon and master regulator of UPR, GRP78 is required for inducing autophagy, which eliminates damaged structures that cannot be repaired otherwise (Li et al. 2008). Under conditions of irremediable ER stress, the character of IRE1α mediated UPR switches from cytoprotection to enhanced programmed cell death, predominantly via CHOP (Lerner et al. 2012).

Since all three ER stress sentinels are principally capable to activate ER stress-associated cell death cascades (Fribley et al. 2009, Morishima et al. 2011), it is believed that the redundancy of the simultaneous activation of the three UPR branches constitutes a strong stimulus towards programmed cell death. It is not known whether or how the cell senses that the malfunction of the ER is irremediable. Anyway, the activation of UPR, particularly when PERK is involved, leads to a state, in which the ER is at least transiently dysfunctional (Dubois et al. 2020). However, the factors modulating UPR fate towards death or life of the cell are not fully understood.

There are several intersections of ER stress and UPR with the inflammatory response. ER stress-induced UPR signaling also activates pro-inflammatory pathways (reviewed in Zhang and Kaufman 2008). It has been shown that ER stress activates acute phase reaction in the liver in response to inflammation (Zhang et al. 2006). On the other hand, ER stress in conjunction with activation of toll like receptors can directly induce inflammation (Hu et al. 2011, Martinon et al. 2010). All the three ER stress sensors induce inflammation by different mechanisms operating via nuclear factor κ-light-chain-enhancer of activated B cells (NF-κB) (Deng et al. 2004, Urano et al. 2000). Furthermore, ROS generated at the ER or in mitochondria upon ER stress can enhance inflammation induction through NF-κB dependent or independent mechanisms. Secondary events caused indirectly by the inflammatory process, such as hypoxic or ischemic episodes, are as well potent inducers of ER stress (Duvigneau et al. 2010). Thus, many conditions that are associated with SIRS may act as potential triggers of ER stress and subsequent UPR. However, whether ER stress seen in SIRS is primarily associated with infection and resulting inflammation or with tissue damage is not clear.

Importantly, UPR also triggers an antioxidant defense program by direct activation of nuclear factor-erythroid-derived 2-related factor 2 (Nrf2) pathway via PERK branch of UPR (Cullinan

et al. 2003, He et al. 2001). Nrf2 activates the transcription of a set of antioxidant and oxidant-detoxifying enzymes including heme oxygenase (HO) -1. HO-1 has been implicated in suppressing ROS-associated ER stress (Chen et al. 2018, Li et al. 2020) however the underlying mechanisms remain elusive. Modulation of the ER stress response could either increase susceptibility to ER dysfunction, or mediate resistance to ER stress associated cell death. Thus, the role of HO in the modulation of the ER stress response is not fully understood.

1.4 Heme oxygenase

HO (enzyme classification (EC) 1.14.14.18) was first described by Tehunen et al. (Tenhunen et al. 1968). Located within the ER it is the rate limiting enzyme in the heme catabolism. In conjunction with nicotinamide adenine dinucleotide phosphate (NADPH) cytochrome P450 reductase (EC 1.6.2.4) it catalyzes the oxidative cleavage of heme (iron protophrphyrin-IX) to equimolar amounts of the linear tetrapyrrole biliverdin, carbon monoxide (CO) and ferrous iron (Fe^{2+}). Biliverdin is further reduced to bilirubin (BR) by biliverdin reductase (EC 1.3.1.24) (**Figure 2**). Initially, the HO reaction was viewed exclusively as a mechanism for heme disposal. With the discovery of the antioxidant and anti-inflammatory properties conferred by HO, research interest was boosted (Maines and Gibbs 2005).

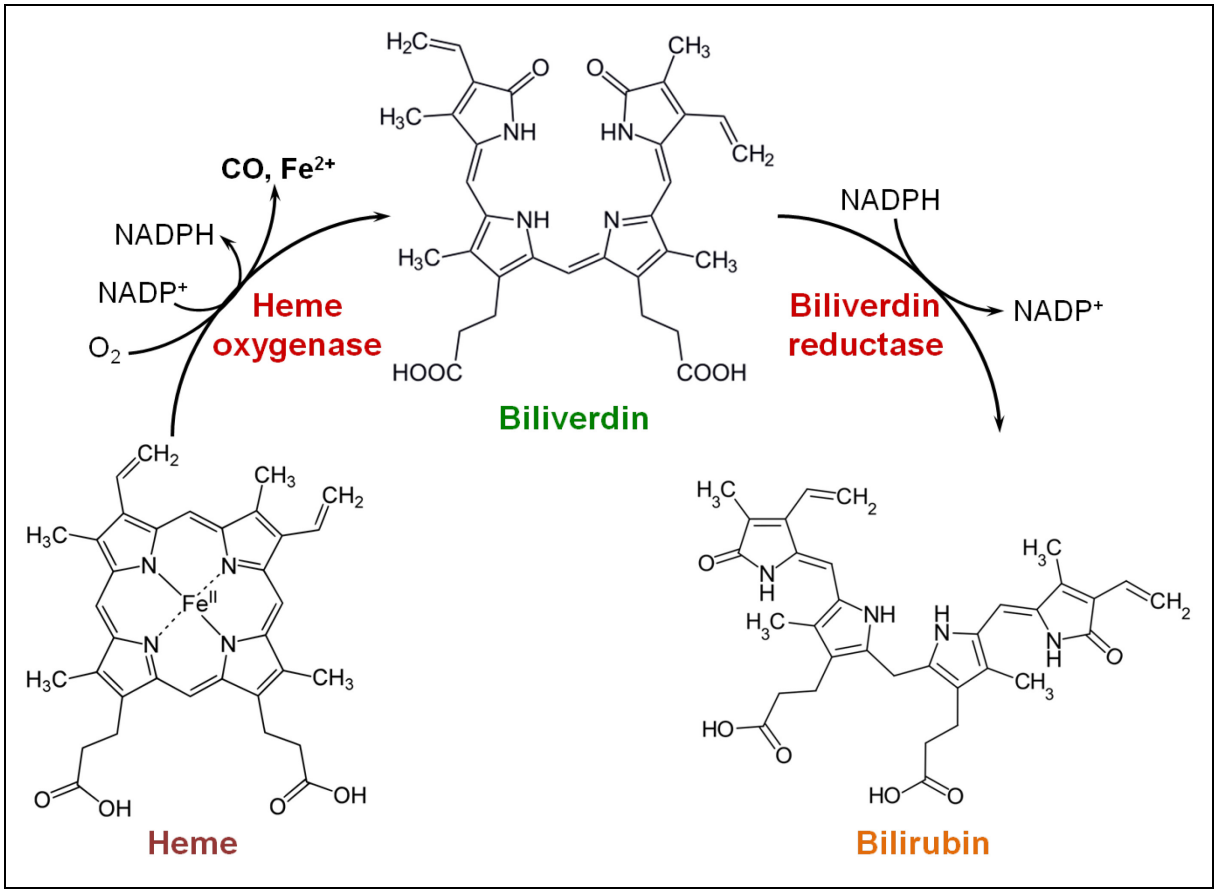

Figure 2: Heme degradation by heme oxygenase. Heme oxygenase catalyzes the degradation of heme to equimolar amounts of biliverdin, carbon monoxide (CO) and ferrous iron (Fe^{2+}) in the presence of oxygen (O_2) and nicotinamide adenine dinucleotide phosphate (NADPH). Biliverdin is reduced to bilirubin by biliverdin reductase.

In mammals, two catalytically active isoforms of HO exist, HO-1 and HO-2. Although catalyzing the same biochemical reaction, they are encoded by independent genes and substantially differ with respect to gene structure, regulation and tissue expression patterns.

HO-1, also referred to as heat shock protein 32, is a 32 kDa protein encoded by the HMOX1 gene. In unstressed conditions, HO-1 is solely expressed in tissues that degrade senescent erythrocytes. However, as a stress-inducible enzyme, HO-1 gene transcription is activated by a vast number of stimuli, including its substrate heme (and its oxidized form, hemin), transition metals, ROS, cytokines, prostaglandines, endotoxines, nitric oxide (NO), altered oxygen tension (hypoxia/hyperoxia) and diverse phytochemicals (reviewed in Medina et al. 2020). Thus, up-regulation of HO-1 is a sensitive marker of cellular stress.

HO-2 is a 36 kDa protein encoded by the HMOX2 gene. It is constitutively expressed in many tissues including brain, testis, cardiovasculature and liver (reviewed in Muñoz-Sánchez and Chánez-Cárdenas 2014).

It is generally assumed that HOs exert their anti-oxidative and anti-inflammatory function essentially via the combined effects of the removal of pro-oxidant heme on the one hand and the generation of biologically-active products from heme catabolism on the other hand. However, the contribution of either mechanism is frequently not known.

Heme is a vital prosthetic group in hemeproteins. The most prominent function of hemeproteins is delivery of oxygen (O_2) to tissues (hemoglobin, myoglobin). It is facilitated by oxygen binding to divalent iron of heme. Further, hemeproteins serve as electron transporters [e.g. Cytochrome c, Cytochrome C oxidase (EC 1.9.3.1)] and catalysts for biosynthesis and biodegradation [e.g. Cytochrome P450 superfamily (EC 1.14.14.1), nitric oxide synthases NOS, (EC 1.14.13.39)] (reviewed in Gozzelino et al. 2010). Besides O_2, other gaseous molecules [NO, CO and hydrogen sulfide (H_2S)] show high affinity to heme-iron. These compounds act as messengers via interaction with hemeproteins that serve as sensors [e.g. soluble guanylate cyclase (EC 4.6.1.2)]. Additionally, NO and CO may act as inhibitors of hemeproteins function. Though indispensable for enzyme function when bound to an apoprotein, free heme is a potent pro-oxidant facilitating iron catalyzed hydroxyl radical formation (Fenton reaction) and membrane lipid peroxidation in diverse subcellular organelles (Halliwell and Gutteridge 1984, reviewed in Kumar and Bandyopadhyay 2005). Finally, free heme has the potential for acting as alarmin, harmful promotors of inflammatory reactions (reviewed in Ryter 2021 and Soares and Bozza 2016).

All three products of the HO reaction, bilirubin, CO and Fe^{2+} are potentially cytotoxic, but at the same time convey concentration dependent antioxidant, anti-inflammatory and vasoactive properties (reviewed in Kirkby and Adin 2006).

BR is well known for its neurotoxic action in newborns. Free unconjugated BR can unbalance the redox homeostasis, affect the mitochondrial membrane integrity and induce apoptosis (Rodrigues et al. 2002). However, at physiological concentrations it is one of the most potent antioxidants in mammalian cells scavenging various ROS including superoxide, peroxyl radicals and peroxynitrites. Due to its lipophilic properties, it is particularly potent in preventing

lipid peroxidation (Stocker et al. 1987). Exogenous administration of bilirubin improved outcome in an experimental sepsis model (Tran et al. 2020).

CO is a dangerous poisonous gas, but at lower concentrations it serves as second messenger that can exert biological functions as diverse as neurotransmission, cytoprotection, anti-inflammation, protection against oxidative injury and regulation of vascular tonus (reviewed in Ryter et al. 2006). The molecular basis for CO biological action relies on its high affinity to heme iron that facilitates the modulation of heme protein function. Binding of CO to active site of soluble guanylate cyclase mediates for example vasodilatation and inhibits platelet aggregation (Brüne and Ullrich 1987). Another protein of relevance in CO signaling is the mitochondrial cytochrome c oxidase. Exposure to CO triggers the release of ROS form mitochondria that activate several anti-inflammatory and anti-oxidant signaling pathways, including p38 mitogen activated protein kinase (MAPK) (Zuckerbraun et al. 2007). MAPK signaling pathway is essentially involved in the anti-inflammatory (Otterbein et al. 2000) and a number of other signaling pathways.

Free ferrous iron is a potent pro-oxidant that catalyzes the formation of ROS and ferryl species via Fenton reaction (Koppenol 2022) which induce lipid peroxidation and oxidative damage to DNA and proteins. Thus, release of iron by HO may contribute to a pro-oxidant state of the cell. Toxicity of an increased level of catalytically active iron could be prevented by an increased synthesis of ferritin. Interestingly, ferritin levels are decreased upon HO inhibition (Eisenstein et al. 1991), suggesting iron mediated up-regulation of ferritin. Ferritin sequesters iron in an almost redox inactive state. Thus, it was supposed that some of the protective effects of HO-1 may be attributed to the lowering of cellular free iron levels (Balla et al. 1992).

The heme degradation product BR exerts potent anti-oxidant, anti-inflammatory and metabolic activity. Application of BR counteracted systemic inflammation induced by endotoxin (Kadl et al. 2007). However, cytoprotective effects of BR are limited, and higher levels of unconjugated BR exert cytotoxic effects (Chuniaud et al. 1996), suggesting that under conditions with enhanced HO activity BR formation may have counterproductive effects.

Thus, HO may confer cytoprotection by multiple mechanisms. However, when heme degradation products overstep critical levels, an accelerated HO reaction can also mediate cell stress. To clarify the role of HO in the development of SIRS induced liver dysfunction, it is important to understand, whether direct (removal of heme) or indirect (activity of the formed

products) effects prevail, and to attribute them to protection or exacerbation of inflammation-associated cell stress.

1.5 NO synthase

The activity HO is interactive with synthesis of NO generated by a family of enzymes called NO synthases (NOS, EC 1.14.13.39). There are three NOS isoforms, the endothelial (eNOS), neuronal (nNOS) and inducible (iNOS) NOS. eNOS and nNOS are expressed constitutively, while iNOS is induced by endotoxin [lipopolysaccharide (LPS)] or inflammatory cytokines (reviewed in Thiemermann 2000). All three NOS isoforms generate NO from L-arginine, NADPH and oxygen. NO is involved in regulation of vascular tone, smooth muscle relaxation, platelet aggregation, synaptic function and cytotoxic function of innate immune cells (reviewed in Robbins and Grisham 1997). It has properties similar to CO which results in a crosstalk between both gaseous messengers mimicking the biological effects of each other, for instance, both are able to activate soluble guanylate cyclase (reviewed in Hartsfield 2002) and regulate the generation of mitochondrial (mt) ROS (Poderoso et al. 1996).

iNOS together with HO-1 are key enzymes of macrophages and both intimately linked to their phenotype. Upon activation macrophages may polarize from resting into pro-inflammatory or anti-inflammatory phenotype. Pro-inflammatory macrophages play an important role for mounting and supporting the inflammatory response. These cells are characterized by an increased expression of the marker enzyme iNOS. iNOS contributes to the synthesis of highly reactive RONS necessary for killing bacteria, but it is also involved in the regulation of several gene expression pathways, including Nrf2 pathway (McNeill et al. 2015). Anti-inflammatory macrophages have tissue remodeling function and are relevant for wound healing and resolution from injury. Anti-inflammatory phenotype is associated with high expression of HO-1 and there is evidence that HO-1 induction can drive phenotypic shift towards anti-inflammatory (Naito et al. 2014). The phenotype of macrophages is dynamic and modulated by the external conditions. Depending on the predominant phenotype, the activity of macrophages is either tissue damaging or tissue protective. The gaseous messengers CO and NO formed by HO-1 and iNOS can regulate mtROS formation (Poderoso et al. 1996, Zuckerbraun et al. 2007). These mtROS play an important role in various innate immune signaling pathways (Garaude et al. 2016), they activate NADPH oxidase (EC 1.6.3.1) (West et al. 2011) and were believed to increase the phagocytic activity of macrophages (Lo et al. 2013). Thus, activity of HO-1 and iNOS may play an important role in regulation of inflammatory response and the processes

related to liver dysfunction in response to systemic inflammation by modulation of macrophage function possibly via mtROS dependent mechanisms.

1.6 Aim of the study

Liver failure upon systemic inflammatory response is supposed to be result of functional impairment induced by metabolic changes going along acute phase response, rather than death of parenchymal cells. Metabolic changes involve reduced capacity of protein folding and accumulation of unfolded proteins in the ER, a condition called ER stress. Induction of subsequent UPR is hallmarked by partial dedifferentiation of the liver and functional impairment. However, the impact of tissue trauma and infection on the induction of hepatic unfolded protein response has not been addressed so far.

Upon systemic inflammation heme oxygenase (HO) and nitric oxide synthase (NOS) activities are markedly increased due to upregulation of stress inducible enzymes HO-1 and inducible NOS (iNOS). The activities of both enzymes are interactive and assumed to be involved in onset and shaping of the UPR and inflammatory response.

Thus, the first aim of this thesis was to dissect the role of trauma (surgery) and infection on the progression of the cellular stress response in a clinically relevant sepsis model.

The second and the third aims were based on the assumption that hepatocytes and macrophages are two major players in the development of liver dysfunction induced by inflammation.

The second aim was to understand whether the changes observed in sepsis model could be recapitulated in hepatocytes.

The third aim was to understand whether the changes observed in vivo could be recapitulated in macrophages.

Outlook: The data obtained are expected to make a contribution to basic understanding of pathomechanisms of diseases accompanied by systemic inflammatory response syndrome, which make a basis for the development of effective therapy.

2 Publications

2.1 Paper I: Tissue Damage, Not Infection, Triggers Hepatic Unfolded Protein Response in an Experimental Rat Peritonitis Model.

Müllebner A, Herminghaus A, Miller I, Kames M, Luís A, Picker O, Bauer I, Kozlov AV, Duvigneau JC.

Frontiers in medicine (2022), 9: 785285.

frontiers in Medicine

ORIGINAL RESEARCH
published: 16 March 2022
doi: 10.3389/fmed.2022.785285

Tissue Damage, Not Infection, Triggers Hepatic Unfolded Protein Response in an Experimental Rat Peritonitis Model

*Andrea Müllebner[1,2], Anna Herminghaus[3], Ingrid Miller[2], Martina Kames[2], Andreia Luís[1], Olaf Picker[3], Inge Bauer[3], Andrey V. Kozlov[1] and Johanna Catharina Duvigneau[2]**

[1] Ludwig Boltzmann Institute for Traumatology, The Research Center in Cooperation With AUVA, Vienna, Austria, [2] Department of Biomedical Sciences, Institute for Medical Biochemistry, University of Veterinary Medicine Vienna, Vienna, Austria, [3] Department of Anesthesiology, University Hospital Düsseldorf, Düsseldorf, Germany

OPEN ACCESS

Edited by:
Claudine Habak,
Emirates College for Advanced Education, United Arab Emirates

Reviewed by:
Rodrigo Tinoco Figueiredo,
Federal University of Rio de Janeiro, Brazil
Ekaterina Kolesanova,
Russian Academy of Medical Sciences (RAMS), Russia

***Correspondence:**
Johanna Catharina Duvigneau
Catharina.Duvigneau@vetmeduni.ac.at

Specialty section:
This article was submitted to Translational Medicine, a section of the journal Frontiers in Medicine

Received: 29 September 2021
Accepted: 10 February 2022
Published: 16 March 2022

Citation:
Müllebner A, Herminghaus A, Miller I, Kames M, Luís A, Picker O, Bauer I, Kozlov AV and Duvigneau JC (2022) Tissue Damage, Not Infection, Triggers Hepatic Unfolded Protein Response in an Experimental Rat Peritonitis Model. Front. Med. 9:785285. doi: 10.3389/fmed.2022.785285

Background: Abdominal surgery is an efficient treatment of intra-abdominal sepsis. Surgical trauma and peritoneal infection lead to the activation of multiple pathological pathways. The liver is particularly susceptible to injury under septic conditions. Liver function is impaired when pathological conditions induce endoplasmic reticulum (ER) stress. ER stress triggers the unfolded protein response (UPR), aiming at restoring ER homeostasis, or inducing cell death. In order to translate basic knowledge on ER function into the clinical setting, we aimed at dissecting the effect of surgery and peritoneal infection on the progression of ER stress/UPR and inflammatory markers in the liver in a clinically relevant experimental animal model.

Methods: Wistar rats underwent laparotomy followed by colon ascendens stent peritonitis (CASP) or surgery (sham) only. Liver damage (aspartate aminotransferase (AST), alanine aminotransferase (ALT) and De Ritis values), inflammatory and UPR markers were assessed in livers at 24, 48, 72, and 96 h postsurgery. Levels of inflammatory (IL-6, TNF-α, iNOS, and HO-1), UPR (XBP1, GRP78, CHOP), and apoptosis (BAX/Bcl-XL) mRNA were determined by qPCR. Splicing of XBP1 (XBP1s) was analyzed by gel electrophoresis, p-eIF2α and GRP78 protein levels using the western blots.

Results: Aspartate aminotransferase levels were elevated 24 h after surgery and thereafter declined with different kinetics in sham and CASP groups. Compared with sham De Ritis ratios were significantly higher in the CASP group, at 48 and 96 h. CASP induced an inflammatory response after 48 h, evidenced by elevated levels of IL-6, TNF-α, iNOS, and HO-1. In contrast, UPR markers XBP1s, p-eIF2α, GRP78, XBP1, and CHOP did not increase in response to infection but paralleled the kinetics of AST and De Ritis ratios. We found that inflammatory markers were predominantly associated with CASP, while UPR markers were associated with surgery. However, in the CASP group, we found a stronger correlation between XBP1s, XBP1 and GRP78 with damage markers, suggesting a synergistic influence of inflammation on UPR in our model.

Conclusion: Our results indicate that independent mechanisms induce ER stress/UPR and the inflammatory response in the liver. While peritoneal infection predominantly triggers inflammatory responses, the conditions associated with organ damage are predominant triggers of the hepatic UPR.

Keywords: sepsis, systemic inflammatory response syndrome (SIRS), ER stress, surgical trauma, colon ascendens stent peritonitis (CASP), unfolded protein response

INTRODUCTION

Abdominal surgery is the most efficient treatment of intra-abdominal sepsis. However, surgical trauma and peritoneal infection lead to the activation of multiple stress and inflammatory pathways. An exaggerated response can cause systemic inflammatory response syndrome (SIRS). Despite worldwide efforts to improve treatment and clinical outcomes, the mortality rate of sepsis, septic shock, and the consecutive multiorgan dysfunction syndrome (MODS) in humans remains very high (1). Notably, sepsis-associated liver failure and dysfunction are associated with a poor prognosis (2).

The liver plays a particular role in SIRS, as it mounts the acute phase response and represents the source but also a target organ of inflammatory mediators. The liver is a major regulator of immune and inflammatory responses at the systemic level (3). In response to infection and inflammation, the liver adapts its metabolism and switches protein synthesis toward the acute phase reactants (4). For these tasks, the hepatocytes critically depend on the functional endoplasmic reticulum (ER). However, SIRS is associated with profound derangements of the hepatic metabolism and the capacity to produce proteins. Recently, these derangements have been attributed to a dysfunctional ER of hepatocytes, a condition termed ER stress. ER stress is meanwhile considered an early sign of hepatocyte dysfunction preceding liver dysfunction caused by sepsis and SIRS (5, 6).

Endoplasmic reticulum stress elicits the unfolded protein response (UPR), an adaptive response that aims at restoring cellular protein homeostasis (7). Three ER stress sentinels drive UPR in a concurrent manner. Activation of inositol-requiring protein 1-2 (IRE1α) leads to alternative splicing of X-Box binding protein 1 (XBP1) mRNA, an early indicator for ER stress. Proteolytic cleavage of activating transcription factor 6 (ATF6) releases its cytosolic portion. The spliced isoform of XBP1 (XBP1s) and the cleaved ATF6 are potent transcription factors that promote an increase in protein-folding capacity of the ER by enhancing the expression of ER chaperones, such as the glucose-regulated protein 78 kDa (GRP78), and ER-associated protein degradation (8, 9). Activation of the protein kinase R-like ER kinase (PERK) causes translational attenuation by directly phosphorylating the α-subunit of the eukaryotic translation initiation factor 2 (eIF2α) (10). Prolonged activation of PERK commits the cell to UPR-induced apoptosis that can be initiated by increased CCAAT/enhancer-binding protein homologous protein (CHOP) expression. CHOP favors a proapoptotic phenotype by downregulating antiapoptotic mitochondrial proteins of the B-cell lymphoma family such as B-cell lymphoma-extra large (Bcl-XL) causing increased levels of proapoptotic proteins, such as Bcl2-associated X protein (BAX) (11). Thus, UPR can initiate apoptosis in a mitochondria-dependent manner, if ER stress remains unresolved (12).

In the last decade, ER stress and UPR have been explored as biomarkers and therapeutic targets in many diseases (13). Activation of ER stress and UPR have been associated with the induction of liver failure in several critical care disease models, e.g., endotoxemia (14), traumatic/hemorrhagic shock (THS) (15, 16), and sepsis (17–19). Besides trauma and burns, intra-abdominal infections are a common cause of sepsis, which therefore represent an important clinical problem in abdominal surgery (20). For translation into clinical practice, the impact of diverse factors, such as inflammation or tissue damage on ER stress activation in the peritonitis needs further characterization using appropriate biomedical research models.

The colon ascendens stent peritonitis (CASP) model closely mimics the clinical progression of sepsis after intra-abdominal surgery. This experimental peritonitis model is of high-clinical relevance since it allows controlling the severity of sepsis (21). It consists of two independent insults, first tissue damage because of the surgery and second infection because of the bacterial leakage from the gut (22). However, the impact of surgery on the markers for the hepatic stress response has not been addressed so far.

We applied a self-resolving model of CASP, with moderate peritonitis induction, in order to minimize secondary, inflammation-induced tissue injury and damage, which is a frequent septic complication. We assumed this model would be particularly suitable to dissect the effect of surgery and peritonitis-induced inflammation on the progression of UPR and inflammation markers in the liver. The clarification of a causal association between UPR signaling and onset of SIRS is of

Abbreviations: ATF4, activating transcription factor 4; ATF6, activating transcription factor 6; BAX, Bcl2 associated X protein; Bcl, B-cell lymphoma; Bcl-XL, Bcl-extra large; BRL3A, buffalo rat liver 3A cell line; CASP, colon ascendens stent peritonitis; CHOP, CCAAT/enhancer-binding protein homologous protein; Cyclo, cyclophilin A; eIF2α, α-subunit of the eukaryotic translation initiation factor 2; ER, endoplasmic reticulum; GRP78, glucose regulated protein 78 kDa; HO-1, heme oxygenase 1; HPRT, hypoxanthine-guanine phosphoribosyltransferase; iNOS, inducible NO synthase; IL-6, interleukin 6; IRE1α, inositol-requiring enzyme-1; LPS, lipopolysaccharide; MODS, multi-organ dysfunction syndrome; NF-κB, Nuclear factor kappa B; PERK, protein kinase R-like endoplasmic reticulum kinase; p-eIF2α, phosphorylated α-subunit of the eukaryotic translation initiation factor 2; SIRS, systemic inflammatory response syndrome; TNF-α, tumor necrosis factor α; THS, traumatic/hemorrhagic shock; TRAF2, tumor necrosis factor α receptor-associated factor 2; UPR, unfolded protein response; XBP1, X-Box binding protein 1; XBP1s, spliced isoform of XBP1.

translational significance, as it implies new medical approaches for preventing liver dysfunction in the clinical situation.

MATERIALS AND METHODS

Animals

In accordance with the ethical guiding principles for animal experiments (23), we aimed at obtaining maximal information from previous animal experiments. We used residual tissue samples of animals investigated in a previous study (24). From animals that did not undergo surgery (untreated control) no more tissue material was available, when we started this study. Because of the limited amount of tissue, we included 8 animals per group, although the previous study comprised 12 animals per group. Animals are described in detail in Herminghaus et al. (24). In brief, liver tissues of 64 adult male Wistar rats (374 ± 23 g body weight) were investigated in this study. Animals were randomly assigned to 8 groups: groups 1–4, sham-operated animals (laparotomy only, 24, 48, 72, and 96 h after surgery) and groups 5–8, CASP with a 14-G stent, 24, 48, 72, and 96 h after surgery (**Figure 1A**).

Colon Ascendens Stent Peritonitis/Sham Surgery

Polymicrobial abdominal infection was induced by leakage of feces into the abdominal cavity *via* a stent implanted in the colonic wall (CASP) as previously described (24). This previous study was approved by the local Animal Care and Use Committee (Landesamt für Natur, Umwelt und Verbraucherschutz, Recklinghausen, Germany), and all the experiments were performed in accordance with the NIH guidelines for animal care. In brief, the volatile anesthetic sevoflurane (3.0 Vol%, FiO_2 0.5) was used to induce and maintain anesthesia. Buprenorphine was applied at 0.05 mg/kg subcutaneously for analgesia. Animals were laparotomized and a 14-G stent penetrating the colonic wall (ca. 0.5 cm distal to the cecum) was fixed. Sham animals underwent anesthesia and laparotomy as stated earlier, but the stent was fixed outside on the wall of the gut without piercing it. After surgery, animals received analgesia (buprenorphine 0.05 mg/kg in 0.6 ml NaCl subcutaneously every 12 h), but no antibiotics and no additional fluid therapy were applied. The overall survival rate in the sham and CASP group were 100 and 94%, respectively. Animals were euthanized by intraperitoneal injection of pentobarbital (120 mg/kg) 24, 48, 72, or 96 h after sham/CASP surgery. Blood was obtained by cardiac puncture. Livers were collected, aliquots were shock frozen in liquid nitrogen, and stored at −80°C until further processing. The experimental scheme is shown in **Figure 1B**.

Plasma Analyses

Plasma levels of alanine aminotransferase (ALT) and aspartate aminotransferase (AST) of all animals included in this study ($n = 8$ per group) and also from untreated control animals ($n = 9$) were taken from a data set determined in a previous study (24) published under Creative Commons-by 4.0 license (25). In brief, plasma was obtained by centrifugation (4°C, 4000 × *g*, 10 min) from blood collected in EDTA tubes and stored at −80°C until further processing. ALT and AST activities were measured in the Central Institute of Clinical Chemistry and Laboratory Medicine of the University Hospital Duesseldorf, Germany (24).

Gene Expression Analyses

Liver tissue (25–50 mg) was homogenized in 1 ml of TriReagent® (Molecular Research Center Inc., Cincinnati, OH, USA). Total RNA was extracted according to the manufacturer's protocol. Extracted RNA was quantified and purity was checked with an Eppendorf BioPhotometer plus UV/VIS (Eppendorf, Wesseling-Berzdorf, Germany) using absorption at 260 nm and the 260/280 nm ratio, respectively. Reverse transcription of 1 µg of total RNA to cDNA was performed using Superscript™ II reverse transcriptase (200 U/reaction; Invitrogen; Carlsbad, CA, USA) and anchored oligo dT primers (3.5 µmol/l final concentration). Equal aliquots of each cDNA were pooled to generate an internal standard used as a reference for the quantification of qPCR.

Quantitative PCR was performed in reactions of 12 µl containing SYBR® green I (0.5×, Sigma Aldrich, Vienna, Austria), iTaq™ DNA polymerase™ (25 U/L; Bio Rad, Hercules, CA, USA), oligonucleotide primers (250 nmol/l each, Invitrogen; Carlsbad, California, USA), dNTP [200 µmol/l each], and $MgCl_2$ (1.5-3 mmol/l). All the reactions were performed in duplicates on a CFX96™ real-time cycler (Bio-Rad, Hercules, California, USA). Details on primer pairs are shown in **Supplementary Table S1**. Randomly assigned no-reverse transcriptase controls corresponding to ∼15% of all the samples investigated, a no-template control, and the internal standard was included in each measurement. ΔCq of no-reverse transcriptase controls to the respective sample was >7 for all the cases, while no-template control never yielded signals.

Data were analyzed using the CFX Manager (version 2.0, Bio-Rad, Hercules, CA, USA) in the linear regression mode. Target gene expression was calculated relative to the internal standard (ΔCq) and normalized by mean ΔCq values of two internal reference genes (hypoxanthine-guanine phosphoribosyltransferase, HPRT, and cyclophilin A, Cyclo), yielding ΔΔCq values, as previously described (26). The ΔΔCq values obtained from the technical replicates were averaged and used for statistical analyses. For visualization, data are presented as fold changes ($2^{-\Delta\Delta Cq}$ values) relative to the mean of the 96 h sham group. The 96 h time point was used as a reference point, owing to the lack of untreated control animals. Our previous study revealed (24) that not only CASP but also the surgical procedure itself transiently affected liver damage markers (AST and ALT) and the mitochondrial function of the liver. However, ALT and AST data obtained from the 96 h sham animals were nearly identical to those of the untreated control animals (**Figures 1C–E**). Therefore, we assume the values of the 96 h sham animals correspond to physiological levels. This is in line with previously published results (19).

Western Blot Analyses

Liver tissues were homogenized 1:10 (w/v) in RIPA lysis buffer (25 mmol/l Tris–HCl (pH 8.0), 0.5% Nonidet P-40,

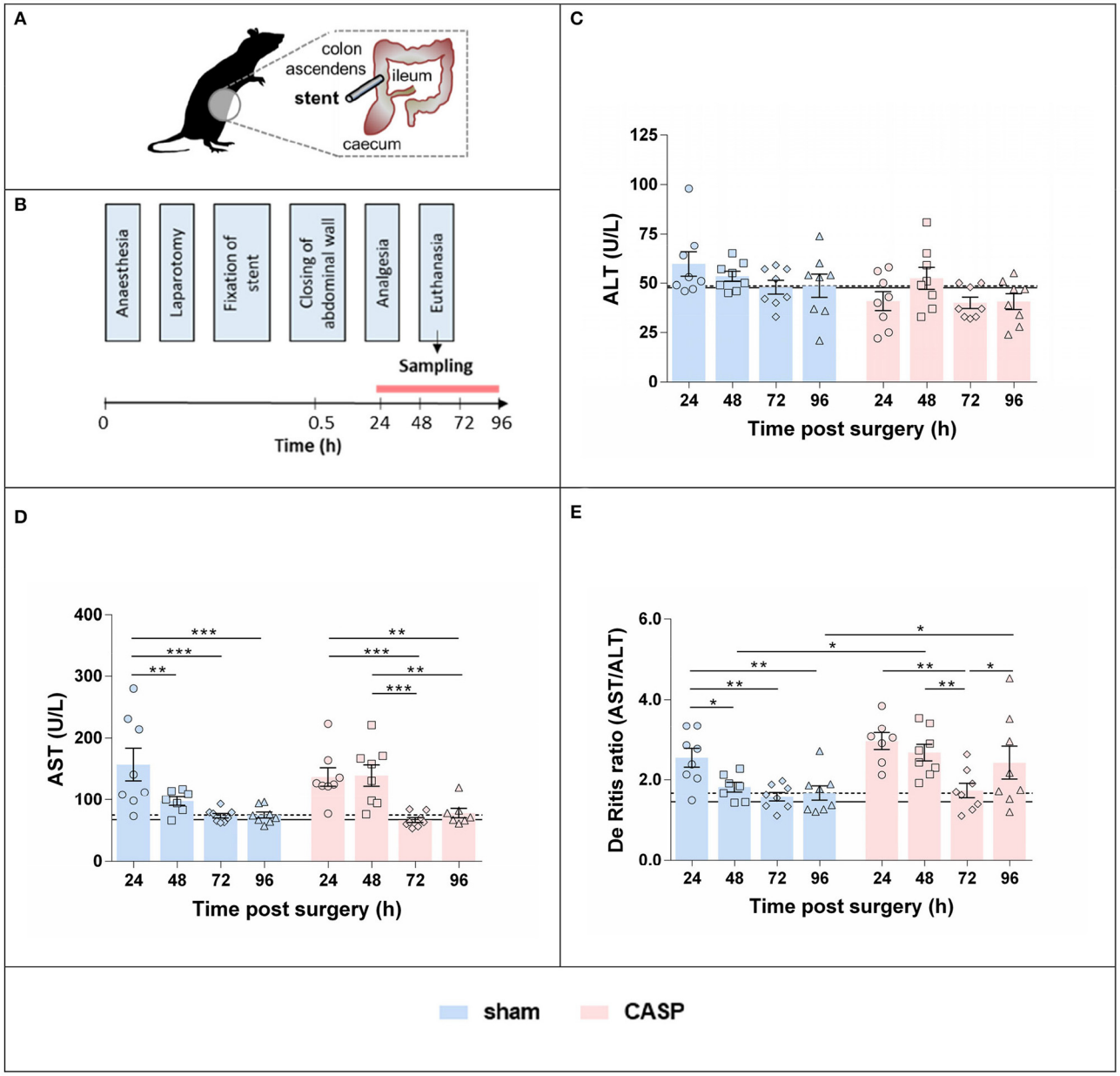

FIGURE 1 | Surgery and peritonitis induce liver damage in a self-resolving model. **(A)** Experimental model for the induction of experimental peritonitis using CASP surgery. **(B)** Plasma and liver samples were collected at consecutive time points after sham and CASP surgery. Plasma levels of **(C)** ALT and **(D)** AST were obtained from a data set determined for a previous study (24) published under Creative Commons-by 4.0 license (25). **(E)** De Ritis ratio was calculated from those data. Data are shown as mean ± SEM per group, with $n = 8$ for all the groups, except for **(D,E)** sham 48 h ($n = 7$), **(D)** CASP 24 h ($n = 7$), and **(D)** CASP 96 h ($n = 7$). The dashed line indicates the mean value of the sham group at 96 h. The solid line indicates the mean value of untreated control animals ($n = 9$). Statistical differences were calculated using two-way ANOVA followed by uncorrected Fisher's LSD test and are indicated by $^{*}p < 0.05$, $^{**}p < 0.01$, $^{***}p < 0.001$.

150 mmol/l NaCl, 0.25% sodium deoxycholate, 0.05% sodium dodecyl sulfate (SDS), 1 mmol/l EDTA, and 0.5 mmol/l DTT) freshly supplemented with protease and phosphatase inhibitor cocktails (Roche, Mannheim, Germany). After centrifugation (12,000×*g*) at 4°C for 10 min, protein concentration in the supernatant was determined using the Bradford method. Western blotting was performed essentially as previously described (15), on specimens of three randomly selected animals per group. Samples (20 µg protein per lane, reduced in Laemmli sample buffer) were separated by sodium dodecyl sulfate-polyacrylamide gel electrophoresis over a separation distance of 7 cm followed by semidry blotting onto nitrocellulose (Hybond ECL; GE Healthcare Life Sciences, Munich, Germany). Blots were first stained with the fluorescent dye ruthenium (II)

tris-(bathophenanthroline disulfonate) and overall protein pattern captured on a Typhoon RGB imager (GE Healthcare Life Sciences, Munich, Germany). Immunostaining was performed with specific antibodies against GRP78 (ALX-210-137, Enzo Life Sciences, 1:5,000) or p-eIF2α (No. 9721, Cell Signaling, 1:1000) followed by cross-adsorbed anti-rabbit-HRPO (No. A16104, Life Technologies). Reactive bands were detected by enhanced chemiluminescence (Clarity™ Western ECL Blotting reagent, Bio-Rad) on a Vilber Fusion FX system (Vilber-Lourmat, Eberhardzell, Germany). The overall protein-staining pattern was used as a loading control and for normalization.

Data Analyses and Statistics

Data were calculated and visualized using GraphPad Prism v6.01 (GraphPad Software Incorporation, La Jolla, California, USA). Outliers were detected by the ROUTs test (Q = 1%) (27) and excluded from analyses. Data were analyzed by two-way ANOVA followed by uncorrected Fisher's LSD test unless otherwise stated. Correlations were calculated using Pearson's correlation coefficient. Differences were considered significant when the p-value was <0.05.

RESULTS

Liver Damage Markers Are Increased 24–48 h After Surgery

The values for the plasma levels of liver damage markers, activities of ALT (**Figure 1C**) and AST (**Figure 1D**) of untreated control animals ($n = 9$), sham and CASP animals enrolled in this study ($n = 8$ per group), were taken from a previously determined data set (see Materials and Methods, Animals and Plasma Analyses). In the acute phase (24-48 h), AST was elevated two-fold compared to the postacute phase (72–96 h) in both sham and CASP groups. We did not observe any significant difference in AST and ALT levels between sham and CASP groups at any time point (24). In contrast, the De Ritis ratio (AST/ALT) was significantly higher in CASP groups compared to shams at 48 and 96 h (**Figure 1E**). The 96 h sham group displayed values for ALT and AST, and also the De Ritis ratio, that did not differ significantly from the non-operated control animals (ALT: $p = 0.9$; AST: $p = 0.3$; De Ritis: $p = 0.4$; two-sided, heteroscedastic Student's t-test), indicating resolution of liver injury.

Abdominal Infection Triggered Stress and Inflammatory Response in the Liver 48 h After CASP

To assess the inflammatory response in the liver, we analyzed gene expression levels of key inflammatory markers. The mRNA levels of stress responsive enzyme heme oxygenase 1 (HO-1; **Figure 2A**) were moderately, albeit, significantly increased in CASP compared to sham-operated animals at 48, 72, and 96 h. The mRNA levels of the proinflammatory cytokines tumor necrosis factor α (TNF-α; **Figure 2B**) and interleukin 6 (IL-6; **Figure 2C**), and inducible NO synthase (iNOS; **Figure 2D**), an enzyme required for bactericidal activity, were significantly higher in CASP compared with sham animals at 48 h after surgery. In addition, iNOS was significantly higher in CASP animals at 96 h (**Figure 2D**). These data show that our experimental CASP model causes abdominal infection, which is capable to trigger an inflammatory response in the liver.

XBP1 Splicing and eIF2α Phosphorylation Are Triggered by Surgical Stress

We studied the activation of canonical UPR signaling in response to CASP and sham operation by quantifying XBP1s and detecting p-eIF2α. XBP1s levels were the highest at 24 h after surgery and declined until 72 h after surgery. Subsequently XBP1s increased again. Changes reached significance between 48 and 72 h in the sham group and 24, and 72 h and 96 h in CASP animals (**Figures 3A,B**). The p-eIF2α continuously increased throughout the observation period in sham and CASP-operated animals (**Figures 3C,D**). Within the sham group, we found significantly higher levels of p-eIF2α at 72 h and 96 h compared with the 24 h time point. The CASP group displayed similar kinetics with significantly higher levels at 96 h compared with the values determined at 24 and 48 h. Although the CASP group displayed higher levels of XBP1s and p-eIF2α at the late time point (96 h), the differences between the sham and CASP group failed to be significant. This suggests that ER stress sentinels, IRE1α and PERK, were activated by surgery-associated stress rather than by moderate peritoneal infection.

Unfolded Protein Response Is Transient and Peaks at 24 h After Surgery

We next examined gene expression of UPR target genes, XBP1 and GRP78. Protein expression of GRP78 was additionally determined. The highest levels of XBP1 (**Figure 4A**) and GRP78 mRNA (**Figure 4B**) were found in sham and CASP groups at 24 h after surgery; however, no differences between the sham and CASP groups were found. In addition, we observed a close correlation of GRP78 mRNA levels with the marker for organ damage De Ritis ratio (**Figure 4C**) with a correlation coefficient (r) of 0.494 ($p < 0.01$) for the sham group and 0.518 ($p < 0.01$) for the CASP group, respectively. Although differences were not significant there was a trend toward lower GRP78 protein levels in the sham group at 96 h compared with the levels at 24 h, while we observed a slight increase at 96 h for the CASP group (**Figure 4D**; **Supplementary Figure S1**).

Unfolded Protein Response Triggered a Proapoptotic Shift in the Liver 48 h After Surgery

Since we found that p-eIF2α levels continued to increase after surgery, which is a sign for sustained activation of the PERK axis of the UPR, we next analyzed markers indicative of apoptosis activation. In both groups, we found the highest levels of CHOP, a downstream target of PERK activation, at 48 h after surgery. Thereafter, CHOP gene expression levels declined (**Figure 5A**). In addition, markers of the mitochondria-triggered apoptotic pathway, involving BAX and Bcl-XL, displayed a transient proapoptotic shift in both groups (**Figure 5B**). Compared with all the other time points, the ratio of the proapoptotic BAX to

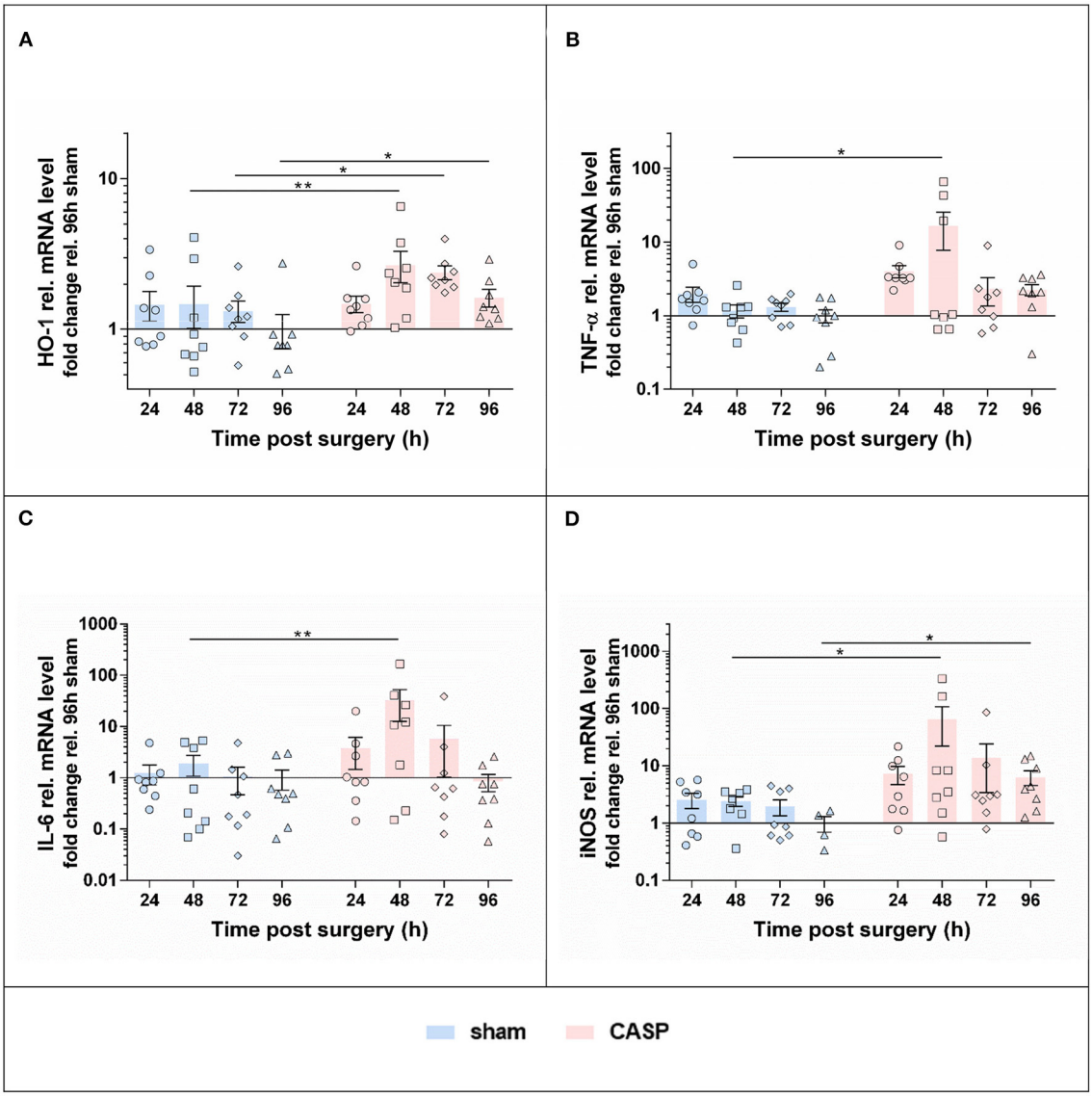

FIGURE 2 | Hepatic inflammatory response induced by abdominal infection peaks at 48 h. Gene expression levels of **(A)** HO-1, **(B)** TNF-α, **(C)** IL-6, and **(D)** iNOS were determined using qPCR in liver samples of rats that underwent sham or CASP surgery. Data are shown as mean ±SEM, with $n = 8$ for all the groups, except for **(D)** sham 48 h ($n = 7$) and **(D)** sham 96 h ($n = 4$). Statistical differences were calculated using two-way ANOVA followed by uncorrected Fisher's LSD test and are indicated by $^{*}p < 0.05$; $^{**}p < 0.01$.

the antiapoptotic Bcl-XL mRNA was significantly increased at 48 h after surgery in both, CASP and sham animals. However, no differences were found between the sham and CASP groups.

Unfolded Protein Response Activation Is Associated With the Surgical Stress

Considering that the degree of tissue damage caused by the surgical procedures was similar in all the experimental animals, the elicited effects are supposed to be influenced mainly by the time passed after surgery. In contrast, effects elicited by the peritoneal infection should distinguish sham animals from the CASP animals. In order to test the hypothesis that tissue damage, not peritoneal infection acts as a direct trigger for the hepatic UPR, we analyzed our data for both main effects, "time after surgery" and "peritoneal infection" and in addition for a potential interaction of both the conditions. We observed that inflammatory markers (TNF-α, IL-6, iNOS, and HO-1) were exclusively associated with the peritoneal infection, while UPR markers (XBPs, p-eIF2α, XBP1, GRP78, and CHOP) exclusively associated surgical stress (**Table 1**). There was no remarkable interaction between peritoneal infection and surgery for most markers. However, the interaction found for GRP78 mRNA in our study indicates that infectious stress in the peritoneum is capable of modulating the altitude of

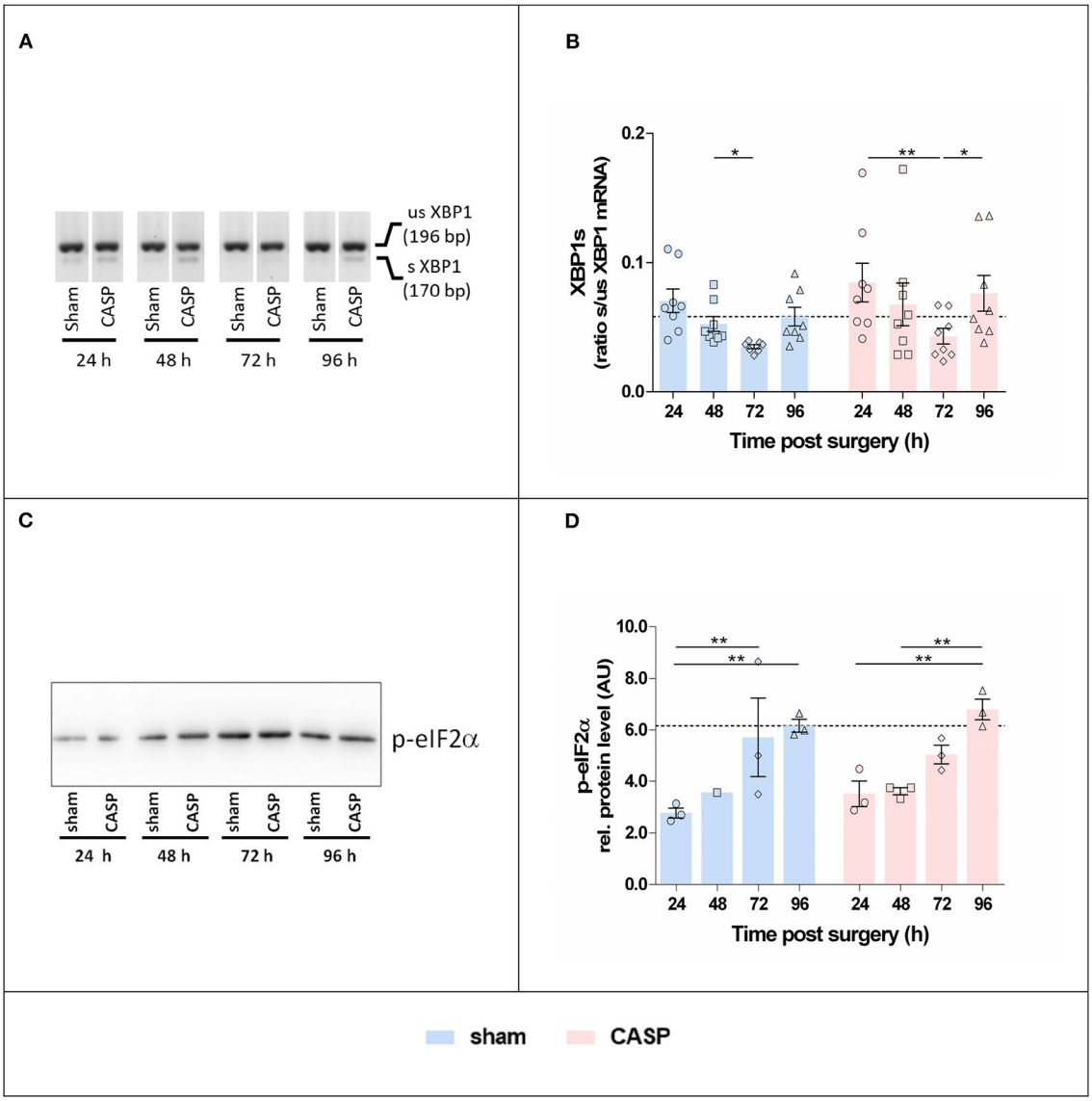

FIGURE 3 | Surgery induces hepatic XBP1 splicing and eIF2α phosphorylation. **(A)** Representative agarose gel electrophoresis of XBP1 PCR products showing the occurrence of the splice variant in the liver. **(B)** XBP1s indicated as the ratio of spliced (s) to unspliced (us) XBP1 mRNA determined by densitometric analyses. Data are given as mean ± SEM ($n = 8$ per group). **(C)** Liver homogenates were analyzed by SDS-PAGE and immunostaining for p-eIF2α. An exemplary blot is shown (the entire blot is shown in **Supplementary Figure S1A**). **(D)** Band intensities were normalized to the total protein of the respective gel lanes. Values are given as mean AU (arbitrary units) ± SEM ($n = 3$ per group, except for sham 48 h $n = 1$). The dashed line indicates the mean value of the sham group at 96 h. Statistical differences were calculated using two-way ANOVA followed by uncorrected Fisher's LSD test and are indicated by $^{*}p < 0.05$, $^{**}p < 0.01$.

hepatic GRP78 gene expression that was triggered by the surgical stress.

Activation of UPR Is Directly Correlated With the Level of Liver Damage During Abdominal Infection

We next analyzed the correlations among organ damage, UPR, or inflammation markers within sham and CASP animals using Pearson correlation (**Figure 6**). We found that UPR target genes GRP78 and XBP1 correlated significantly with liver damage markers De Ritis ratio (GRP78: sham $r = 0.49$, $p < 0.01$ and CASP $r = 0.52$, $p < 0.01$; XBP1: sham $r = 0.50$, $p < 0.01$ and CASP $r = 0.48$, $p < 0.01$) and AST (GRP78: sham $r = 0.52$, $p < 0.01$ and CASP $r = 0.59$, $p < 0.01$; XBP1: CASP $r = 0.60$, $p < 0.01$) in animals of both groups (**Figure 6**). Interestingly, these correlations were stronger among each other in animals of the CASP group. In addition, a strong positive correlation of XBP1s with liver damage markers (De Ritis ratio: $r = 0.56$, $p < 0.01$; AST: $r = 0.53$, $p < 0.01$) and with GRP78 ($r = 0.91$, $p < 0.01$) protein expression was found

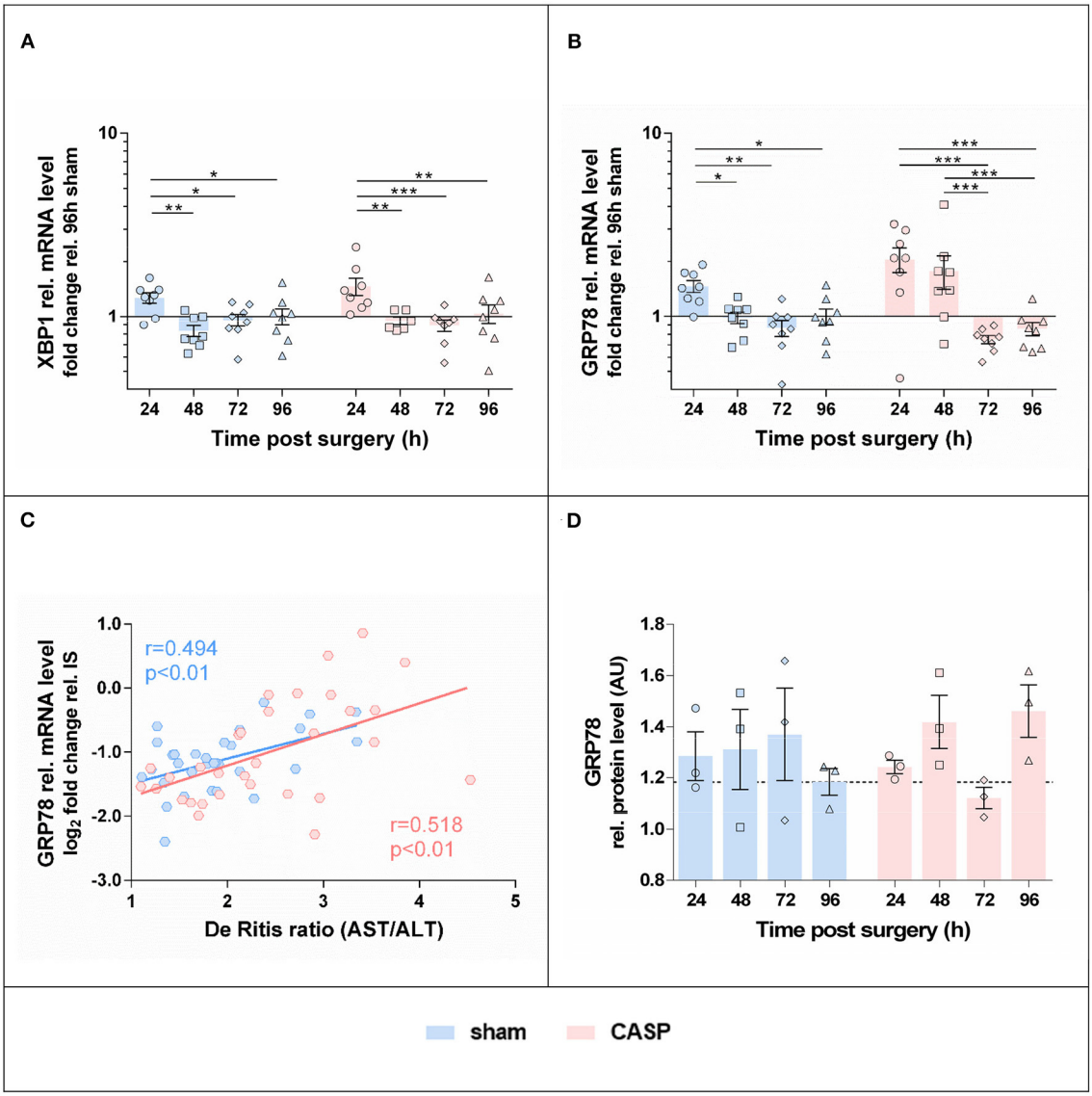

FIGURE 4 | Gene expression of UPR markers in the liver is highest at 24 h after surgery. Gene expression levels of **(A)** XBP1 and **(B)** GRP78 in the liver of sham and CASP operated rats were determined by means of qPCR. Data are shown as mean ± SEM ($n = 8$ per group). **(C)** Pearson correlation between GRP78 mRNA level and De Ritis ratio of sham ($n = 31$) and CASP ($n = 31$) operated animals. **(D)** GRP78 protein abundance in liver homogenates of single animals was analyzed by SDS-PAGE and immunostained for GRP78 (blot is shown in **Supplementary Figure S1B**). Band intensities of specific staining were normalized to the total protein of the respective gel lanes. Values are given as mean AU (arbitrary units) ± SEM ($n = 3$ per group). The dashed line indicates the mean value of the sham group at 96 h. Statistical differences were calculated using two-way ANOVA followed by uncorrected Fisher's LSD test and are indicated by $^{*}p < 0.05$; $^{**}p < 0.01$, and $^{***}p < 0.005$.

in CASP animals. Moreover, only in the CASP animals, the gene expression of the inflammatory marker TNF-α correlated with XBP1 mRNA ($r = 0.5$, $p < 0.01$). In sham animals, we found inverse correlations of CHOP and BAX/Bcl-XL with XBP1 mRNA (CHOP: $r = -0.42$, $p < 0.05$; BAX/Bcl-XL: $r = -0.54$, $p < 0.01$), which were not present in CASP animals. In contrast, no correlations between liver damage and markers of the inflammatory response were found. Taken together, our data suggest that not peritoneal infection, but organ damage triggers hepatic UPR.

Infectious Stimulants Are Weak, but Organ Damage-Triggering Factors Are Strong Inducers of UPR in the Liver

Since an upregulated hepatic UPR has been shown in several inflammatory animal models, including our own (15, 28), the question arises, which condition acts as a predominant trigger; the inflammation-inducing stimuli, or the tissue damage, which is accompanying severe inflammatory processes. To address this question more profoundly, we determined clustering of representative markers by reanalyzing data sets from

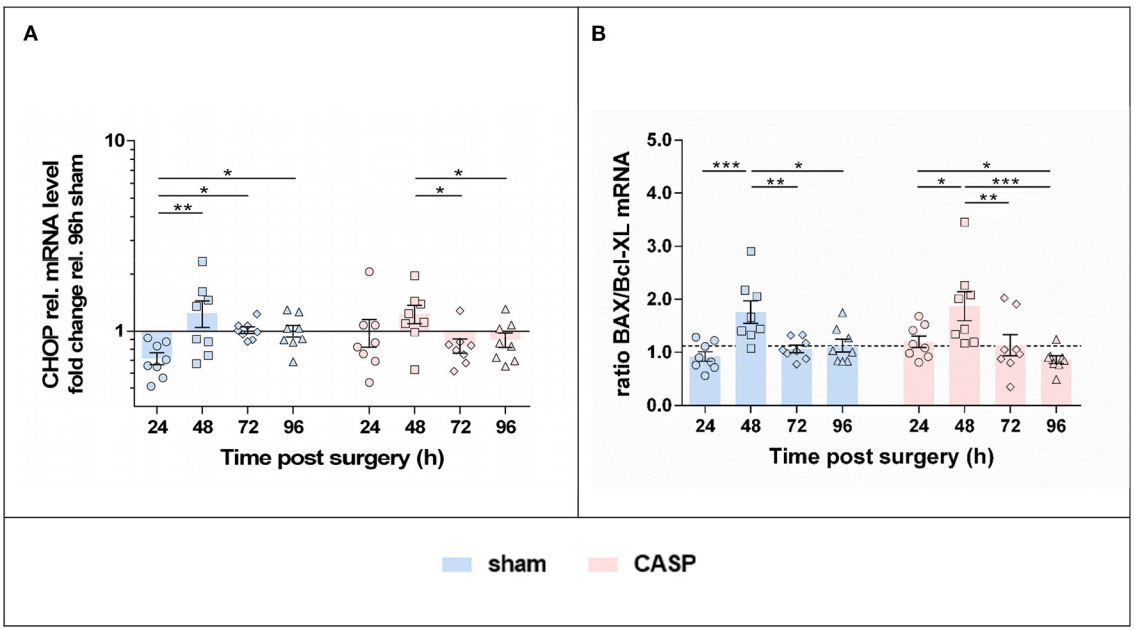

FIGURE 5 | UPR triggers a pro-apoptotic shift with maximum at 48 h after surgery. Gene expression levels of **(A)** CHOP, **(B)** BAX and Bcl-XL mRNA were determined by means of qPCR in liver samples after sham and CASP surgery. Data from BAX and Bcl-XL expression are presented as a ratio. The dashed line indicates the mean value of the sham group at 96 h. All data are shown as mean ± SEM ($n = 8$ per group). Statistical difference was calculated using two-way ANOVA followed by uncorrected Fisher's LSD test and is indicated by $^{*}p < 0.05$, $^{**}p < 0.01$, and $^{***}p < 0.005$.

two different acute experimental models, a THS model and an endotoxic shock model (*i.v.* application of LPS), which were part of studies previously published (15, 28). While the THS model induces initially acute tissue damage, *via* ischemia/reperfusion injury, intravenous LPS application leads acutely to a fulminant inflammatory response. Thus, analyzing a very early time point (2 h) in both models, we expected to see the predominantly triggered responses, without superimposing secondary effects. The applied analytical approach, of ranking the normalized effects of investigated markers (refer to Methods to **Supplementary Figure S2** in **Supplementary Material**), allows a direct comparison of marker clustering in both models. We found significant differences between the THS (2 h after trauma and hemorrhage) and the endotoxic shock group (LPS, 2 h). The LPS group showed higher cumulative ranks of inflammatory markers (iNOS, TNF-α) with lower ALT ranks, and lower ranks for UPR (CHOP, XBP1, XBP1s, and GRP78) compared with the THS animals. In contrast, the THS group showed higher ranks of ER-stress markers (CHOP, XBP1, and XBP1s) and higher ALT ranks, while an association with the inflammatory markers was nearly absent (**Supplementary Figure S2**). Of note: HO-1 levels were significantly increased compared with controls in both models, supporting the observation of HO-1 as an exquisite marker of the general hepatic cell stress.

In addition, our experiments performed with an immortalized liver cell line (BRL3A) described in the **Supplementary Material** (Methods to **Supplementary Figure S3**), support the finding of the weak capacity of inflammatory mediators to directly induce hepatic UPR. Although the BRL3A cells are capable of exquisitely responding to ER stress inducers, such as tunicamycin and thapsigargin (**Supplementary Figure S3A**), incubation with inflammatory mediators raised the expression of IL-6, without clearly affecting the UPR response markers, GRP78 and CHOP (**Supplementary Figure S3B**).

These additional data support the assumption that not infectious stimuli, but the conditions associated with organ damage are the predominant triggers of the hepatic UPR seen in our CASP model.

DISCUSSION

Animal Model

Abdominal infections are an important clinical problem. In Germany, abdominal infections cause 28.7% of all sepsis cases (29). Primary peritonitis caused by diverticulitis or Morbus Crohn, or secondary peritonitis through anastomotic failure after surgical procedures is a frequent problem in the clinical setting.

The CASP model is a well-established and clinically relevant animal model of polymicrobial sepsis. The stent used in CASP leads to continuous leakage of feces into the abdomen, and therefore, closely mimics the clinical course of diffuse peritonitis in patients with steadily increasing systemic infection and inflammation (22). The severity of sepsis and resulting mortality can be controlled in CASP models, as it is directly depending on the size of the stent (21). Mortality occurs already at early time points in the experimental models of severe sepsis, such as CASP with large stent, or cecal ligation and puncture models (22). In the model of moderate

TABLE 1 | Main effects of peritoneal infection and surgical stress on inflammatory markers, unfolded protein response, and interaction of both the conditions determined by two-way ANOVA.

Variable		Main effect (*p*-value)		Interaction (*p*-value)
		Peritoneal infection	Surgery	
AST	Activity	0.638	**<0.0001**	0.133
ALT	Activity	**0.008**	0.157	0.289
De Ritis ratio	(AST/ALT)	**0.002**	**0.0002**	0.396
TNF-α	mRNA	**0.002**	0.132	0.516
IL-6	mRNA	**0.035**	0.112	0.233
iNOS	mRNA	**0.0004**	0.4690	0.872
HO-1	mRNA	**0.000**	0.141	0.314
p-eIF2α	Protein	0.733	**0.0008**	0.697
XBP1s	mRNA	0.074	**0.007**	0.975
GRP78	mRNA	0.202	**<0.0001**	**0.044**
XBP1	mRNA	0.404	**<0.0001**	0.625
GRP78	Protein	0,765	0.680	0.134
CHOP	mRNA	0.897	**0.006**	0.118
BAX/Bcl-XL	mRNA	0.995	**<0.0001**	0.164

Significant effects ($p < 0.05$) are indicated by bold values.

peritonitis, which was applied in this study, the survival rate was more than 90% until 96 h after surgery (24). Therefore, this model is characterized as non-lethal but self-resolving peritonitis. Using this model, we previously demonstrated that CASP transiently compromised liver mitochondria early (24–48 h) after surgery (24). The transient nature of CASP-induced effects on functional parameters of the liver confirms the moderate and self-resolving character of the present peritonitis model.

Organ/Cell Damage

The levels of the liver damage markers AST, as published previously (24), and the De Ritis ratio were only moderately elevated. AST and De Ritis ratio were significantly higher at the early time point (24 h) in response to the surgical stress. Thereafter, these values declined successively supporting the self-resolving character of the CASP model. Abdominal infection only slightly modulated AST values, which resulted in moderately, albeit significantly higher De Ritis ratios in the CASP groups at 48 and 96 h after surgery. Thus, the surgical procedure exerted an acute, but transient stress that was associated with a moderate liver-damaging potential. Moderate peritonitis contributed little to liver damage, which occurred predominantly in response to surgery. We assume that this reaction was the consequence of tissue damage related to the surgery. The increased expression of ER stress response genes in the blood cells of patients 1 day after cardiac surgery with cardiopulmonary bypass supports our assumption (30).

Hepatic Inflammatory Response

In contrast to organ damage markers, expression of markers of inflammation in liver tissues showed a strong response to and a clear association with the abdominal infection. In CASP compared with the sham animals, gene expression of proinflammatory markers was maximally and significantly increased at 48 h. Thereafter, gene expression levels declined with HO-1 and iNOS still being significantly higher in the sham group up to the latest time point investigated (96 h). We attribute this late effect to the continuously increasing systemic response to infection and inflammation induced by CASP, as shown before (22). These data show that surgery contributes little if anything to the inflammatory response in the liver, which is essentially triggered by the abdominal infection. Of note, we have determined the inflammatory markers at gene expression levels, which reflect a quick response to infection. Thus, it can be assumed that in the present model, abdominal infection induced by CASP takes about 2 days (48 h) to reach the maximum. This is also the time point, at which high-mortality rates can be observed in severe sepsis models and septic patients (21, 31, 32). We assumed that UPR would follow the same kinetics if triggered by infectious stimuli.

Hepatic Unfolded Protein Response

Contrary to this assumption, the kinetics of expression of ER stress and UPR-related markers were different from those of the proinflammatory markers. The changes observed for the UPR-related markers were moderate, but most strikingly, markers associated with IRE1α activation were maximal at 24 h after surgery. Furthermore, we could not determine a significant effect of CASP on the UPR-related markers investigated.

Unfolded protein response activation in consequence of tissue damage (33), particularly because of hypoxia or ischemia/reperfusion (15, 16), has been demonstrated in the last couple of years. Thus, we assume that hepatic ER stress and UPR are a consequence of circulating damage-associated signals (possibly danger-associated molecular patterns) rather than inflammatory mediators.

This association was addressed more profoundly by reanalyzing data sets from two different acute models, a THS model and an endotoxic shock model (*i.v.* application of lipopolysaccharide (LPS)), which were part of studies previously published (15, 28). Both experimental models are associated with a substantial loss of animals (up to 50%) and are, in contrast to the CASP model, characterized by a nearly immediate response of the liver (15, 28). Therefore, we considered a very early time point (2 h) most suitable to dissect the direct impact of induced tissue damage vs. induced inflammation on the manifestation of the hepatic ER stress response.

The infectious stimulus, LPS, triggered predominantly an increased inflammatory response that was initially not associated with substantial organ damage (28) and only a weakly upregulated hepatic UPR at this time point. In contrast, THS, which triggered significant organ damage (15), was associated with a strongly upregulated hepatic UPR, while an inflammatory response was absent at this early time point. Of importance, in the THS model XBP1 and XBP1s nearly instantly followed organ damage as indicated by the increased levels of ALT (15). These data indicate that conditions associated with organ damage rather than infectious stimuli operate as direct triggers of the hepatic

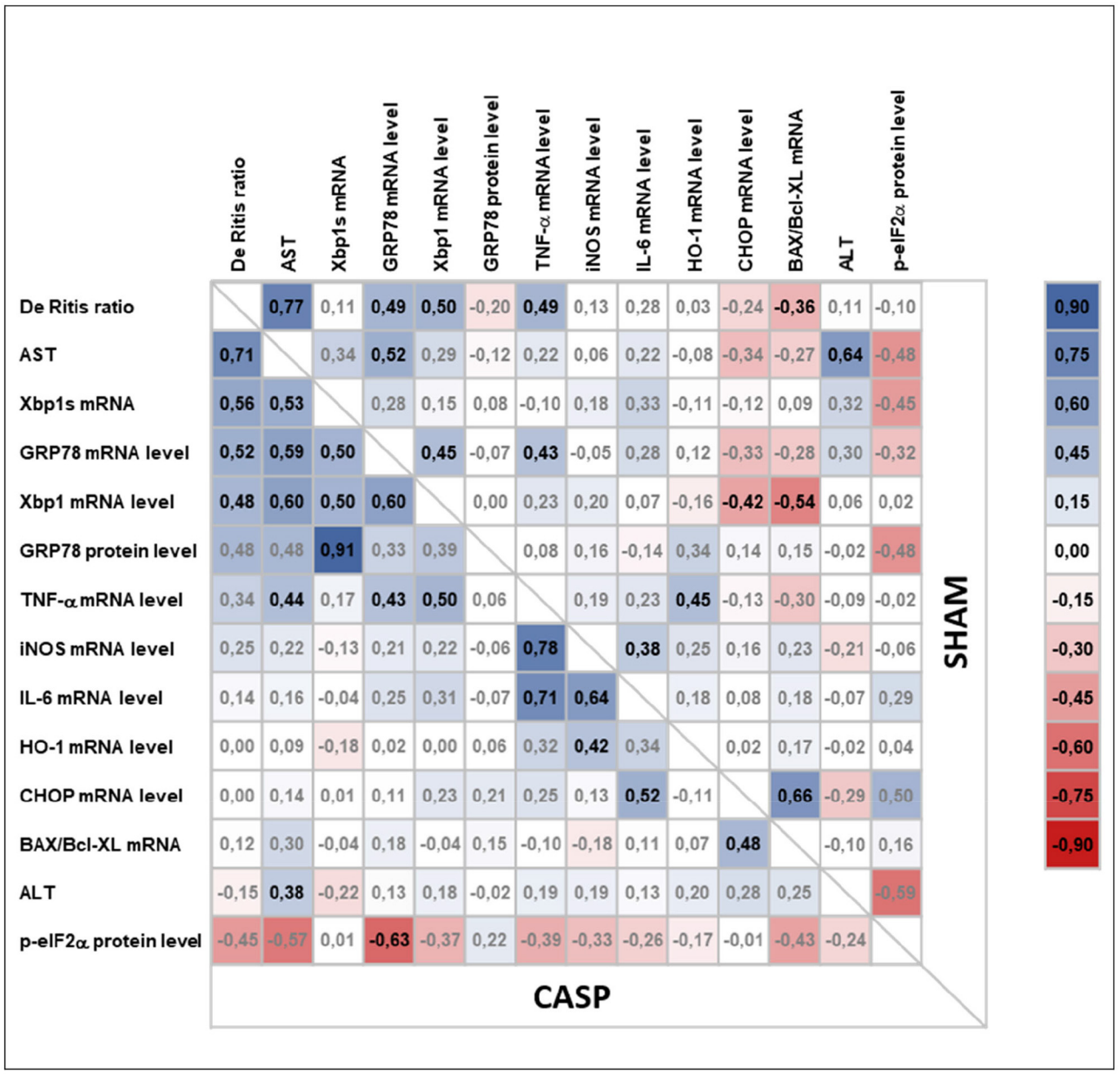

FIGURE 6 | Pearson correlation analysis of liver damage markers, UPR, and inflammatory response in animals subjected to surgery (sham) or CASP. Markers for organ damage (plasma ALT and AST and De Ritis ratio) and levels of hepatic markers for UPR (XBP1s mRNA, XBP1 mRNA, GRP78 mRNA/protein, p-eIF2α protein, CHOP mRNA), inflammatory response (IL-6 mRNA, TNF-α mRNA, iNOS mRNA), general stress response (HO-1 mRNA), as well as BAX/Bcl-XL mRNA ratio as a marker for a proapoptotic phenotype were correlated with each other in both, CASP and sham animals, using Pearson correlation ($n = 4$–8 for all mRNA data, $n = 1$–3 for all the protein data). In the upper right and the lower left part correlation coefficients (r) calculated from sham and CASP animals, respectively, are shown. A correlation plot was prepared using Microsoft Excel 2016. Positive correlations are highlighted in blue, negative correlations in red. Significant correlations are indicated by bold letters.

UPR. This assumption is further supported by our additional experiments using cultured immortalized liver cells, in which we show that inflammatory mediators were capable to induce an inflammatory response, but not a substantial ER stress response.

We found that UPR, which was triggered primarily by tissue damage, is associated with IRE1α and PERK activation. IRE1α activation, through the expression of XBP1s, has been extensively associated with cell survival (34). In the CASP model, IRE1α was temporarily activated early (24 h) after surgery, while the PERK-eIF2α-p-eIF2α pathway was activated throughout the entire observation period. Phosphorylation of eIF2α inhibits translation initiation resulting in a reduction of protein load in the ER, except for transcripts related to ER stress resolution (35). Persistent PERK-ATF4-CHOP signaling can commit the cell to

apoptosis (36). Indeed, CHOP levels peaked 48 h after surgery and resulted in transiently higher BAX/Bcl-XL ratios indicating a proapoptotic switch at the consecutive time point (48 h) in the present model. In addition, eIF2α phosphorylation and CHOP activation are associated with metabolic dysregulation during hepatic ER stress (37).

Although individual UPR-related targets increased only moderately in this model, the entity of upregulated UPR-related markers following tissue trauma because of the surgery likely reflects an early effort to rescue tissue function upon danger signaling, as was previously suggested (38).

In addition, both the XBP1 and the downstream target GRP78 correlated significantly with AST and De Ritis ratio in the present CASP model. Although a correlation does not imply a causal relationship, it is noteworthy that organ damage markers did not correlate with inflammatory markers, but with ER stress markers. Pharmacological induction of ER stress has been shown to result in increased mortality after trauma (33). In contrast, inhibition of ER stress has been shown to protect livers against ischemia/reperfusion injury in a model of hepatectomy (39). This indicates that possibly danger-associated molecular patterns, released in substantial amounts during trauma or surgery, but also secondary to substantial systemic inflammatory conditions are triggers of liver cell death employing mechanisms that involve ER stress pathways.

Interaction of Hepatic UPR With CASP-Induced Inflammatory Response Pathways

Even though abdominal infection had no significant effect on the expression of UPR markers, we found a stronger association between XBP1s and GRP78 with liver damage markers in rats that underwent CASP. Furthermore, CASP altered the kinetics of GRP78 gene expression following surgical trauma toward a later decline, suggesting cooperation between inflammatory and ER stress pathways. To the best of our knowledge, no experiments could show a direct induction of UPR by inflammatory mediators, such as cytokines. However, the secondary organ damage, which is typically accompanying inflammatory conditions, could well explain the increased ER stress response seen in SIRS. Vice versa, ER stress is capable to trigger inflammatory pathways acting as synergizing components in several pathologies (40). Both UPR branches, IRE1α and PERK can directly activate nuclear factor kappa B (NF-κB) (41, 42) leading to the production of inflammatory cytokines. ER stress activating IRE1α is further linked to TNF-α-mediated cell death through the adaptor protein tumor necrosis factor α receptor-associated factor 2 (TRAF2) and NF-κB (43). Therefore, cell death signals synergize in response to inflammation triggered by TNF-α, which also employs NF-κB. TNF-α levels in the plasma of CASP animals were elevated 96 h after surgery in the present model (24). The increased De Ritis ratio in the CASP group at this time point possibly reflects a converged synergism of cell death pathways. Although the low mortality of this CASP model indicates that the elicited inflammatory response may be self-resolving, it was sufficient to transiently affect mitochondrial function in the liver (24). Interestingly, mitochondrial damage driven by caspase 2 has been described as a mechanism underlying hepatocyte death upon ER stress that operated *via* NLRP3 inflammasome activation (44, 45).

Given the good outcome of our experimental rats, which were young and showed no clinical signs when enrolled in the study, we assume that the damage triggered hepatic UPR was well balanced and exerted a beneficial role in the present CASP model. However, since ER stress is a critical inflammation triggering factor, the role of surgery modulating UPR warrants closer consideration in patients suffering from comorbidities, i.e., metabolic diseases (46). Based on our results, we suggest therapeutic approaches, which target the ER to maintain liver function in conditions associated with inflammatory processes, such as sepsis. Of note, certain anesthetics or antibiotics have been shown to modulate ER stress induction in the liver (47–50). Thus, the choice of an appropriate anesthetic protocol during surgery followed by a suitable antibiotic therapy might help to shape UPR and limit consecutive liver damage.

Limitations

This study was focused on the progression of ER stress/UPR markers exclusively in the liver as a remote target organ in the peritonitis and abdominal surgery, because of its central role for the system. However, we did not analyze the local effects of peritonitis. Several studies have already highlighted the relevance of intestinal ER stress in peritonitis that is tightly linked to deranged intestinal tissue homeostasis and immunity (51, 52), and particularly the impairment of the intestinal barrier function (53). Further studies will be necessary to clarify the source or the nature of the compounds that trigger the ER stress/UPR and inflammatory response in the liver.

CONCLUSION

Using a clinically relevant experimental sepsis model, we found that surgical trauma activates hepatic UPR, presumably because of tissue injury. UPR activation occurred early and preceded the inflammatory response in the liver. This indicates that hepatic UPR and the inflammatory response are triggered by different mechanisms. Our data further suggest that secondary tissue injury, as it occurs in septic complications, may influence the severity of ER stress and UPR-mediated liver cell dysfunction. Thus, the hepatic ER appears to be an important target for shaping UPR in order to prevent liver dysfunction in abdominal surgery and severe SIRS.

DATA AVAILABILITY STATEMENT

The original contributions presented in the study are included in the article/**Supplementary Material**, further inquiries can be directed to the corresponding author.

ETHICS STATEMENT

The animal study was reviewed and approved by Landesamt für Natur, Umwelt und Verbraucherschutz, Recklinghausen, Germany (experiments were performed in accordance with the NIH Guidelines for Animal Care).

AUTHOR CONTRIBUTIONS

AM wrote the first draft of the manuscript, performed the statistical analysis and the graphical data presentation. AH and OP performed and supervised animal experiments. IM performed and interpreted WB analysis. AM and MK performed and interpreted PCR analysis. AL provided critical feedback and revised the manuscript. JD, IB, and AK designed and supervised the study. JD and AK provided critical feedback and wrote the final version of the manuscript. All authors gave intellectual input and approved the final version of the manuscript.

FUNDING

AM was supported by the Austrian Research Promotion Agency with a Ph.D. Grant: Industrienahe Dissertation (849090). MK was supported by an Internship for female students from the Austrian Research Promotion Agency (FFG). AL received funding from the European Union's Horizon 2020 Research and Innovation Program under the Marie Skłodowska-Curie Grant Agreement No. 675448.

ACKNOWLEDGMENTS

We thank H. P. Satzer, J. Paier-Pourani, and I. Kehrer for contributing the data of the cultured hepatocyte cells (BRL3A) treated with ER stressors, tunicamycin and thapsigargin, and inflammatory mediators, generated from white blood cells, which were included in the **Supplemental Material**.

SUPPLEMENTARY MATERIAL

The Supplementary Material for this article can be found online at: https://www.frontiersin.org/articles/10.3389/fmed.2022.785285/full#supplementary-material

REFERENCES

1. Hatfield KM, Dantes RB, Baggs J, Sapiano MRP, Fiore AE, Jernigan JA, Epstein L. Assessing variability in hospital-level mortality among US medicare beneficiaries with hospitalizations for severe sepsis and septic shock. *Crit Care Med.* (2018) 46:1753–60. doi: 10.1097/CCM.0000000000003324
2. Yan J, Li S, Li S. The role of the liver in sepsis. *Int Rev Immunol.* (2014) 33:498–510. doi: 10.3109/08830185.2014.889129
3. Strnad P, Tacke F, Koch A, Trautwein C. Liver-guardian, modifier and target of sepsis. *Nat Rev Gastroenterol Hepatol.* (2017) 14:55–66. doi: 10.1038/nrgastro.2016.168
4. Moshage H. Cytokines and the hepatic acute phase response. *J Pathol.* (1997) 181:257–66. doi: 10.1002/(SICI)1096-9896(199703)181:3<257::AID-PATH756>3.0.CO;2-U
5. Khan MM, Yang WL, Wang P. Endoplasmic reticulum stress in sepsis. *Shock.* (2015) 44:294–304. doi: 10.1097/SHK.0000000000000425
6. Thiessen SE, Van den Berghe G, Vanhorebeek I. Mitochondrial and endoplasmic reticulum dysfunction and related defense mechanisms in critical illness-induced multiple organ failure. *Biochim Biophys Acta Mol Basis Dis.* (2017) 1863:2534–45. doi: 10.1016/j.bbadis.2017.02.015
7. Hetz C, Zhang K, Kaufman RJ. Mechanisms, regulation and functions of the unfolded protein response. *Nat Rev Mol Cell Biol.* (2020) 21:421–38. doi: 10.1038/s41580-020-0250-z
8. Yamamoto K, Sato T, Matsui T, Sato M, Okada T, Yoshida H, et al. Transcriptional induction of mammalian ER quality control proteins is mediated by single or combined action of ATF6alpha and XBP1. *Dev Cell.* (2007) 13:365–76. doi: 10.1016/j.devcel.2007.07.018
9. Lee A-H, Iwakoshi NN, Glimcher LH. XBP-1 regulates a subset of endoplasmic reticulum resident chaperone genes in the unfolded protein response. *Mol Cell Biol.* (2003) 23:7448–59. doi: 10.1128/mcb.23.21.7448-7459.2003
10. Ron D. Translational control in the endoplasmic reticulum stress response. *J Clin Invest.* (2002) 110:1383–8. doi: 10.1172/JCI16784
11. Hu H, Tian M, Ding C, Yu S. The C/EBP homologous protein (CHOP) transcription factor functions in endoplasmic reticulum stress-induced apoptosis and microbial infection. *Front Immunol.* (2019) 10:1–13. doi: 10.3389/fimmu.2018.03083
12. Kaufman RJ. Orchestrating the unfolded protein response in health and disease. *J Clin Invest.* (2002) 110:1389–98. doi: 10.1172/JCI0216886
13. Almanza A, Carlesso A, Chintha C, Creedican S, Doultsinos D, Leuzzi B, et al. Endoplasmic reticulum stress signalling—from basic mechanisms to clinical applications. *FEBS J.* (2019) 286:241–78. doi: 10.1111/febs.14608
14. Kozlov A V, Duvigneau JC, Miller I, Nürnberger S, Gesslbauer B, Kungl A, et al. Endotoxin causes functional endoplasmic reticulum failure, possibly mediated by mitochondria. *Biochim Biophys Acta Mol Basis Dis.* (2009) 1792:521–30. doi: 10.1016/j.bbadis.2009.03.004
15. Duvigneau JC, Kozlov A V, Zifko C, Postl A, Hartl RT, Miller I, et al. Reperfusion does not induce oxidative stress but sustained endoplasmic reticulum stress in livers of rats subjected to traumatic-hemorrhagic shock. *Shock.* (2010) 33:289–98. doi: 10.1097/SHK.0b013e3181aef322
16. Jian B, Hsieh CH, Chen J, Choudhry M, Bland K, Chaudry I, et al. Activation of endoplasmic reticulum stress response following trauma-hemorrhage. *Biochim Biophys Acta Mol Basis Dis.* (2008) 1782:621–6. doi: 10.1016/j.bbadis.2008.08.007
17. Kleber A, Kubulus D, Rössler D, Wolf B, Volk T, Speer T, et al. Melatonin modifies cellular stress in the liver of septic mice by reducing reactive oxygen species and increasing the unfolded protein response. *Exp Mol Pathol.* (2014) 97:565–71. doi: 10.1016/j.yexmp.2014.10.009
18. Qian W-J, Cheng Q-H. Endoplasmic reticulum stress-mediated apoptosis signal pathway is involved in sepsis-induced liver injury. *Int J Clin Exp Pathol.* (2017) 10:9990−7.
19. Thiessen SE, Derese I, Derde S, Dufour T, Pauwels L, Bekhuis Y, et al. The role of autophagy in critical illness-induced liver damage. *Sci Rep.* (2017) 7:1–12. doi: 10.1038/s41598-017-14405-w
20. Hecker A, Reichert M, Reuß CJ, Schmoch T, Riedel JG, Schneck E, et al. Intra-abdominal sepsis: new definitions and current clinical standards. *Langenbeck's Arch Surg.* (2019) 404:257–71. doi: 10.1007/s00423-019-01752-7
21. Lustig MK, Bac VH, Pavlovic D, Maier S, Gründling M, Grisk O, et al. Colon ascendens stent peritonitis—a model of sepsis adopted to the rat:

physiological, microcirculatory and laboratory changes. *Shock.* (2007) 28:59–64. doi: 10.1097/SHK.0b013e31802e454f
22. Maier S, Traeger T, Entleutner M, Westerholt A, Kleist B, Hüser N, et al. Cecal ligation and puncture versus colon ascendens stent peritonitis: two distinct animal models for polymicrobial sepsis. *Shock.* (2004) 21:505–11. doi: 10.1097/01.shk.0000126906.52367.dd
23. Russel WMS, Burch RL. *The Principles of Humane Experimental Technique.* (1959) Available at: https://caat.jhsph.edu/principles/the-principles-of-humane-experimental-technique (accessed September 23, 2021)
24. Herminghaus A, Papenbrock H, Eberhardt R, Vollmer C, Truse R, Schulz J, et al. Time-related changes in hepatic and colonic mitochondrial oxygen consumption after abdominal infection in rats. *Intensive care Med Exp.* (2019) 7:4. doi: 10.1186/s40635-018-0219-9
25. Cerative Commons Corporation, Creative Commons Licence. (1996) Available online at: https://creativecommons.org/licenses/by/4.0/ (accessed September 23, 2021)
26. Müllebner A, Moldzio R, Redl H, Kozlov AV, Duvigneau JC. Heme degradation by heme oxygenase protects mitochondria but induces ER stress via formed bilirubin. *Biomolecules.* (2015) 5:679–701. doi: 10.3390/biom5020679
27. Motulsky HJ, Brown RE. Detecting outliers when fitting data with nonlinear regression - A new method based on robust nonlinear regression and the false discovery rate. *BMC Bioinformatics.* (2006) 7:1–20. doi: 10.1186/1471-2105-7-123
28. Nürnberger S, Miller I, Catharina Duvigneau J, Kavanagh ET, Gupta S, Hartl RT, et al. Impairment of endoplasmic reticulum in liver as an early consequence of the systemic inflammatory response in rats. *Am J Physiol Gastrointest Liver Physiol.* (2012) 303:1373–83. doi: 10.1152/ajpgi.00056.2012
29. SepNet Critical Care Trials Group. Incidence of severe sepsis and septic shock in German intensive care units: the prospective, multicentre INSEP study. *Intensive Care Med.* (2016) 42:1980–1989. doi: 10.1007/s00134-016-4504-3
30. Clavier T, Demailly Z, Semaille X, Thill C, Selim J, Veber B, et al. Weak response to endoplasmic reticulum stress is associated with postoperative organ failure in patients undergoing cardiac surgery with cardiopulmonary bypass. *Front Med.* (2020) 7:613518. doi: 10.3389/fmed.2020.613518
31. Mishra SK, Choudhury S. Experimental protocol for cecal ligation and puncture model of polymicrobial sepsis and assessment of vascular functions in mice. *Methods Mol Biol.* (2018) 1717:161–87. doi: 10.1007/978-1-4939-7526-6_14
32. Davies R, O'Dea K, Gordon A. Immune therapy in sepsis: are we ready to try again? *J Intensive Care Soc.* (2018) 19:326–44. doi: 10.1177/1751143718765407
33. Abdullahi A, Barayan D, Vinaik R, Diao L, Yu N, Jeschke MG. Activation of ER stress signalling increases mortality after a major trauma. *J Cell Mol Med.* (2020) 24:9764–73. doi: 10.1111/jcmm.15548
34. Lin JH Li H, Yasumura D, Cohen HR, Zhang C, Panning B, Shokat KM, et al. IRE1 signaling affects cell fate during the unfolded protein response. *Science.* (2007) 318:944–9. doi: 10.1126/science.1146361
35. Szegezdi E, Logue SE, Gorman AM, Samali A. Mediators of endoplasmic reticulum stress-induced apoptosis. *EMBO Rep.* (2006) 7:880–5. doi: 10.1038/sj.embor.7400779
36. McCullough KD, Martindale JL, Klotz L-O, Aw T-Y, Holbrook NJ. Gadd153 sensitizes cells to endoplasmic reticulum stress by down-regulating Bcl2 and perturbing the cellular redox state. *Mol Cell Biol.* (2001) 21:1249–59. doi: 10.1128/mcb.21.4.1249-1259.2001
37. Chikka MR, McCabe DD, Tyra HM, Rutkowski DT. C/EBP homologous protein (CHOP) contributes to suppression of metabolic genes during endoplasmic reticulum stress in the liver. *J Biol Chem.* (2013) 288:4405–15. doi: 10.1074/jbc.M112.432344
38. Soares MP, Gozzelino R, Weis S. Tissue damage control in disease tolerance. *Trends Immunol.* (2014) 35:483–94. doi: 10.1016/j.it.2014.08.001
39. Ben Mosbah I, Alfany-Fernández I, Martel C, Zaouali MA, Bintanel-Morcillo M, Rimola A, et al. Endoplasmic reticulum stress inhibition protects steatotic and non-steatotic livers in partial hepatectomy under ischemia-reperfusion. *Cell Death Dis.* (2010) 1:1–12. doi: 10.1038/cddis.2010.29
40. Zhang K, Kaufman RJ. From endoplasmic-reticulum stress to the inflammatory response. *Nature.* (2008) 454:455–62. doi: 10.1038/nature07203
41. Kaneko M, Niinuma Y, Nomura Y. Activation signal of nuclear factor-kappa B in response to endoplasmic reticulum stress is transduced via IRE1 and tumor necrosis factor receptor-associated factor 2. *Biol Pharm Bull.* (2003) 26:931–5. doi: 10.1248/bpb.26.931
42. Deng J, Lu PD, Zhang Y, Scheuner D, Kaufman RJ, Sonenberg N, et al. Translational repression mediates activation of nuclear factor kappa B by phosphorylated translation initiation factor 2. *Mol Cell Biol.* (2004) 24:10161–8. doi: 10.1128/MCB.24.23.10161-10168.2004
43. Schmitz ML, Shaban MS, Albert BV, Gökçen A, Kracht M. The crosstalk of endoplasmic reticulum (ER) stress pathways with NF-κB: complex mechanisms relevant for cancer, inflammation and infection. *Biomedicines.* (2018) 6:1–18. doi: 10.3390/biomedicines6020058
44. Lebeaupin C, Proics E, de Bieville CHD, Rousseau D, Bonnafous S, Patouraux S, et al. ER stress induces NLRP3 inflammasome activation and hepatocyte death. *Cell Death Dis.* (2015) 6:e1879. doi: 10.1038/cddis.2015.248
45. Bronner DN, Abuaita BH, Chen X, Fitzgerald KA, Nuñez G, He Y, et al. Endoplasmic reticulum stress activates the inflammasome via NLRP3- and caspase-2-driven mitochondrial damage. *Immunity.* (2015) 43:451–62. doi: 10.1016/j.immuni.2015.08.008
46. Hotamisligil GS. Endoplasmic reticulum stress and the inflammatory basis of metabolic disease. *Cell.* (2010) 140:900–17. doi: 10.1016/j.cell.2010.02.034
47. Liu D, Jin X, Zhang C, Shang Y. Sevoflurane relieves hepatic ischemia-reperfusion injury by inhibiting the expression of Grp78. *Biosci Rep.* (2018) 38:1–10. doi: 10.1042/BSR20180549
48. Seo EH, Piao L, Park HJ, Lee JY, Sa M, Oh CS, et al. Impact of general anaesthesia on endoplasmic reticulum stress: propofol vs. isoflurane. *Int J Med Sci.* (2019) 16:1287–94. doi: 10.7150/ijms.36265
49. Bellizzi Y, Anselmi Relats JM, Cornier PG, Delpiccolo CML, Mata EG, Cayrol F, et al. Contribution of endoplasmic reticulum stress, MAPK and PI3K/Akt pathways to the apoptotic death induced by a penicillin derivative in melanoma cells. *Apoptosis.* (2021) 2021:1–15. doi: 10.1007/s10495-021-01697-7
50. Burban A, Sharanek A, Guguen-Guillouzo C, Guillouzo A. Endoplasmic reticulum stress precedes oxidative stress in antibiotic-induced cholestasis and cytotoxicity in human hepatocytes. *Free Radic Biol Med.* (2018) 115:166–78. doi: 10.1016/j.freeradbiomed.2017.11.017
51. Eugene SP, Reddy VS, Trinath J. Endoplasmic reticulum stress and intestinal inflammation: a perilous union. *Front Immunol.* (2020) 11:1–10. doi: 10.3389/fimmu.2020.543022
52. Coleman OI, Haller D, ER. Stress and the UPR in Shaping Intestinal Tissue Homeostasis and Immunity. *Front Immunol.* (2019) 10:1–13. doi: 10.3389/fimmu.2019.02825
53. Sun S, Duan Z, Wang X, Chu C, Yang C, Chen F, et al. Neutrophil extracellular traps impair intestinal barrier functions in sepsis by regulating TLR9-mediated endoplasmic reticulum stress pathway. *Cell Death Dis.* (2021) 12:1–12. doi: 10.1038/s41419-021-03896-1

Conflict of Interest: The authors declare that the research was conducted in the absence of any commercial or financial relationships that could be construed as a potential conflict of interest.

Publisher's Note: All claims expressed in this article are solely those of the authors and do not necessarily represent those of their affiliated organizations, or those of the publisher, the editors and the reviewers. Any product that may be evaluated in this article, or claim that may be made by its manufacturer, is not guaranteed or endorsed by the publisher.

Tissue damage, not infection, triggers hepatic unfolded protein response in an experimental rat peritonitis model

Supplementary Material

Supplementary Table 1: Sequence and source of primer pairs used in this study.

Target	Accession number	Primer sequences	Position on plus strand	Product Length	Source
Cyclo	M19533	TAT CTG CAC TGC CAA GAC TGA GTG	381	127	(1)
		CTT CTT GCT GGT CTT GCC ATT CC	507		
HPRT	NM_012583	CTC ATG GAC TGA TTA TGG ACA GGA C	179	123	(2)
		GCA GGT CAG CAA AGA ACT TAT AGC C	301		
TNF-α	X66539	TGC CTC AGC CTC TTC TCA TT	94	376	(1)
		TGT GGG TGA GGA GCA CAT AG	469		
IL-6	NM_012589.1	CCG GAG AGG AGA CTT CAC AG	154	161	(3)
		ACA GTG CAT CAT CGC TGT TC	314		
iNOS	NM_012611.3	AGG CAA GCC CTC ACC TAC TT	2654	161	(3)
		GTG GGG TTG TTG CTG AAC TT	2814		
HO-1	NM_012580.2	CCA GCC ACA CAG CAC TAC	441	293	(1)
		GCG GTC TTA GCC TCT TCT G	733		
GRP78	NM_013083.2	GTT CTG CTT GAT GTG TGT CC	1424	349	(1)
		TTT GGT CAT TGG TGA TGG TG	1772		
XBP1	NM_001004210.1	GAG TCC AAG GGG AAT GGA GT	435	196	(4)
		ACA GGG TCC AAC TTG TCC AG	630		
CHOP	NM_024134.2	TTG GGG GCA CCT ATA TCT CA	219	263	(1)
		CTC CTT CAT GCG CTG TTT CC	481		
BAX	NM_017059.2	AAA GTG CCC GAG CTG ATC A	471	153	(5)
		AGC CAC AAA GAT GGT CAC TGT CT	623		
Bcl-XL	NM_001033672.1	AAT GAA CTC TTT CGG GAT GGG	717	126	(5)
		CCA ACT TGC AAT CCG ACT CA	842		

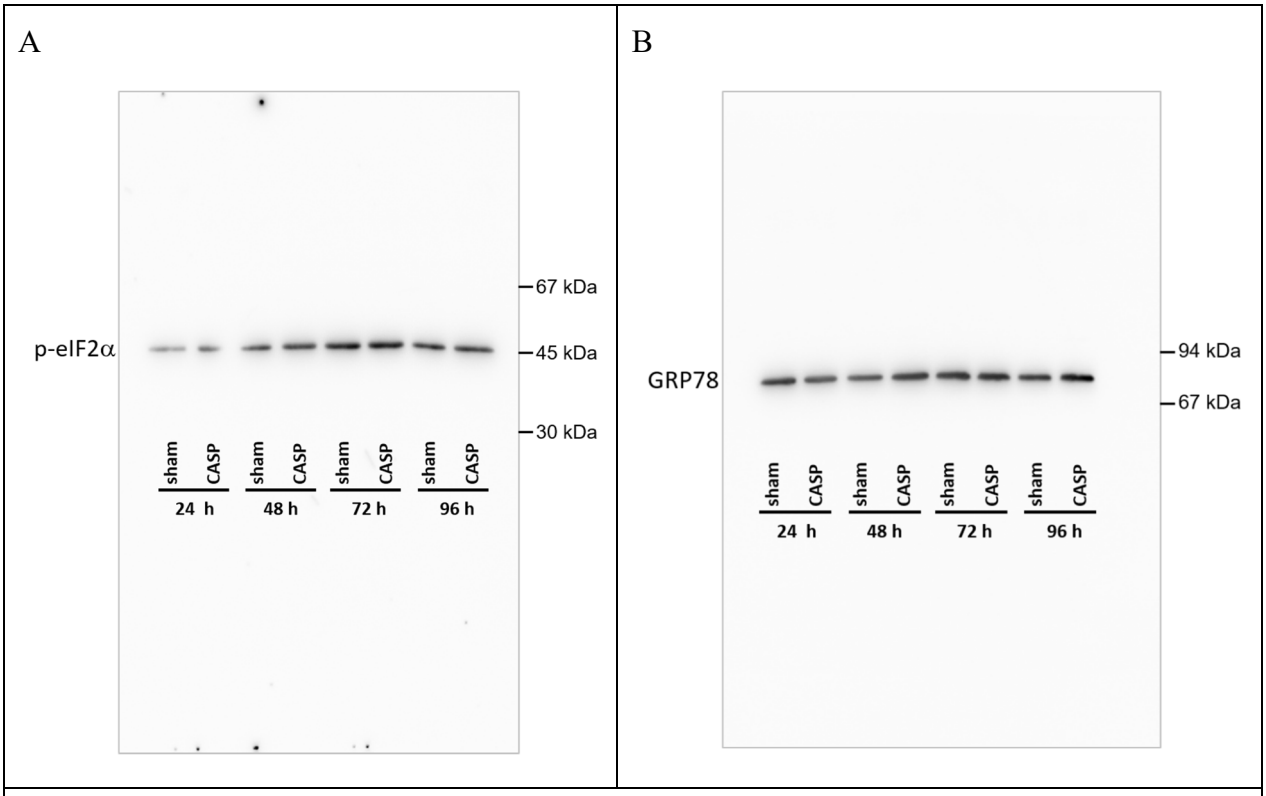

Supplementary Figure 1: p-eIF2α and GRP78 protein abundance in liver homogenates after sham or CASP surgery. Liver homogenates were analyzed by SDS-PAGE and immunostained for p-eIF2α or GRP78. Exemplary whole blots of p-eIF2α (A) and GRP78 (B) staining are shown.

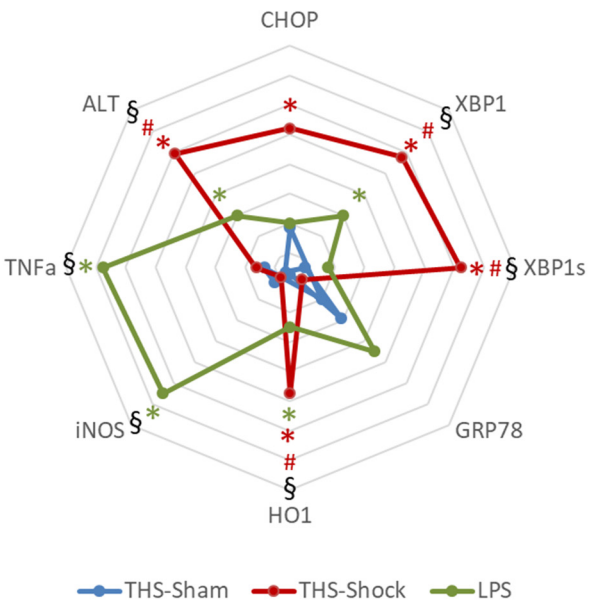

Supplementary Figure 2: Hepatic UPR is associated primarily with organ damage, rather than with induction of inflammatory response. Radar chart showing mean ranks of normalized values from rats subjected to an inflammatory stimulus (LPS *i.v.* 2 h, n=7, green line) or tissue damage (traumatic/hemorrhagic shock, THS-Shock, 2 h after onset of hemorrhage, n=8, red line), and the respective sham control (THS-Sham, n=8, blue line) for visualizing predominating type of response. Values were calculated from data sets of previous studies, in which experimental details can be found (5,6). Values for plasma levels of organ damage marker (ALT) and mRNA expression levels of ER stress (CHOP, GRP78, XBP1, XBP1s), inflammatory (iNOS, TNF-α) and general cell stress (HO-1) response markers were normalized for allowing comparison and ranking as is described beneath in the methods to supplementary figure 2. Higher mean group ranks indicate higher differences to the untreated control animals (n=7/8). For indicating significant differences to the respective control groups normalized data were used and Kruskal Wallis, followed by Dunn test was performed (*, $p<0.05$, relative to untreated control; #, $p<0.05$, relative to THS-Sham). Differences between THS and LPS group were calculated with ranked values using non-parametric Wilcoxon test (IBM SPSS Statistics 27), and are indicated (§, $p<0.05$ significant differences between).

Methods to supplementary figure 2:

Association of UPR and inflammatory response with liver damage and induction of inflammatory response in comparable *in-vivo* models

Two data sets from previously published studies (5,6) were reanalysed. Data were obtained from a study using an endotoxic shock model, 2 h after injection of LPS (6 mg/kg, *i.v.*; n = 6/7) reflecting immediate response to an infectious/inflammatory stimulus. Details regarding the groups' description and the experimental approach can be found elsewhere (6). The second data set was taken from a study using an experimental model of traumatic/hemorrhagic shock (THS) consisting of surgery and severe haemorrhage followed by inadequate volume resuscitation corresponding to a time point of 2h after onset of haemorrhage and includes THS (n=8) and sham (n=8) animals. Details regarding the groups' description and the experimental approach can be

found elsewhere (5). In both studies a group of corresponding untreated control animals were included for comparison and levels for organ damage (plasma ALT), as well as hepatic ER stress response (CHOP, GRP78, XBP1 and XBP1s mRNA), inflammatory response (iNOS, TNF-α mRNA) and general cell stress response (HO-1 mRNA) levels were recorded.

For allowing direct comparison, the two data sets were normalized, using respective untreated control values as reference. From this group the median was calculated and all data were expressed relative to the median of the reference animals. To calculate differences between groups normalized data were used and Kruskal-Wallis, followed by Dunn test (GraphPad Prism v6.01; GraphPad Software, Inc., La Jolla, CA, USA) was applied. To enable visualization of the elicited effects independently of the magnitude, the normalized values of the experimental animals (THS, sham, LPS) were ranked in increasing order according to their effect size and mean group ranks were calculated. Statistical differences between mean ranks of LPS and THS-Shock group were calculated using non-parametric Wilcoxon test (IBM SPSS Statistics 27; IBM, New York, USA).

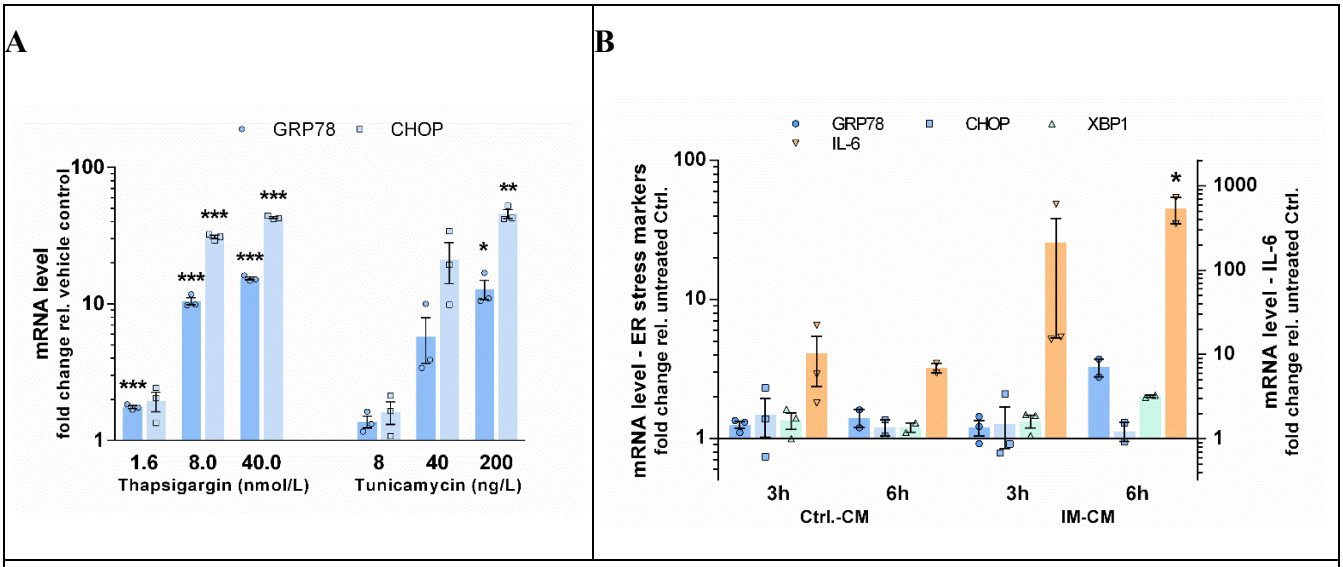

Supplementary Figure 3: Effect of ER stressors and inflammatory mediators (IM) on expression of ER stress markers in immortalized rat liver cells. BRL3A cells were incubated with (A) classical ER stressors or (B) conditioned medium (CM), which was generated using white blood cells treated without (Ctrl.-CM) or with LPS to elicit production of inflammatory mediators (IM-CM) as described beneath in the methods to supplementary figure 3. Levels of mRNA were calculated relative to vehicle (A) or untreated (B) controls. Data are shown as mean +/-SEM (n=2/3). Levels of UPR marker mRNA (GRP78, CHOP, XBP1) are presented on primary, IL-6 mRNA levels on the secondary Y-axis in B. Significant differences were calculated relative to vehicle (A) or untreated (B) control (Student's t-test, paired, 2 sided; *, $p<0.05$; **, $p<0.01$; ***, $p<0.005$).

Methods to supplementary figure 3:

Cell culture

Adherently growing cells from buffalo rat liver 3A cell line (BRL3A, ECACC) were cultivated in Coon's F-12 medium with 5% fetal calf serum (PAA). For the experiments, cells were grown in six-well plates until reaching a confluency of 70–80%. BRL3A cells were incubated with different concentrations of thapsigargin (1.6, 8, 40 nmol/L), tunicamycin (8, 40, 200 ng/L) or vehicle (dimethyl sulfoxide) for 6 h and for 3 h or 6 h with RPMI-1640 medium (untreated control), control conditioned medium or inflammatory mediator containing conditioned medium. Thereafter, RNA was extracted, reverse transcribed and used for qPCR analyses, as described in Materials and Methods, Gene Expression Analyses.

Preparation of conditioned media

Medium containing inflammatory mediators was generated as described elsewhere (3). Briefly, conditioned medium was prepared from isolated rat white blood cells set at a density of 1×10^6 cells/mL. Cells were incubated for 24 h at 37°C with RPMI-1640 medium alone (Ctr.-CM) or supplemented with LPS (E. coli Serotype 026:B6, 6 µg/ml; IM-CM) to obtain control or inflammatory mediators containing medium, respectively. The cell suspension was centrifuged (10 min, 400×g, 4°C), the supernatants harvested and stored at −80°C until being used. Inflammatory cytokines were determined by Myriad RBMTM (Austin, TX, USA), and were exclusively present in the inflammatory mediators containing medium (IFNγ, 4.6 pg/mL; IL-1α, 290 pg/mL; TNF-α, 0.6 pg/mL; MCP1, 1335 pg/mL).

References:

1. Kozlov A V., Catharina Duvigneau J, Hyatt TC, Raju R, Behling T, Hartl RT, Staniek K, Miller I, Gregor W, Redl H, et al. Effect of estrogen on mitochondrial function and intracellular stress markers in rat liver and kidney following trauma-hemorrhagic shock and prolonged hypotension. *Mol Med* (2010) **16**:254–261. doi:10.2119/molmed.2009.00184

2. Müllebner A, Moldzio R, Redl H, Kozlov A V., Duvigneau JC. Heme degradation by heme oxygenase protects mitochondria but induces ER stress via formed bilirubin. *Biomolecules* (2015) **5**:679–701. doi:10.3390/biom5020679

3. Weidinger A, Dungel P, Perlinger M, Singer K, Ghebes C, Duvigneau JC, Müllebner A, Schäfer U, Redl H, Kozlov A V. Experimental data suggesting that inflammation mediated rat liver mitochondrial dysfunction results from secondary hypoxia rather than from direct effects of inflammatory mediators. *Front Physiol* (2013) **4 JUN**:138. doi:10.3389/fphys.2013.00138

4. Müllebner A, Moldzio R, Redl H, Kozlov AV, Duvigneau JC. Heme degradation by heme oxygenase protects mitochondria but induces ER stress via formed bilirubin. *Biomolecules* (2015) **5**: doi:10.3390/biom5020679

5. Duvigneau JC, Kozlov A V., Zifko C, Postl A, Hartl RT, Miller I, Gille L, Staniek K, Moldzio R, Gregor W, et al. Reperfusion does not induce oxidative stress but sustained endoplasmic reticulum stress in livers of rats subjected to traumatic-hemorrhagic shock. *Shock* (2010) **33**:289–298. doi:10.1097/SHK.0b013e3181aef322

6. Nürnberger S, Miller I, Catharina Duvigneau J, Kavanagh ET, Gupta S, Hartl RT, Hori O, Gesslbauer B, Samali A, Kungl A, et al. Impairment of endoplasmic reticulum in liver as an early consequence of the systemic inflammatory response in rats. *Am J Physiol - Gastrointest Liver Physiol* (2012) **303**:1373–1383. doi:10.1152/ajpgi.00056.2012

2.2 Paper II: Heme Degradation by Heme Oxygenase Protects Mitochondria but Induces ER Stress via Formed Bilirubin.

Müllebner A, Moldzio R, Redl H, Kozlov AV, Duvigneau JC.

Biomolecules (2015), 5 (2): 679–701.

Biomolecules **2015**, *5*, 679-701; doi:10.3390/biom5020679

OPEN ACCESS

biomolecules

ISSN 2218-273X

www.mdpi.com/journal/biomolecules/

Article

Heme Degradation by Heme Oxygenase Protects Mitochondria but Induces ER Stress via Formed Bilirubin

Andrea Müllebner [1], Rudolf Moldzio [1], Heinz Redl [2], Andrey V. Kozlov [2] and J. Catharina Duvigneau [1,*]

[1] Institute for Medical Biochemistry, Veterinary University Vienna, Veterinaerplatz 1, 1210 Vienna, Austria; E-Mails: andrea.muellebner@vetmeduni.ac.at (A.M.); rudolf.moldzio@vetmeduni.ac.at (R.M.)

[2] Ludwig Boltzmann Institute for Experimental and Clinical Traumatology, Donaueschingenstraße 13, 1200 Vienna, Austria; E-Mails: office@trauma.lbg.ac.at (H.R.); andrey.kozlov@trauma.lbg.ac.at (A.V.K.)

* Author to whom correspondence should be addressed; E-Mail: catharina.duvigneau@vetmeduni.ac.at; Tel.: +43-1-25077-4201; Fax: +43-1-25077-4290.

Academic Editors: Michael Breitenbach and Peter Eckl

Received: 3 February 2015 / Accepted: 16 April 2015 / Published: 30 April 2015

Abstract: Heme oxygenase (HO), in conjunction with biliverdin reductase, degrades heme to carbon monoxide, ferrous iron and bilirubin (BR); the latter is a potent antioxidant. The induced isoform HO-1 has evoked intense research interest, especially because it manifests anti-inflammatory and anti-apoptotic effects relieving acute cell stress. The mechanisms by which HO mediates the described effects are not completely clear. However, the degradation of heme, a strong pro-oxidant, and the generation of BR are considered to play key roles. The aim of this study was to determine the effects of BR on vital functions of hepatocytes focusing on mitochondria and the endoplasmic reticulum (ER). The affinity of BR to proteins is a known challenge for its exact quantification. We consider two major consequences of this affinity, namely possible analytical errors in the determination of HO activity, and biological effects of BR due to direct interaction with protein function. In order to overcome analytical bias we applied a polynomial correction accounting for the loss of BR due to its adsorption to proteins. To identify potential intracellular targets of BR we used an *in vitro* approach involving hepatocytes and isolated mitochondria. After verification that the hepatocytes possess HO activity at a similar level as liver tissue by using our improved post-extraction spectroscopic assay, we elucidated the effects of increased HO activity and

the formed BR on mitochondrial function and the ER stress response. Our data show that BR may compromise cellular metabolism and proliferation via induction of ER stress. ER and mitochondria respond differently to elevated levels of BR and HO-activity. Mitochondria are susceptible to hemin, but active HO protects them against hemin-induced toxicity. BR at slightly elevated levels induces a stress response at the ER, resulting in a decreased proliferative and metabolic activity of hepatocytes. However, the proteins that are targeted by BR still have to be identified.

Keywords: heme oxygenase activity; bilirubin; hemin; endoplasmic reticulum; mitochondria

1. Introduction

Heme oxygenase (HO), residing at the endoplasmic reticulum membrane, is the rate-limiting enzyme in the degradation of heme, yielding equivalent amounts of carbon monoxide (CO), ferrous iron (Fe^{2+}), and biliverdin (BV). BV is subsequently reduced to bilirubin (BR) by the cytosolic BV reductase (BVR). Stressful conditions lead to an increase in HO activity due to induction of HO-1 [1], a member of the heat shock protein family (HSP32). Up-regulation of HO in the liver is caused by multiple stimuli that include cytokines, bacterial toxins, hypoxia, and increased amounts of the HO substrate, protoheme IX (heme). HO-1 was shown to mediate tissue protection, since its inhibition increased tissue injury, while tissues were protected when HO-1 was upregulated prior to an acute experimental insult [2]. The cytoprotective effects of HO-1 are partly attributed to the degradation of excessive free heme and partly to the generation of the heme degradation products CO and BR, which are able to mimic HO-1-mediated effects [3–5]. Although BR was found to exert anti-oxidant activity, which together with BV effectively protects the water/membrane interface [6,7], it is not clear to what extent BR formed in the HO reaction may contribute to the protection against heme-induced oxidative damage to subcellular structures.

Besides its relevance as diagnostic marker for liver diseases [8], BR was for a long time considered a waste product of heme degradation. However, elevated levels of unconjugated BR are able to induce cytotoxic effects, which are well documented for developing neuronal cells [9–12]. Free unconjugated BR was found to unbalance the redox homeostasis [13], or to affect the mitochondrial membrane integrity and to induce apoptosis [14]. The liver is one of the organs with a relatively high HO activity and involved in the elimination of BR. Thus, especially under conditions of elevated HO activity BR levels may exceed physiologic levels.

Determination of HO activity by means of BR quantification following the classical photometric extraction assay [15–17] is sensitive to higher protein concentrations making direct comparison between different sample types difficult. Thus, improvements of these assays should take the high affinity of lipophilic BR to proteins into account. Additionally, this affinity suggests that functional interaction with lipid and protein-rich structures, such as mitochondria or ER, are likely to occur. Increased levels of BR are formed during enhanced HO activity [5] and may target intracellular structures. However, it is not clear whether such an interaction would contribute to protective effects of the HO reaction or whether it may compromise cellular function and thereby limit the cytoprotective properties of the HO reaction.

In order to approach this topic we addressed the following questions using rat liver, cultured hepatocytes and isolated mitochondria as *in vitro* systems:

(1) How to account for the amount of BR that is adsorbed by protein and thus not considered when applying the classical photometric extraction assay for the determination of HO activity?
(2) Are the *in vitro* model systems suitable to investigate the effects of BR that is released following HO reaction?
(3) Does the HO reaction rescue hepatic mitochondria from hemin-mediated toxicity?
(4) Is the anti-oxidative property of BR involved in the protective effect of HO towards mitochondria?
(5) How does BR formation relate to the metabolic activity and the proliferative response of cultured hepatocytes under conditions of accelerated HO activity?
(6) Which subcellular structure in the hepatocyte is sensitive to increased levels of BR?

2. Aims of This Study

This study aimed at determining the potential limits of the protective range of the HO reaction in liver cells due to the formation of BR. In contrast to previous reports we focus this study more on the biological/analytical impact of the high affinity of BR to proteins in the liver. We consider two major consequences of the high affinity, namely errors in the determined quantity of BR as a measure for HO activity and the direct interaction of BR with mitochondria and ER. These effects were investigated using rat livers, cultured hepatocytes, and isolated mitochondria.

3. Results and Discussion

At increased protein concentrations the precise quantification of BR is a problem, because BR may adsorb to proteins, as known for albumin [18]. In the first part of the study we focused on the improvement of the HO assay, since determination of HO activity using BR quantification was compromised by higher protein concentrations [19].

3.1. Protein Adsorption of BR and Subsequent Interference with the Quantification Can Be Corrected Using a Polynomial that Accounts for the Protein Amount Present in the Assay

Quantification of BR, the end product from the HO/BVR reaction, is least laborious and therefore the most frequently used approach to determine HO activity [15,16]. BV and its reduction product BR are components exclusively formed by the HO/BVR system and generally tissue or cell homogenates possess sufficient BVR activity assuring the complete conversion of BV to BR and thus allowing the determination of BR by means of HPLC [20] or by photo spectroscopy [15,17].

Although extraction of BR from the aqueous phase into an organic solvent [17] significantly enhances the sensitivity of the assay, because BR is the only component absorbing around 450 nm in the organic extract, the load of unspecific protein has to be reduced, as it was shown to interfere with the assay [19]. Therefore generally microsomal-enriched fractions are prepared, which contain less protein [21]. However, the use of microsomal preparations bears the risk of partially losing HO activity. It was shown that pathogenic stimuli may induce translocation of HO-1 into the cell nucleus [22] or into

mitochondria [23]. This translocation increased the enzymatic activity to convert heme in the target compartment [23], while the activity in the microsomal fraction decreased [22].

The problem to correctly quantify BR can be solved in two ways. Either BR calibration curves are used, which contain the same amount of protein, as was the case in a recently presented study for the determination of BR by ELISA [24], or the effect of protein adsorption has to be considered using a mathematical approach. The latter has the advantage of circumventing the laborious and time-consuming preparation of appropriate calibration curves. However, both approaches allow an improved comparison of the capacities of cells or tissues to convert heme, since preparation steps that may introduce biases are reduced.

To quantify BR formed by the HO reaction we used calibration curves which we obtained by adding known amounts of BR to an equivalent amount of assay buffer followed by extraction into chloroform (Figure 1A). When adding protein the amount of BR extractable from the buffer decreased in a non-linear fashion (Figure 1B). At constant protein concentrations, however, the relation between input BR and extractable BR remained linear (Figure 1C). Therefore it was possible to develop a polynomial for calculating a correction factor f, which takes into account the adsorption of BR to protein, which is dependent on the amount x of protein.

The corrected BR amount is: $br_{corr} = br \times f$

br = BR concentration (calculated from the calibration curve using the differential OD)

$f = -0.076 \times x^2 + 0.704 \times x + 1.027$

x = protein content present in the assay in mg

Using this equation, we were able to achieve a nearly linear relationship between the amount of BR formed in the reaction and the amount of tissue homogenate subjected to the assay for determination of HO-activity (Figure 1D). The data presented in Figure 1 show that the high affinity of BR to proteins may result in underestimation of HO-activity, which can be corrected using the polynomial. In addition to improvement of the analytical procedure determining HO activity, this result stimulated us to explore the biological impact of a presumed interaction of BR with intracellular protein. Since BR is formed by the HO/BVR reaction within the cell, in close vicinity to the ER, we focused our studies on the effects of BR on mitochondria and ER, structures that are rich in protein and membrane lipids.

3.2. BRL3A Cells Have Similar HO Activities as Liver Tissue

We first verified the suitability of the hepatocyte line BRL3A regarding its HO activity, since we aimed at studying the effects of BR formed by the HO reaction in a cell culture model. In the liver different cell types contribute to the activity of HO, composed of the activity of both enzymes, HO-1 and HO-2. Under physiological conditions the determined HO activity nearly exclusively consists of the activity of HO-2, while an increase accounts for the induction of HO-1, which occurs in all liver cells to different degrees [25]. Since the amount of BR formed depends on the level of the HO activity, we first examined whether BRL3A cells would be able to convert heme at comparable rates as homogenized liver. Cells were cultured and treated with various amounts of hemin, that is protoporphyrin IX containing ferric iron, or vehicle for 16 h, and examined for HO activity as described in the Materials and Methods section (Figure 2). Basal levels of HO activity (Figure 2, grey bars) were similar to those

found in homogenates obtained from livers of control rats (dashed line in Figure 2). An incubation for 16 h with varying concentrations of hemin resulted in a dose dependent increase in HO activity, indicative for HO-1 induction (Figure 2, black bars).

These findings show that BRL3A cells are suitable to study the role of HO and the effects mediated by the products of heme degradation.

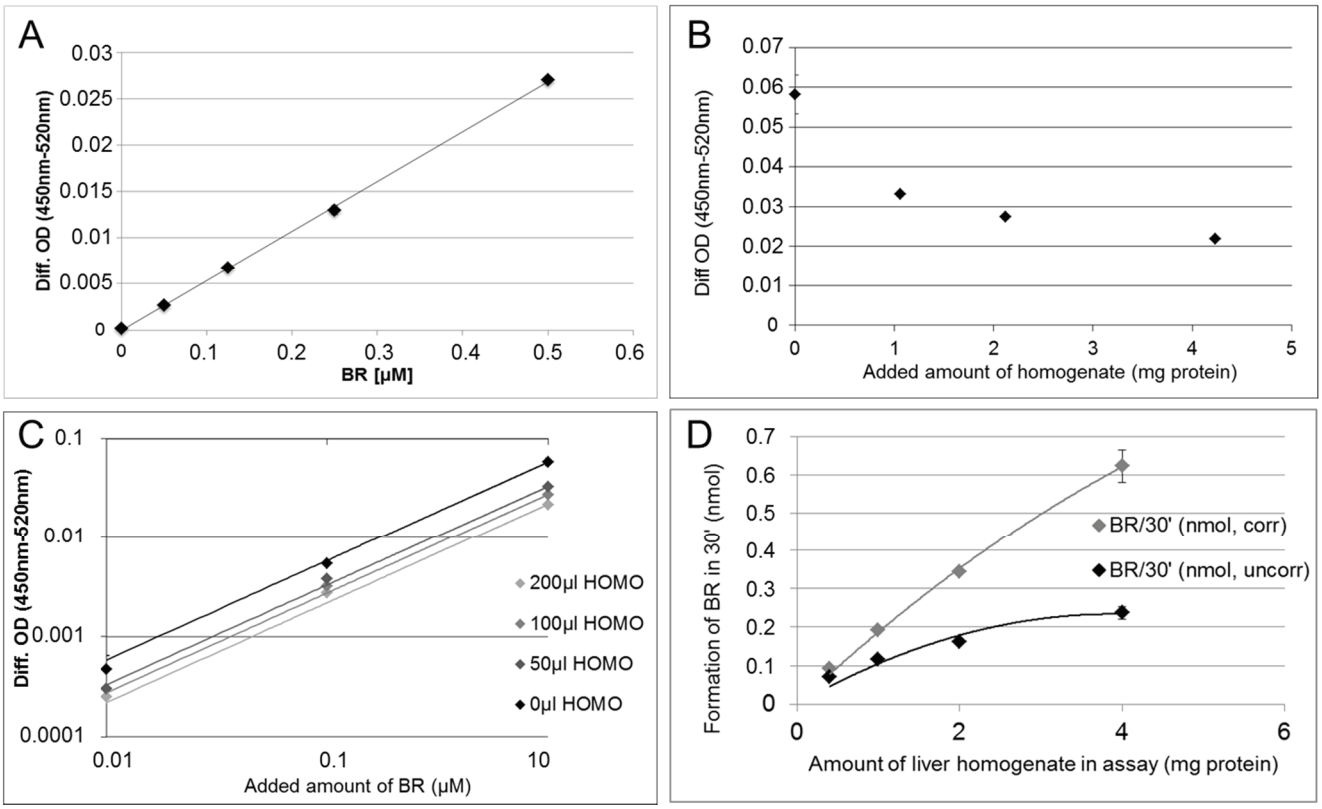

Figure 1. The tight interaction of BR with protein leads to underestimation of enzyme activities using the classical HO-assay. (**A**) Relationship between input and extractable amount of BR from HO-assay buffer (amount of BR was calculated using OD at 450 nm corrected for background OD at 520 nm (Diff. OD)) was linear (no protein added); (**B**) Presence of protein (liver homogenate: HOMO) in assay buffer supplemented with BR (1 µM) decreased the extractable amount of BR (Diff. OD); (**C**) Relationship between input and extractable amount of BR (0.01–1 µM) from HO-assay buffer (Diff. OD) was linear at constant protein concentration (added tissue homogenate (HOMO) with constant protein concentration of 10 mg protein/mL); (**D**) Using the polynomial for correcting the BR amount, the activity of HO (formation of BR/30 min) depended nearly linearly on the amount of liver homogenate used for the assay.

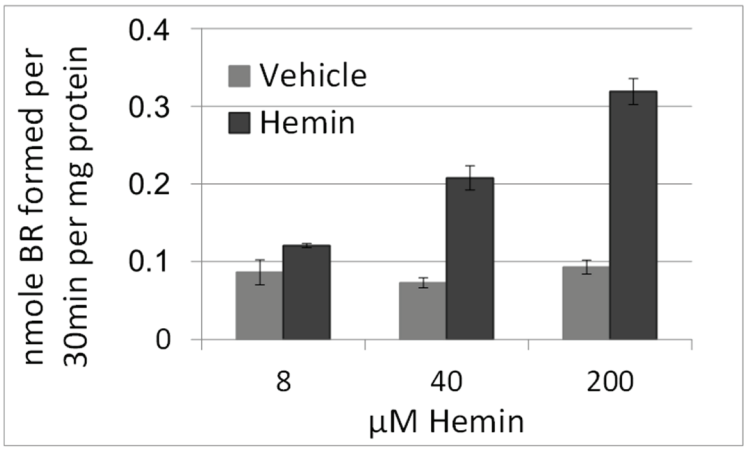

Figure 2. HO activity in hepatocytes after treatment with hemin. Cells were treated with vehicle (DMSO, grey bars) or hemin (8, 40, 200 µM, black bars) for 16 h. HO activity was determined in homogenized cells as described in the Materials and Methods section. The capacity to convert hemin increased in function to the concentration present in medium. HO activity, expressed as capacity of 1 mg cell protein to produce BR was similar to that obtained in the liver of control rats (n = 5, dashed line). Data are given as means (±SD) obtained from one experiment with n = 2 replicates.

3.3. HO Reaction Rescues Mitochondria from Hemin-Mediated Impairment of Respiration and Subsequent Fragmentation

We next questioned whether HO in BRL3A cells would protect mitochondria of BRL3A cells against hemin-induced toxicity via formed BR. It is known that mitochondria are particularly sensitive to increased intracellular levels of heme [26]. Although heme may reach much higher concentrations, we used levels that have been reported previously as the intracellular threshold for inducing heme toxicity [26].

Heme toxicity is based on the oxidative modification and consequent damage exerted to membranes and associated proteins when exceeding critical levels. Heme induces HO-1 by directly interacting with the heme-sensitive transcription factors BACH1 and BACH2 [27], resulting in its subsequent degradation by the up-regulated HO activity. HO may provide protection in two ways, either by consumption of heme or by the release of BR, exerting putative anti-oxidative properties, or by both. In the following experiments we examined the effect of HO on hemin-mediated impairment of mitochondrial function. BRL3A cells were treated with 20 µM hemin and mitochondria were visualized using JC-1 (Figure 3), as a measure for membrane potential (Figure 3A1–C1). Membrane potential initially decreased in cells treated with hemin, and this effect was most pronounced when its degradation was inhibited by zinc protoprophyrin IX (ZnIXPP), a competitive inhibitor of HO (Figure 3D). Continuous inhibition of hemin degradation resulted in an increased mitochondrial fragmentation (Figure 3C1). Cells treated with hemin or vehicle alone did not show any effects on their mitochondria (Figure 3A,B).

In order to rule out the possibility that the inhibitor itself may have caused mitochondrial dysfunction, we incubated isolated mitochondria with either hemin or ZnIXPP at various concentrations and examined respiration in terms of oxygen consumption (Figure 4).

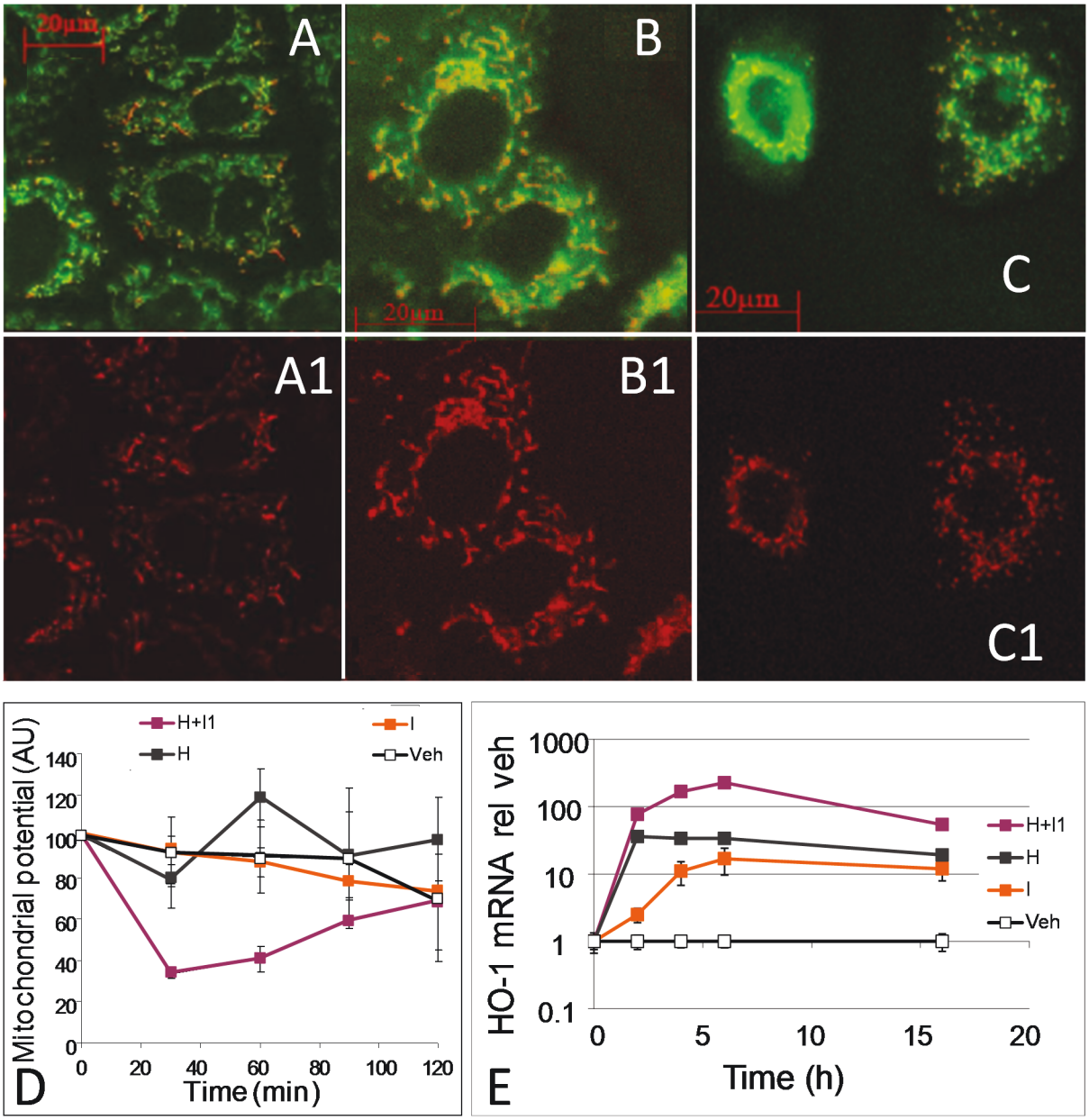

Figure 3. Effect of hemin and zinc protoprophyrin IX on mitochondrial function and morphology in hepatocytes. Liver cells (BRL3A) were incubated with JC-1 for 30 min, thereafter vehicle (DMSO, **A**) or hemin (20 µM); (**B**,**C**)) was added. Zinc protoporphyrin (ZnIXPP), a competitive inhibitor of HO (0.2 µM); was added 10 min before (**C**). Cells were analyzed after 2 h. **A1**, **B1** and **C1** show energized mitochondria (fluorescence at 590 nm). Competitive inhibition of HO by ZnIXPP resulted in delayed fragmentation of mitochondria (**C1**); (**D**) Effect of hemin (H, grey line), HO-inhibitor ZnIXPP (I, orange line), and hemin plus inhibitor (H+I1, violet line) in the concentrations indicated above on quantification of mitochondrial potential (intensity of background normalized JC-1 fluorescence (emission at 590 nm) was used as a parameter for mitochondrial potential); (**E**) Effect of hemin (H, grey line), HO-inhibitor ZnIXPP (I, orange line), and hemin plus inhibitor (H+I, violet line) in the concentrations indicated above on HO-1 mRNA expression in BRL3A cells determined by qPCR. Data are given as means (±SD) obtained from one representative experiment using $n = 4$ replicates.

We found that isolated liver mitochondria responded with a significant decrease of oxygen consumption at a concentration of 20 μM hemin (Figure 4), which is in line with our previous cell culture experiment. In contrast to hemin, ZnIXPP did not affect mitochondrial respiration, suggesting that iron ions play the principal role in the induction of mitochondrial dysfunction. Thus, our results show that functional HO in parenchymal liver cells protects mitochondria against hemin-mediated respiratory dysfunction. It is possible that the heme degradation products contribute to this effect, although initial levels present are presumably too low, as the levels of hemin are still high. However, longer incubation time may raise BR until reaching effective concentration.

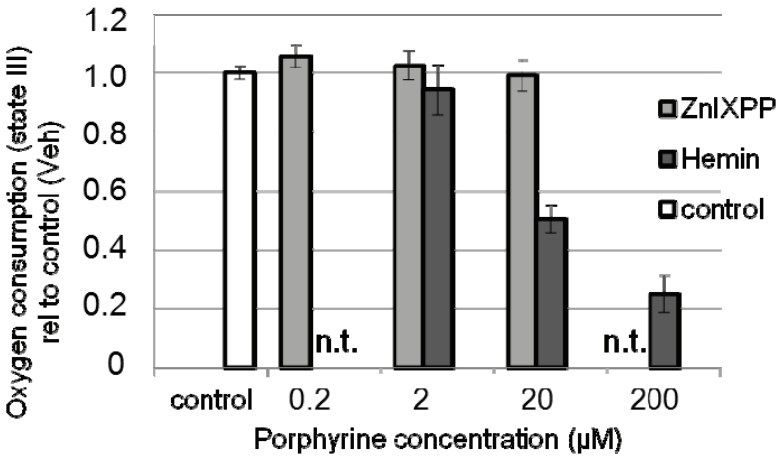

Figure 4. Hemin compromizes respiration of mitochondria. Isolated mitochondria were supplemented with succinate/rotenon to promote respiration of complex II. Transition to state III was induced by adding ADP and oxygen consumption was determined immediately after adding vehicle, hemin in the following concentrations: 2, 20 and 200 μM. In order to exclude effects of the HO inhibitor we also tested ZnIXPP (HO inhibitor) in the following concentrations: 0.2, 2 and 20 μM. Concentrations not tested are indicated (n.t.). State III respiration is indicated relative to the control (vehicle alone, set to 1). Data are given as means (±SD) obtained from one experiment with $n = 5$ replicates.

3.4. Bilirubin Does not Prevent Hemin-Induced Repression of Respiration in Liver Mitochondria

In order to understand whether BR is able to mediate the preservation of mitochondrial function seen in cells with functional HO, we used isolated mitochondria treated with hemin and BR simultaneously (Figure 5). As was shown before (Figures 3 and 4), a nearly immediate dose-dependent decrease of oxygen consumption occurred in mitochondria treated with increasing amounts of hemin. Addition of BR at physiological concentrations tended to further decrease mitochondrial respiration, however, without being significant. Additionally, BR was not able to restore the hemin-mediated depression of respiration (Figure 5). This suggests that in cells treated with hemin, the removal of heme by HO and not the release of BR, mediates the protection of mitochondria.

Interestingly, others showed that BR was able to modulate membrane integrity and redox status [14] of mitochondria, to modulate cytochrome c oxidase activity [28], and to induce apoptotic cell death, which involves mitochondrial pathways [14,29,30], without reporting on changes of respiratory parameters. Thus BR may target other cellular functions that are more sensitive to BR.

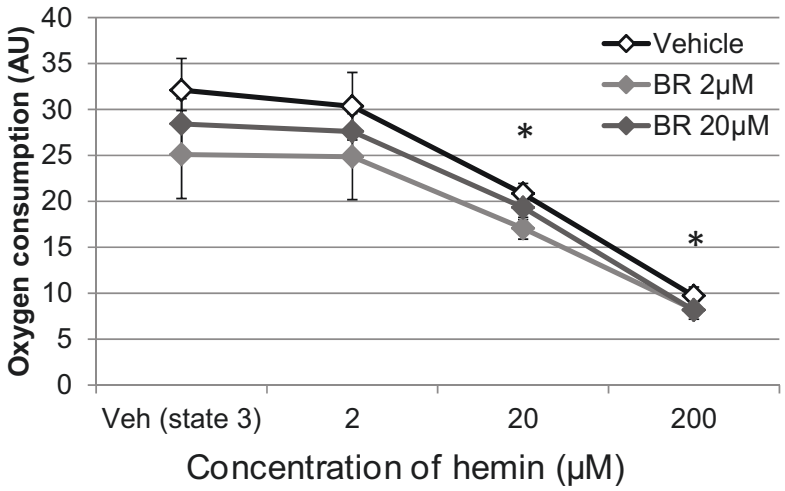

Figure 5. BR was not able to prevent hemin-mediated decrease of mitochondrial respiration. Liver mitochondria were isolated as described in the Materials and Methods section and treated with BR in the indicated concentration or with DMSO (Veh). State 3 respiration of complex II was induced by adding ADP and effects on oxygen consumption were determined after adding hemin in the indicated concentrations. Data are given as means (±SD), obtained from one experiment with $n = 2$ (control)/4 (BR) replicates, indicating significant differences (*) to the control (Veh state 3).

3.5. Formation of BR and Excretion to the Cell Culture Medium Is Accelerated in Response to hemin, but Decreases Cell Proliferation Rate

We next questioned how much BR is produced by BRL3A cells that are cultured in the presence of hemin, and whether an increased amount of BR extracted from the cell culture medium would reflect the underlying capacity to convert hemin determined *ex vivo* (see Figure 2). The presence of BR in the cell culture medium may represent an additional measure for HO activity *(in-situ* HO activity), provided that BR is not degraded. BR was extracted from medium and extracted into $CHCl_3$, and quantified by means of photo spectroscopy using calibration curves.

Cells treated with 20 μM hemin responded with increasing BR production, compared to control (Figure 6A). We next questioned whether BR production and excretion into the medium would reflect the HO activity determined *ex vivo*. If so, we would expect that an amount of 20 nmol hemin should be converted to 20 nmol BR by 1 mg BRL3A cell protein within 66 h. Considering a fully upregulated HO-1 (approximately within 12 h) we expected 1.6 nmole BR to be produced. However in the time period between 12 h and 24 h we were able to extract only 0.16 nmole BR per mg cell protein (Figure 6B). Although unbound BR may freely diffuse through cell membranes [31], once bound to albumin, a part will be redirected into hepatocytes via vesicular uptake [32]. Furthermore, it was shown that BR may be oxidized by cytochrome P450 2A [33,34], and a part of BR may have been conjugated. Therefore an unknown amount of BR has possibly escaped from quantification. Although the appearance of BR in the cell culture may not properly represent the underlying HO activity *in situ*, the data show that BR formation occurs much slower than expected. With increasing BR concentrations however, the proliferation of the producing cells slowed down, reaching only 80% of the cell number of the control, verified by estimation of the underlying cell number at each time point (Figure 6A, inset Y-axis).

Due to the tight interaction of BR it is possible, that the newly formed BR modulates cell function by binding to suitable proteins. Bilirubin was reported to inhibit proliferation in several cell types [35–37].

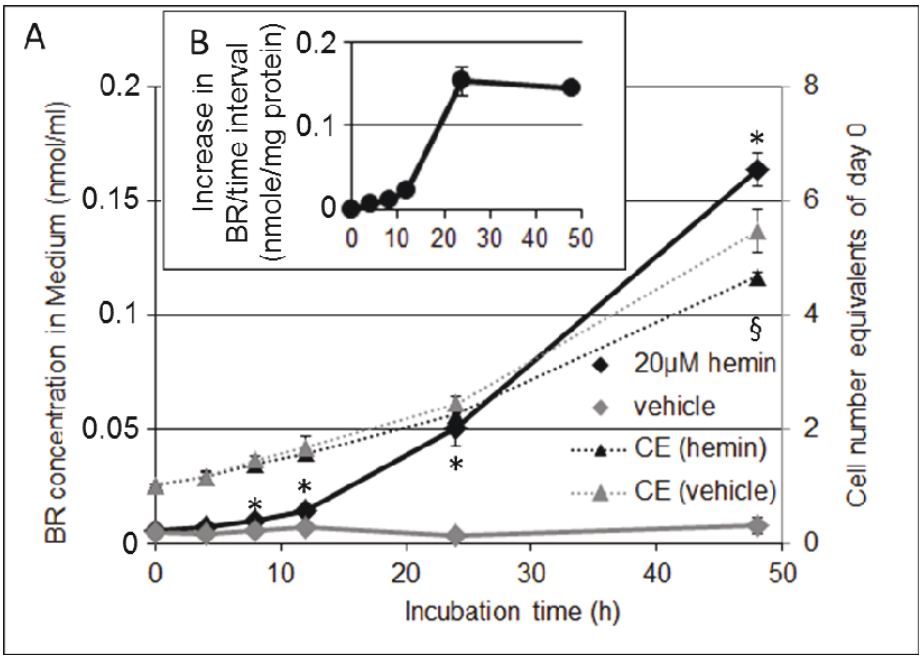

Figure 6. Production of BR by liver cells (BRL3A) as a function of the incubation time. (**A**) Cells were treated with vehicle (DMSO, grey symbols) or hemin (20 µM, black symbols) for the indicated time. BR was extracted from medium (diamonds; solid lines). Underlying cell number equivalents (CE, inset Y-axis) were determined (triangles) using crystal violet assay and expressed relative to the values of day 0 (dotted lines). After 48 h, equivalents of hemin-treated cells were significantly lower compared to the vehicle-control (§); (**B**) Hemin treatment increased the total amount of BR that was newly formed (nmole) per time interval when calculated per mg cell protein. Protein content of cell samples was determined at 48 h using the Bradford method and extrapolated from cell equivalents for each time point. Data are given as means (±SD), obtained from one experiment with $n = 4$ replicates.

To elucidate the role of BR in regulating proliferation of BRL3A cells we incubated cells with varying concentrations of unconjugated BR and determined cell number (crystal violet assay; [38–40]) and metabolic activity (MTT assay; [41]) at different time points (12 h and 48 h; Figure 7). Considering that an increase in HO would only slowly increase physiologic levels of BR, we used physiologic concentrations of BR, which range between 5 and 32 µM in human serum [42] and about half as much in rodents [43], of which around 4% appears as water-soluble glucuronides [44]. We found that physiologic levels of BR (4–20 µM) decreased the proliferation rate about 20%, but affected the metabolic activity to a much higher degree (50% activity after 48h at the highest BR concentration tested).

3.6. BR Increases Expression of Markers for ER Stress and Unfolded Protein Response

Decreased metabolic activity is frequently interpreted as a decrease in mitochondrial energy provision. However, also compromised ER function may lead to decreased cell proliferation rates, especially as a response to ER stressing agents [45].

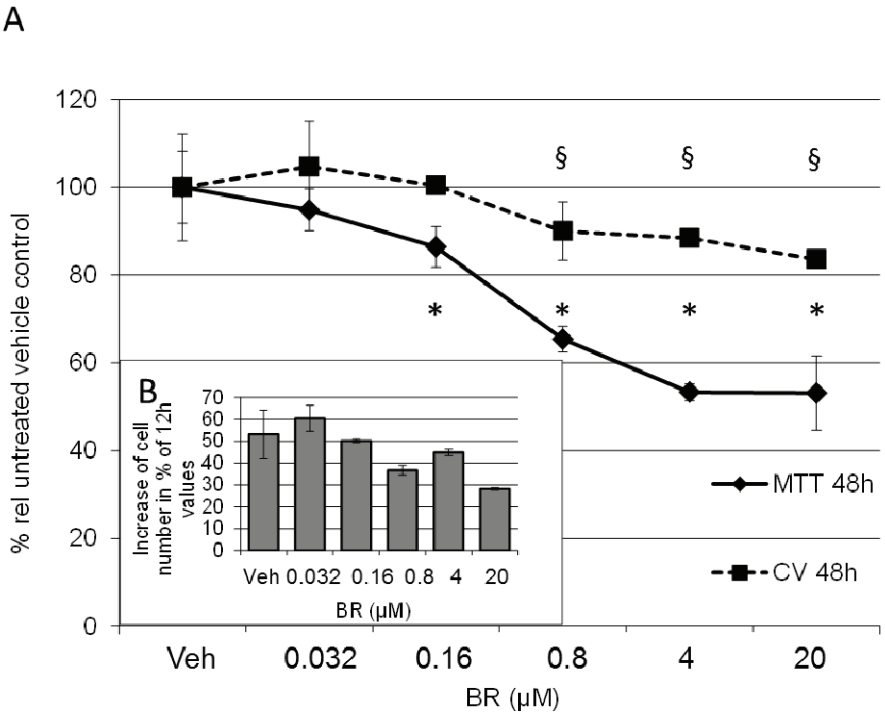

Figure 7. BR results in decreased proliferation and metabolic activity of BRL 3A cells. (**A**) Cells were treated with vehicle (Veh) or BR in the concentrations indicated, and incubated for 48 h. Cell number (squares and dotted line) was determined using crystal violet assay, and expressed in % relative to the vehicle control (CV 48 h). Data are given as means (±SD) obtained from two experiments with $n = 2$ replicates. Metabolic activity of treated cells was determined by MTT assay (diamonds and full line). Data are given as means (±SD) obtained from one experiment with $n = 4$ replicates (MTT 48 h). Significant differences to the control are indicated as (*, §); (**B**) Determination of cell numbers within one experiment at consecutive time points (12 h and 48 h) showed a decreased proliferation rate in the presence of BR. Data are given as % increase relative to the values determined at 12 h.

We have found that BR concentrations reduced the metabolic activity of BRL3A indicative for enhanced cell stress. It is known that induction of ER stress decelerates growth rate, involving sXBP1 [46] and promotes apoptosis via CHOP [47,48]. We therefore analyzed the expression of markers for ER stress, X-Box binding protein 1 (XBP1), glucose regulated protein 78 (GRP78) HO-1, CRBP homologous protein (CHOP), and interleukin 6 (IL6) as a marker for an inflammatory response, in BR-treated BRL3A cells. Already after 8 h at concentrations between 4 µM and 20 µM BR elicited an ER stress response (Figure 8), which was accompanied by elevated levels of the XBP1 splice variant, a typical ER-stress marker [49]. Additionally, we determined increased levels of IL6, suggesting onset of an inflammatory response, a pathologic reaction mediated by classical ER stressors [50]. Our data indicate that BR may affect proper function of ER. BR may induce protein mis-folding and aggregation due to its particular chemical properties. We showed that BR, which is newly formed in the HO reaction, tightly binds to proteins. At higher concentrations BR is known to lead to aggregates which are favored at lower pH [51]. Additionally, BR is able to associate with calcium [52], which is high in the ER lumen, and to precipitate with other amphiphilic compounds. This phenomenon is known to occur in the bile leading to the formation of pigmented gallstones containing calcium bilirubinate [53]. In neuronal cells, both

mitochondrial and ER function are sensitive to elevated concentrations of BR [54]. In parenchymal hepatocytes, in contrast, BR affects primarily the ER. If the concept remains valid that BR works as a potent anti-oxidant within the cell, an elevated level of BR is supposed to disturb the finely tuned redox equilibrium. However, it is well possible that under conditions of excessive oxidative stress BR would help to reinstall a disturbed equilibrium.

Thus, we cannot answer the question, whether the observed changes would be beneficial under pathologic conditions, or not. It was found, however, that treatment of obese mice with BR over a longer period, relieved signs of metabolic diseases [55]. Interestingly, in this pathologic model, markers for ER stress decreased. Further studies are needed to clarify the significance of BR-mediated interaction with the ER and the induction of a stress response.

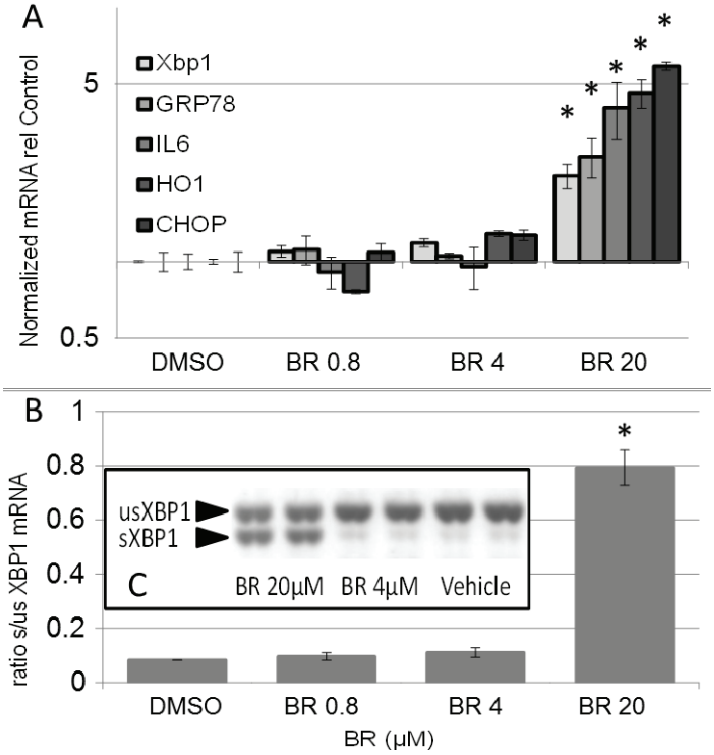

Figure 8. Physiologic range of BR induces ER stress response in BRL 3A cells. (**A**) Cells were treated with vehicle (DMSO) or BR in the concentrations indicated, and incubated for 8 h. RNA was extracted and expression of cell stress markers X-Box binding protein 1 (XBP1), glucose regulated protein 78 (GRP78), interleukin 6 (IL6), HO-1, CRBP homologous protein (CHOP) and the internal reference genes (cyclophilin A, hypoxanthine ribosyltransferase, glycerinaldehyde dehydrogenase) used for basket normalisation was determined by means of real-time PCR. Target mRNA was normalized to the internal references and calculated relative to the vehicle control (DMSO); (**B**) BR induced unconventional XBP1 splicing. PCR products were separated using electrophoresis and visualized by ethidium bromide staining. PCR products consisting of spliced (sXBP1) and unspliced variants (usXBP1) were quantified by means of densitometry using the public domain Scion Image program (http://www.scioncorp.com/), and intensities were expressed as a ratio (spliced to unspliced isoforms). Data are given as means (±SD) obtained from one experiment with $n = 2$ replicates, indicating significant differences (*).

4. Experimental Section

4.1. Chemicals

All reagents were obtained from Sigma-Aldrich (Vienna, Austria) unless otherwise noted. All porphyrins were dissolved in DMSO and used as a 500× stock solution.

4.2. Cell Culture

The adherently growing Buffalo rat liver cell line (BRL3A, European Collection of Cell Cultures, Salisbury, UK) was cultivated in Coon's F-12 medium with 5% FCS (PAA, Linz, Austria). At a confluency of 70%–80% cells were passaged using 0.25% trypsin/EDTA and diluted 1/10 for further culture. Maximal six consecutive passages were used.

4.3. Animals

Rats were injected with lipopolysaccharide (LPS) at a dose of 8 mg/kg (i.v.). Adult male Sprague-Dawley rats weighing 280 ± 21 g (Animal Research Laboratories, Himberg, Austria) were divided into two groups: a control group receiving saline i.v., and a group receiving 8 mg lipopolysaccharide/kg i.v. (LPS; *E. coli* 026:B6, Difco, Detroit, MI, USA). At different time points (0, 2, 4, 8, and 12 h (n = 3/6)), the animals were killed; liver tissue was taken for analytical examination, aliquoted and stored at −80 °C until analysis. All animals received humane care according to the criteria outlined in the "Guide for the Care and Use of Laboratory Animals" prepared by the National Academy of Sciences and published by the National Institutes of Health (NIH publication 86-23, revised 1985).

4.4. Determination of Cell Number by Crystal Violet Assay

BRL3A cells were seeded at a density of 5–10 × 10^4/mL in 24-wells using Coon's F-12 medium (5% FCS). The next day medium was exchanged for medium containing hemin (20 μM) or BR (0.032 μM, 0.16 μM, 0.8 μM, 4 μM, and 20 μM) or vehicle (DMSO). Cells were incubated for the given time points (4 h, 8 h, 12 h, 24 h and 48 h or 12 h and 48 h). Thereafter culture medium was removed, cells were washed 3× with PBS and fixed with 4% paraformaldehyde in PBS. After washing 3× with dH_2O cells were stained using crystal violet staining solution (0.5% in ethanol (10%)) and incubated for 15 min. Thereafter cells were washed three times, plates were dried, and kept in the dark until analysis. In each well 500 μL acetic acid (10%) was added. Stained cells were solubilized by pipetting. One hundred μL of the solution was transferred into a 96-well plate, and extinction at 590 nm was determined using a plate reader.

4.5. Determination of Metabolic Activity by MTT Assay

BRL3A cells were prepared as described above in Section 4.4. The next day medium was exchanged for medium containing BR (0.032 μM, 0.16 μM, 0.8 μM, 4 μM, and 20 μM) or vehicle (DMSO). Cells were incubated for 48 h. Six hour prior to the end of the experiment, medium was exchanged for MTT-containing medium (0.5 mg/mL) which was freshly prepared. Following a 6 h incubation period, supernatant was aspirated and formazan crystals were dissolved in sterile DMSO (same volume as the

culture medium) by incubating at 37 °C for 30 min. After shaking, 100 µL aliquots were transferred into 96-wells and the absorbance was read at 550 nm using a plate reader.

4.6. Cellular Heme Oxygenase Activity by Determination of BR Production in Medium

For determination of BR production, cells were plated in 6-well plates at a density of 5×10^4/mL. The next day medium was supplemented with 0.5% hemin solution (solved in DMSO) to a final concentration of 12.5 µg/mL (corresponding to 20 µM). At each time point (4 h, 8 h, 12 h, 24 h, and 48 h) an aliquot of 200 µL medium was removed and supplemented with 100 µL saturated KCl and 2 mL $CHCl_3$. After vortexing (3 × 30 s) and centrifugation (250× *g*) the organic phase was harvested, and bilirubin concentration was determined using photo spectroscopy (U-3000, Hitachi, Tokyo, Japan). The samples were repeatedly (3 times) scanned between 600 and 380 nm using the following settings: slit: 2 nm, 120 nm/min, PMT: autogain, high resolution, and the difference in absorption between 450 and 520 nm determined. Samples were run in triplicates and obtained values were averaged. Calculation of the formed bilirubin was obtained using a standard calibration curve. This standard was generated by adding known amounts of bilirubin to Coon's F12 medium supplemented with 5% FCS, followed by the subsequent extraction of bilirubin. HO activity was calculated as nmole bilirubin formed per ml per 30 min.

4.7. Laser Scanning Microscopy

BRL3A cells were grown in Lab-Tek two-chambered cover glasses (Nalge Nunc, Rochester, NY, USA) with cell culture medium (Coon's F-12 medium). For confocal microscopic investigations, cells were stained with JC-1 (2 µM MitoProbe, Invitrogen, Carlsbad, CA, USA). After 20 min, cells were treated with Zn(II) protoporphyrin IX (0.1; 1; 10 mg/L; Frontier Scientific, Logan, UT, USA). Subsequently hemin was added at a concentration of 12.5 mg/L. Control cells were treated with DMSO (vehicle control). Thereafter cells were washed with Coon's F-12 medium. Fluorescence of JC-1 at 590 nm was used as parameter for mitochondrial potential. Imaging was performed with an inverted confocal microscope (LSM 510, Zeiss, Oberkochen, Germany) and 63× oil immersion objective. Image analysis was performed with the histogram toolbar (LSM 510, Zeiss). Regions of interests were marked manually and total fluorescence intensity was defined as mean x area + area x threshold.

4.8. Gene Expression

RNA was isolated from BRL3A treated with BR (0.8 µM, 4 µM, 20 µM) for 8 h and processed as described elsewhere [56]. Primer sequences used for amplification are given in Table 1. Primer sequences for XBP-1 were newly designed (and amplification efficiency was verified by dilution series (accessory information is given in the Appendix Figure A1, Tables A1 and A2). Expression of target genes was measured using a CFX96™ (Bio-Rad, Hercules, CA, USA). Each reaction contained SYBR® green I as reporter (0.5×), iTaq™ polymerase™ (0.625 U/reaction; BioRad), the primers (250 nmol/L each, Invitrogen) with a final concentration of 200 µmol/L dNTP (each) and 3 mmol/L $MgCl_2$ in the provided reaction buffer with a final volume of 12 µL. Data were collected in the regression mode and calculated against an internal standard (IS) consisting of pooled cDNA samples of all experiments. We used a modified comparative ΔΔCq method. First the gene specific Cqs were subtracted from the mean Cq of

the IS obtained for the same gene giving rise to ΔCq. The values were then subtracted from the normalization factor, which was calculated by averaging the ΔCqs of the internal reference genes (cyclophilin A, hypoxanthinribosyl transferase, glycerinaldehyde dehydrogenase) of the same sample (ΔΔCq). The obtained ΔΔCq values of the replicates were averaged and expressed as $2^{-\Delta\Delta Cq}$ in fold changes relative to the IS.

Table 1. Primers used for analysis of gene expression by real-time PCR.

	Accession	Sense Primer	Antisense Primer	Source
XBP-1	NM_001004210.2	gag tcc aag ggg aat gga gt	aca ggg tcc aac ttg tcc ag	Designed for this study
GRP78	S63521	gtt ctg ctt gat gtg tgt cc	ttt ggt cat tgg tga tgg tg	[57]
IL6	NM_012589.1	ccg gag agg aga ctt cac ag	aca gtg cat cat cgc tgt tc	[58]
HO-1	NM_012580.2	cca gcc aca cag cac tac	gcg gtc tta gcc tct tct g	[59]
CHOP	NM_024134.2	ttg ggg gca cct ata tct ca	ctc ctt cag tcg ctg ttt cc	[60]
GAPDH	M17701	cat gcc gcc tgg aga aac ctg cca	tgg gct ggg tgg tcc agg ggt ttc	[61]
HPRT	NM_012583	ctc atg gac tga tta tgg aca gga c	gca ggt cag caa aga act tat agc c	[62]
Cyc	M19533	tat ctg cac tgc caa gac tga gtg	ctt ctt gct ggt ctt gcc att cc	[62]

4.9. Determination of Unconventional Splicing of XBP1

For the quantitative determination of the spliced variant of XBP-1 mRNA, 10 μL from the PCR reaction product were separated on a 2% agarose gel and after staining with ethidium bromide visualized by 300 nm UV transillumination. Density of both products, the unspliced and the spliced variant, was quantified via computer assisted densitometric scanning using the public domain Scion Image program (http://www.scioncorp.com/), and the ratio of the spliced to the unspliced variant was determined in each sample.

4.10. Heme Oxygenase Activity of Liver Tissue

Liver tissue was homogenized 1:10 (gram tissue/mL buffer) in a buffer containing 300 mM sucrose, 20 mM TRIS and 2 mM EDTA at a pH of 7.4. Approximately 1 mg of protein was added to a reaction mixture containing 500 nmole NADPH in a 100 mM potassium phosphate buffer with 1 mM EDTA (pH: 7.4), supplemented by 20 nmoles of hemin. The mixture was incubated under constant agitation in darkness for 30 min at 37 °C. Afterwards, the reaction was stopped by transferring the samples on ice. After addition of 1/5 volume of saturated KCl, the formed bilirubin was extracted into chloroform (4× the assay volume). Samples were then processed as described in Section 4.6. Samples were run in duplicates and obtained values were averaged and corrected for the absorption measured in corresponding samples incubated at 0 °C. Calculation of the formed bilirubin was obtained using a standard calibration curve. This standard was generated by adding known amounts of bilirubin to a pool of tissue homogenate followed by the subsequent extraction of bilirubin. Protein concentration of liver homogenate was determined using Coomassie Brilliant Blue [63]. HO activity was corrected for the BR lost due to adsorption by proteins using the correction factor described in Section 3.1 and calculated as nmole bilirubin formed per mg protein per 30 min.

4.11. Heme Oxygenase Activity of BRL3A Cells

BRL3A cells were seeded at a density of 5–10 × 10^4/mL in 6-well plates using Coon's F-12 medium (5% FCS). The next day medium was exchanged for medium containing hemin (20 μM) or vehicle (DMSO). Cells were incubated for 16 h. Medium was discarded, cell layer was washed once with prewarmed PBS and the cells were detached by adding 800 μL of 0.25% trypsin/EDTA. After complete detachment cell suspension of each well was transferred into 5 mL vials containing 4 ml culture medium to stop the trypsin activity. Cells were gently pelleted (400× *g*, RT) (10 min) and supernatant was aspirated. The tube was then placed in liquid nitrogen to snap freeze and stored at −80 °C until being used. For the determination of HO activity, the cell pellet was quickly unfrozen and dissolved in 60 μL buffer containing 300 mM sucrose, 20 mM TRIS and 2 mM EDTA at a pH of 7.4. Approximately 0.3 mg of protein (50 μL) was added to a reaction mixture containing 500 nmole NADPH in a 100 mM potassium phosphate buffer with 1 mM EDTA (assay buffer, pH 7.4), supplemented by 20 nmoles of hemin. The mixture was incubated under constant agitation in darkness for 30 min at 37 °C. Afterwards, the reaction was stopped by transferring the samples on ice. After addition of 1/5 volume of saturated KCl, the formed bilirubin was extracted into chloroform (4× the assay volume). Samples were then processed as described in Section 4.6. Samples were run in duplicates and obtained values were averaged and corrected for the absorption measured in solvent alone. Calculation of the formed bilirubin was obtained using regression analysis of standard calibration curves. These standards were generated by adding known amounts of bilirubin to assay buffer followed by the subsequent extraction of bilirubin. Protein concentration of liver homogenate was determined using Coomassie Brilliant Blue [63]. HO activity was corrected for the BR lost due to adsorption by proteins using the correction factor described in Section 3.1 and calculated as nmole bilirubin formed per mg protein per 30 min.

4.12. Preparation of Liver Mitochondria

Sprague-Dawley rats weighing 280 ± 21 g (Animal Research Laboratories, Himberg, Austria) were euthanized by decapitation. The protocol was approved by the City Government of Vienna, Austria, and all experiments were performed under the conditions described in the Guide for the Care and Use of Laboratory Animals of the National Institutes of Health. Immediately after decapitation, liver was extracted and placed in ice-cold sucrose buffer (0.25 M sucrose, 10 mM Tris-HCl, 1 mM EDTA, 0.1% ethanol, pH = 7.4), diced and rinsed with the same buffer to remove remaining blood. After blotting dry with paper, the liver pieces were weighed and the same buffer was added in a ratio of 1:6 liver/buffer (w/v) and homogenized using a Potter-Elvehjem homogenizer. Rat liver mitochondria (RLM) were prepared as described previously [64] and stored at 0 °C for 4–5 h in a buffer containing 0.25 M sucrose, 10 mM TRIS-HCl, 0.5 mM EDTA (pH 7.2), and 0.5 g/L essentially fatty-acid-free bovine serum albumin.

4.13. Hepatic Mitochondrial Function

Respiratory parameters of mitochondria isolated from control and LPS-treated rats were determined with a Clark-type oxygen electrode (OROBOROS Ltd, Innsbruck, Austria). Rat liver mitochondria (0.5 mg/mL) were incubated in a buffer consisting of 105 mM·KCl, 20 mM TRIS-HCl, 1 mM diethylenetriaminepentaacetic acid, 5 mM·KH_2PO_4, and 1 mg/mL fatty acid-free bovine serum albumin

(pH 7.4, 25 °C). Respiration was stimulated by the addition of 10 mM succinate in the presence of rotenone (1 μg/mL; complex II). The transition to state 3 respiration was induced by addition of 200 μM ADP and used as parameter for ATP synthesis.

4.14. Data Analysis and Statistics

Data processing and graphics were made using Excel or SPSS 15 (SPSS Inc., Chicago, IL, USA). Data from experiments performed with cells and isolated mitochondria were analyzed by one-way ANOVA followed by LSD post hoc test using SPSS. Data from experiments using liver tissues obtained from animals were subjected to non-parametric analysis using Kruskal-Wallis. Differences to the control were considered significant when $p < 0.05$, and are indicated. The numbers of independent samples (n) are indicated in figure legends.

5. Conclusions

We found that HO activity can be determined in each type of sample by the modified photometric extraction assay when the adsorption of BR to protein is accounted for. Additionally this shows that BR that is newly formed by the HO reaction may tightly adsorb to intracellular protein, and thereby modulate the function of sensitive target structures. We found that HO protected mitochondria from hemin-induced toxicity. BR at concentrations that were only slightly higher than the physiological concentrations was capable of inhibiting cell metabolism and proliferation and inducing a stress response at the ER. In BRL3A cells the primary target modulated by BR was the ER, which indicates that HO may modulate ER function *via* newly formed BR.

Acknowledgments

The authors thank Annika Cronstedt-Fell, Jasmin Weeger, and Carmen Konzett for skilled assistance in performing and analyzing cell culture experiments. The technical support of Susanne Haindl, performing the experiments with isolated mitochondria, is greatly acknowledged. The study was supported by FWF (Austria, project P211221-B11 assigned to Andrey V. Kozlov).

Author Contributions

Andrea Müllebner planned the experiments, performed qPCR experiments, analyzed data, wrote first version and revised the manuscript. Rudolf Moldzio performed viability assays and analyzed the data. Heinz Redl designed part of the study and supervised the animal experiments. Andrey V. Kozlov and J. Catharina Duvigneau designed the study, performed experiments with mitochondria, optimized the assay for the determination of the heme oxygenase activity and contributed to the writing and editing of the manuscript.

Abbreviations

BR	Bilirubin
BV	Biliverdin
Diff. OD	background corrected optical density

Appendix

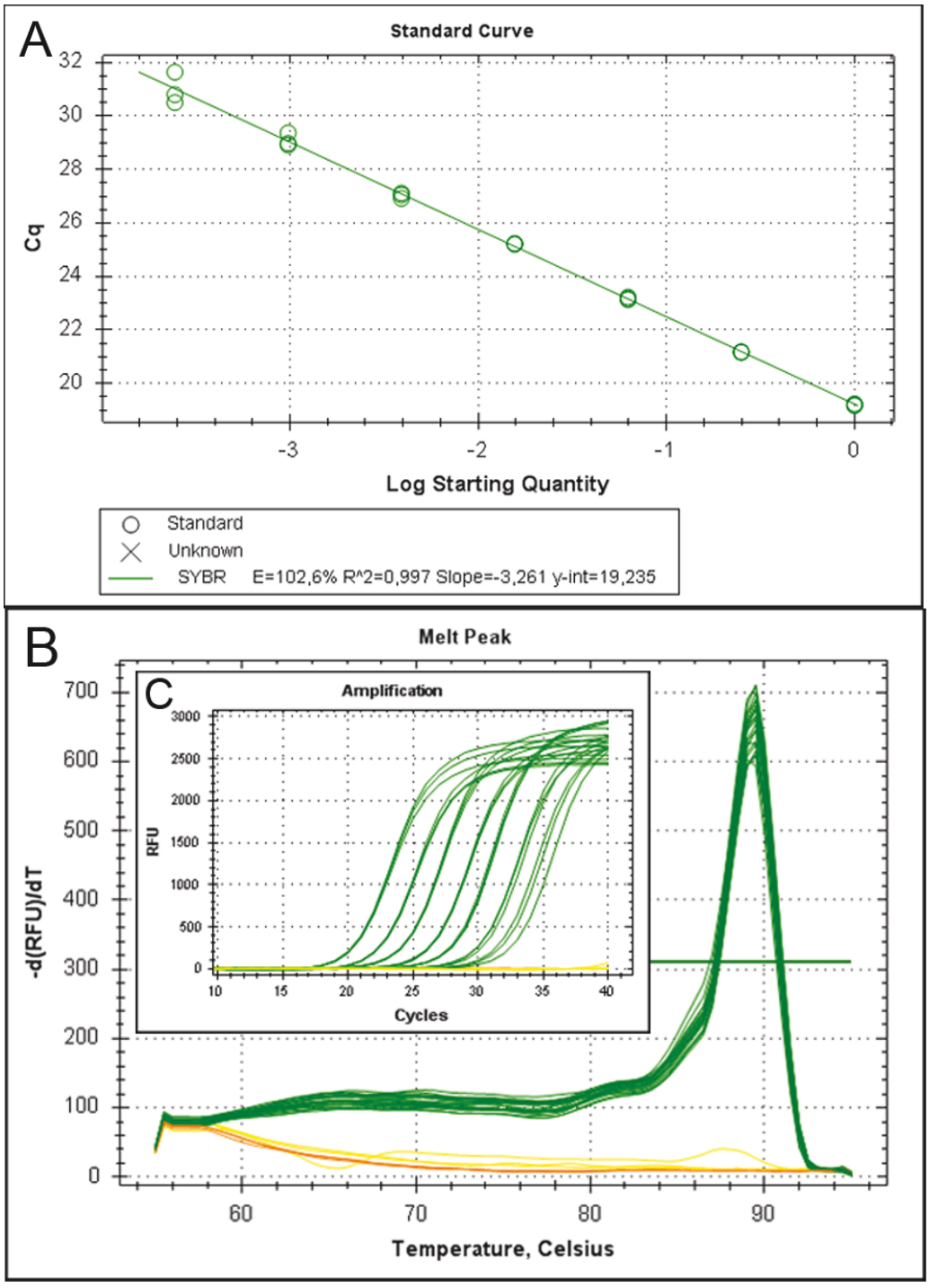

Figure A1. The suitability of the newly designed primers was verified in separate experiments by performing dilution series using the PCR products (Table A2) as well as dilution series of a cDNA pool (**A**). In melt curve (**B**) and amplification plots (**B**) samples are shown in green while controls (no reverse transcription control and no template control) are shown in yellow and orange respectively.

Table A1. Information about Intron-spanning primers.

Target	Accession number	Start on plus strand	Stop on plus strand	Product-length (bp)	Exon junctions in	Intron size (bp)
XBP-1, transcript variant 1, mRNA (usXBP-1)	NM_001004210.1	435	454	196	Forward Primer	~300
		630	611		Product	~740
XBP-1, transcript variant 2, mRNA (sXBP-1)	NM_001271731.1	454	473	170	Forward Primer	~300
		623	604		Product	~740

Table A2. Optimized protocol and validation studies using amplificate dilution series

Target	Annealing temp (°C)/time (sec)	Extension temp (°C)/time (sec)	ΔCt (RT+ to RT−)	slope	Correlation-Coefficient (Pearson) R^2	Verified dynamic range
XBP-1	65/30	72/20	not detected	−3.537	0.997	10^5

Conflicts of Interest

The authors declare no conflict of interest.

References

1. Alam, J.; Cook, J.L. Transcriptional regulation of the heme oxygenase-1 gene via the stress response element pathway. *Curr. Pharm. Des.* **2003**, *9*, 2499–2511.
2. Kubulus, D.; Mathes, A.; Pradarutti, S.; Raddatz, A.; Heiser, J.; Pavlidis, D.; Wolf, B.; Bauer, I.; Rensing, H. Hemin arginate-induced heme oxygenase 1 expression improves liver microcirculation and mediates an anti-inflammatory cytokine response after hemorrhagic shock. *Shock* **2008**, *29*, 583–590.
3. Wang, W.W.; Smith, D.L.; Zucker, S.D. Bilirubin inhibits iNOS expression and NO production in response to endotoxin in rats. *Hepatology* **2004**, *40*, 424–433.
4. Yamaguchi, T.; Horio, F.; Hashizume, T.; Tanaka, M.; Ikeda, S.; Kakinuma, A.; Nakajima, H. Bilirubin is oxidized in rats treated with endotoxin and acts as a physiological antioxidant synergistically with ascorbic acid *in vivo*. *Biochem. Biophys. Res. Commun.* **1995**, *214*, 11–19.
5. Zelenka, J.; Muchova, L.; Zelenkova, M.; Vanova, K.; Vreman, H.J.; Wong, R.J.; Vitek, L. Intracellular accumulation of bilirubin as a defense mechanism against increased oxidative stress. *Biochimie* **2012**, *94*, 1821–1827.
6. Jansen, T.; Hortmann, M.; Oelze, M.; Opitz, B.; Steven, S.; Schell, R.; Knorr, M.; Karbach, S.; Schuhmacher, S.; Wenzel, P.; *et al*. Conversion of biliverdin to bilirubin by biliverdin reductase contributes to endothelial cell protection by heme oxygenase-1-evidence for direct and indirect antioxidant actions of bilirubin. *J. Mol. Cell Cardiol.* **2010**, *49*, 186–195.
7. Stocker, R. Antioxidant activities of bile pigments. *Antioxid. Redox. Signal.* **2004**, *6*, 841–849.
8. Fevery, J. Bilirubin in clinical practice: A review. *Liver Int.* **2008**, *28*, 592–605.
9. Amit, Y.; Boneh, A. Bilirubin inhibits protein kinase C activity and protein kinase C-mediated phosphorylation of endogenous substrates in human skin fibroblasts. *Clin. Chim. Acta* **1993**, *223*, 103–111.

10. Chuniaud, L.; Dessante, M.; Chantoux, F.; Blondeau, J.P.; Francon, J.; Trivin, F. Cytotoxicity of bilirubin for human fibroblasts and rat astrocytes in culture. Effect of the ratio of bilirubin to serum albumin. *Clin. Chim. Acta* **1996**, *256*, 103–114.
11. Fernandes, A.; Falcao, A.S.; Silva, R.F.; Gordo, A.C.; Gama, M.J.; Brito, M.A.; Brites, D. Inflammatory signalling pathways involved in astroglial activation by unconjugated bilirubin. *J. Neurochem.* **2006**, *96*, 1667–1679.
12. Vitek, L.; Ostrow, J.D. Bilirubin chemistry and metabolism; harmful and protective aspects. *Curr. Pharm. Des.* **2009**, *15*, 2869–2883.
13. Qaisiya, M.; Coda Zabetta, C.D.; Bellarosa, C.; Tiribelli, C. Bilirubin mediated oxidative stress involves antioxidant response activation via Nrf2 pathway. *Cell Signal.* **2014**, *26*, 512–520.
14. Rodrigues, C.M.; Sola, S.; Brites, D. Bilirubin induces apoptosis via the mitochondrial pathway in developing rat brain neurons. *Hepatology* **2002**, *35*, 1186–1195.
15. McCoubrey, W.K., Jr. Detection of heme oxygenase 1 and 2 proteins and bilirubin formation. *Curr. Protoc. Toxicol.* **2001**, doi:10.1002/0471140856.tx0903s00.
16. Sunderman, F.W., Jr.; Downs, J.R.; Reid, M.C.; Bibeau, L.M. Gas-chromatographic assay for heme oxygenase activity. *Clin. Chem.* **1982**, *28*, 2026–2032.
17. Tenhunen, R. Method for microassay of microsomal heme oxygenase activity. *Anal. Biochem.* **1972**, *45*, 600–607.
18. Novak, M.; Polacek, K.; Melichar, V. Competition between bilirubin and non-esterified fatty acids for binding to albumin. *Biol. Neonat.* **1962**, *4*, 310–315.
19. McNally, S.J.; Ross, J.A.; James, G.O.; Wigmore, S.J. Optimization of the paired enzyme assay for heme oxygenase activity. *Anal. Biochem.* **2004**, *332*, 398–400.
20. Ryter, S.W.; Tyrrell, R.M. An HPLC method to detect heme oxygenase activity. *Curr. Protoc. Toxicol.* **2001**, doi:10.1002/0471140856.tx0906s05.
21. Vreman, H.J.; Stevenson, D.K. Heme oxygenase activity as measured by carbon monoxide production. *Anal. Biochem.* **1988**, *168*, 31–38.
22. Lin, Q.; Weis, S.; Yang, G.; Weng, Y.H.; Helston, R.; Rish, K.; Smith, A.; Bordner, J.; Polte, T.; Gaunitz, F.; *et al*. Heme oxygenase-1 protein localizes to the nucleus and activates transcription factors important in oxidative stress. *J. Biol. Chem.* **2007**, *282*, 20621–20633.
23. Converso, D.P.; Taille, C.; Carreras, M.C.; Jaitovich, A.; Poderoso, J.J.; Boczkowski, J. HO-1 is located in liver mitochondria and modulates mitochondrial heme content and metabolism. *FASEB J.* **2006**, *20*, 1236–1238.
24. Rucker, H.; Amslinger, S. Identification of heme oxygenase-1 stimulators by a convenient ELISA-based bilirubin quantification assay. *Free Radic. Biol. Med.* **2015**, *78*, 135–146.
25. Bauer, I.; Wanner, G.A.; Rensing, H.; Alte, C.; Miescher, E.A.; Wolf, B.; Pannen, B.H.; Clemens, M.G.; Bauer, M. Expression pattern of heme oxygenase isoenzymes 1 and 2 in normal and stress-exposed rat liver. *Hepatology* **1998**, *27*, 829–838.
26. Nath, K.A.; Grande, J.P.; Croatt, A.J.; Likely, S.; Hebbel, R.P.; Enright, H. Intracellular targets in heme protein-induced renal injury. *Kidney Int.* **1998**, *53*, 100–111.
27. Sun, J.; Hoshino, H.; Takaku, K.; Nakajima, O.; Muto, A.; Suzuki, H.; Tashiro, S.; Takahashi, S.; Shibahara, S.; Alam, J.; *et al*. Hemoprotein Bach1 regulates enhancer availability of heme oxygenase-1 gene. *EMBO J.* **2002**, *21*, 5216–5224.

28. Malik, S.G.; Irwanto, K.A.; Ostrow, J.D.; Tiribelli, C. Effect of bilirubin on cytochrome C oxidase activity of mitochondria from mouse brain and liver. *BMC Res. Notes* **2010**, doi:10.1186/1756-0500-3-162.
29. Keshavan, P.; Schwemberger, S.J.; Smith, D.L.; Babcock, G.F.; Zucker, S.D. Unconjugated bilirubin induces apoptosis in colon cancer cells by triggering mitochondrial depolarization. *Int. J. Cancer* **2004**, *112*, 433–445.
30. Paradisi, F.; Graziano, L. Mitochondrial swelling induced by unconjugated bilirubin *in vitro*. *Experientia* **1973**, *29*, 1376–1377.
31. Zucker, S.D.; Goessling, W.; Hoppin, A.G. Unconjugated bilirubin exhibits spontaneous diffusion through model lipid bilayers and native hepatocyte membranes. *J. Biol. Chem.* **1999**, *274*, 10852–10862.
32. Pascolo, L.; Del, V.S.; Koehler, R.K.; Bayon, J.E.; Webster, C.C.; Mukerjee, P.; Ostrow, J.D.; Tiribelli, C. Albumin binding of unconjugated [3H]bilirubin and its uptake by rat liver basolateral plasma membrane vesicles. *Biochem. J.* **1996**, *316*, 999–1004.
33. Bu-Bakar, A.; Arthur, D.M.; Aganovic, S.; Ng, J.C.; Lang, M.A. Inducible bilirubin oxidase: A novel function for the mouse cytochrome P450 2A5. *Toxicol. Appl. Pharmacol.* **2011**, *257*, 14–22.
34. De, M.F.; Lord, G.A.; Kee, L.C.; Pons, N. Bilirubin degradation by uncoupled cytochrome P450. Comparison with a chemical oxidation system and characterization of the products by high-performance liquid chromatography/electrospray ionization mass spectrometry. *Rapid Commun. Mass. Spectrom.* **2006**, *20*, 1209–1217.
35. Ollinger, R.; Bilban, M.; Erat, A.; Froio, A.; McDaid, J.; Tyagi, S.; Csizmadia, E.; Graca-Souza, A.V.; Liloia, A.; Soares, M.P.; *et al*. Bilirubin: A natural inhibitor of vascular smooth muscle cell proliferation. *Circulation* **2005**, *112*, 1030–1039.
36. Taille, C.; Almolki, A.; Benhamed, M.; Zedda, C.; Megret, J.; Berger, P.; Leseche, G.; Fadel, E.; Yamaguchi, T.; Marthan, R.; *et al*. Heme oxygenase inhibits human airway smooth muscle proliferation via a bilirubin-dependent modulation of ERK1/2 phosphorylation. *J. Biol. Chem.* **2003**, *278*, 27160–27168.
37. Tell, G.; Gustincich, S. Redox state, oxidative stress, and molecular mechanisms of protective and toxic effects of bilirubin on cells. *Curr. Pharm. Des.* **2009**, *15*, 2908–2914.
38. Gillies, R.J.; Didier, N.; Denton, M. Determination of cell number in monolayer cultures. *Anal. Biochem.* **1986**, *159*, 109–113.
39. Kueng, W.; Silber, E.; Eppenberger, U. Quantification of cells cultured on 96-well plates. *Anal. Biochem.* **1989**, *182*, 16–19.
40. Tremezaygues, L.; Seifert, M.; Tilgen, W.; Reichrath, J. 1,25-dihydroxyvitamin D_3 protects human keratinocytes against UV-B-induced damage: *In vitro* analysis of cell viability/proliferation, DNA-damage and -repair. *Dermatoendocrinology* **2009**, *1*, 239–245.
41. Edwards, V.; Markovic, E.; Matisons, J.; Young, F. Development of an *in vitro* reproductive screening assay for novel pharmaceutical compounds. *Biotechnol. Appl. Biochem.* **2008**, *51*, 63–71.
42. Berk, P.D.; Korenblat, K.M. Approach to the Patient with Jaundice or Abnormal Liver Test Results. In *Cecil Medicine*; Goldman, L., Ausiello, D., Eds.; Elsevier: Philadelphia, PA, USA, 2011.

43. Wolford, S.T.; Schroer, R.A.; Gohs, F.X.; Gallo, P.P.; Brodeck, M.; Falk, H.B.; Ruhren, R. Reference range data base for serum chemistry and hematology values in laboratory animals. *J. Toxicol. Environ. Health* **1986**, *18*, 161–188.
44. Arias, I.M.; Alter, H.J.; Boyer, J.L.; Cohen, D.E.; Fausto, N.; Schafritz, D.A.; Wollkoff, A.W. *The Liver, Biology and Pathobiology*; Wiley: Chinchester, UK, 2009; pp. 0–1216.
45. Yoshida, J.; Ishibashi, T.; Nishio, M. Antiproliferative effect of Ca^{2+} channel blockers on human epidermoid carcinoma A431 cells. *Eur. J. Pharmacol.* **2003**, *472*, 23–31.
46. Thorpe, J.A.; Schwarze, S.R. IRE1alpha controls cyclin A1 expression and promotes cell proliferation through XBP-1. *Cell Stress Chaperones.* **2010**, *15*, 497–508.
47. Gu, X.; Li, K.; Laybutt, D.R.; He, M.L.; Zhao, H.L.; Chan, J.C.; Xu, G. Bip overexpression, but not CHOP inhibition, attenuates fatty-acid-induced endoplasmic reticulum stress and apoptosis in HepG2 liver cells. *Life Sci.* **2010**, *87*, 724–732.
48. Pfaffenbach, K.T.; Gentile, C.L.; Nivala, A.M.; Wang, D.; Wei, Y.; Pagliassotti, M.J. Linking endoplasmic reticulum stress to cell death in hepatocytes: Roles of C/EBP homologous protein and chemical chaperones in palmitate-mediated cell death. *Am. J. Physiol. Endocrinol. Metab.* **2010**, 298, E1027–E1035.
49. Van, S.A.; van't Wout, E.F.; Stolk, J.; Hiemstra, P.S. A quantitative method for detection of spliced X-box binding protein-1 (XBP1) mRNA as a measure of endoplasmic reticulum (ER) stress. *Cell Stress Chaperones* **2012**, *17*, 275–279.
50. Zhang, K.; Shen, X.; Wu, J.; Sakaki, K.; Saunders, T.; Rutkowski, D.T.; Back, S.H.; Kaufman, R.J. Endoplasmic reticulum stress activates cleavage of CREBH to induce a systemic inflammatory response. *Cell* **2006**, *124*, 587–599.
51. Brodersen, R. Bilirubin Solubility and interaction with albumin and phospholipid. *J. Biol. Chem.* **1979**, *254*, 2364–2369.
52. Van der Veere, C.N.; Schoemaker, B.; van der, M.R.; Groen, A.K.; Jansen, P.L.; Oude Elferink, R.P. Rapid association of unconjugated bilirubin with amorphous calcium phosphate. *J. Lipid. Res.* **1995**, *36*, 1697–1707.
53. Suzuki, N. On bilirubin-metal complex compounds in relation to black pigments of gallstones. *Tohoku J. Exp. Med.* **1966**, *90*, 195–205.
54. Calligaris, R.; Bellarosa, C.; Foti, R.; Roncaglia, P.; Giraudi, P.; Krmac, H.; Tiribelli, C.; Gustincich, S. A transcriptome analysis identifies molecular effectors of unconjugated bilirubin in human neuroblastoma SH-SY5Y cells. *BMC Genomics* **2009**, doi:10.1186/1471-2164-10-543.
55. Dong, H.; Huang, H.; Yun, X.; Kim, D.S.; Yue, Y.; Wu, H.; Sutter, A.; Chavin, K.D.; Otterbein, L.E.; Adams, D.B.; *et al*. Bilirubin increases insulin sensitivity in leptin-receptor deficient and diet-induced obese mice through suppression of ER stress and chronic inflammation. *Endocrinology* **2014**, *155*, 818–828.
56. Weidinger, A.; Mullebner, A.; Paier-Pourani, J.; Banerjee, A.; Miller, I.; Lauterbock, L.; Duvigneau, J.C.; Skulachev, V.P.; Redl, H.; Kozlov, A.V. Vicious inducible nitric oxide synthase-mitochondrial reactive oxygen species cycle accelerates inflammatory response and causes liver injury in rats. *Antioxid. Redox Signal.* **2015**, *22*, 572–586.

57. Althausen, S.; Paschen, W. Homocysteine-induced changes in mRNA levels of genes coding for cytoplasmic- and endoplasmic reticulum-resident stress proteins in neuronal cell cultures. *Mol. Brain Res.* **2000**, *84*, 32–40.
58. Weidinger, A.; Dungel, P.; Perlinger, M.; Singer, K.; Ghebes, C.; Duvigneau, J.C.; Mullebner, A.; Schafer, U.; Redl, H.; Kozlov, A.V. Experimental data suggesting that inflammation mediated rat liver mitochondrial dysfunction results from secondary hypoxia rather than from direct effects of inflammatory mediators. *Front. Physiol.* **2013**, doi:10.3389/fphys.2013.00138.
59. Di, F.C.; Marfella, R.; Cuzzocrea, S.; Piegari, E.; Petronella, P.; Giugliano, D.; Rossi, F.; D'Amico, M. Hyperglycemia in streptozotocin-induced diabetic rat increases infarct size associated with low levels of myocardial HO-1 during ischemia/reperfusion. *Diabetes* **2005**, *54*, 803–810.
60. Nurnberger, S.; Miller, I.; Duvigneau, J.C.; Kavanagh, E.T.; Gupta, S.; Hartl, R.T.; Hori, O.; Gesslbauer, B.; Samali, A.; Kungl, A.; *et al*. Impairment of endoplasmic reticulum in liver as an early consequence of the systemic inflammatory response in rats. *Am. J. Physiol. Gastrointest. Liver Physiol.* **2012**, *303*, G1373–G1383.
61. Zhu, L.J.; Altmann, S.W. mRNA and 18S-RNA coapplication-reverse transcription for quantitative gene expression analysis. *Anal. Biochem.* **2005**, *345*, 102–109.
62. Peinnequin, A.; Mouret, C.; Birot, O.; Alonso, A.; Mathieu, J.; Clarencon, D.; Agay, D.; Chancerelle, Y.; Multon, E. Rat pro-inflammatory cytokine and cytokine related mRNA quantification by real-time polymerase chain reaction using SYBR green. *BMC Immunol.* **2004**, doi:10.1186/1471-2172-5-3.
63. Bradford, M.M. A rapid and sensitive method for the quantitation of microgram quantities of protein utilizing the principle of protein-dye binding. *Anal Biochem.* **1976**, *72*, 248–254.
64. Staniek, K.; Nohl, H. H_2O_2 detection from intact mitochondria as a measure for one-electron reduction of dioxygen requires a non-invasive assay system. *Biochim. Biophys. Acta* **1999**, *1413*, 70–80.

2.3 Paper III: Interaction between Mitochondrial Reactive Oxygen Species, Heme Oxygenase, and Nitric Oxide Synthase Stimulates Phagocytosis in Macrophages.

Müllebner A, Dorighello GG, Kozlov AV, Duvigneau JC.

Frontiers in medicine (2017), 4: 252.

frontiers in Medicine

ORIGINAL RESEARCH
published: 22 January 2018
doi: 10.3389/fmed.2017.00252

Interaction between Mitochondrial Reactive Oxygen Species, Heme Oxygenase, and Nitric Oxide Synthase Stimulates Phagocytosis in Macrophages

*Andrea Müllebner[1,2], Gabriel G. Dorighello[3], Andrey V. Kozlov[2] and J. Catharina Duvigneau[1]**

[1] Institute for Medical Biochemistry, University of Veterinary Medicine Vienna, Vienna, Austria, [2] Ludwig Boltzmann Institute for Experimental and Clinical Traumatology, Vienna, Austria, [3] Department of Structural and Functional Biology, Biology Institute, University of Campinas, Campinas, Brazil

OPEN ACCESS

Edited by:
Mikhail Kirov,
Northern State Medical University, Russia

Reviewed by:
Lars Jakob Bjertnæs, University of Tromsø, Norway
Evgeny Suborov, North-Western State Medical University named after I.I. Mechnikov, Russia

***Correspondence:**
J. Catharina Duvigneau
catharina.duvigneau@vetmeduni.ac.at

Specialty section:
This article was submitted to Intensive Care Medicine and Anesthesiology, a section of the journal Frontiers in Medicine

Received: 30 September 2017
Accepted: 19 December 2017
Published: 22 January 2018

Citation:
Müllebner A, Dorighello GG, Kozlov AV and Duvigneau JC (2018) Interaction between Mitochondrial Reactive Oxygen Species, Heme Oxygenase, and Nitric Oxide Synthase Stimulates Phagocytosis in Macrophages. Front. Med. 4:252. doi: 10.3389/fmed.2017.00252

Background: Macrophages are cells of the innate immune system that populate every organ. They are required not only for defense against invading pathogens and tissue repair but also for maintenance of tissue homeostasis and iron homeostasis.

Aim: The aim of this study is to understand whether heme oxygenase (HO) and nitric oxide synthase (NOS) contribute to the regulation of nicotinamide adenine dinucleotide phosphate oxidase (NOX) activity and phagocytosis, two key components of macrophage function.

Methods: This study was carried out using resting J774A.1 macrophages treated with hemin or vehicle. Activity of NOS, HO, or NOX was inhibited using specific inhibitors. Reactive oxygen species (ROS) formation was determined by Amplex® red assay, and phagocytosis was measured using fluorescein isothiocyanate-labeled bacteria. In addition, we analyzed the fate of the intracellular heme by using electron spin resonance.

Results: We show that both enzymes NOS and HO are essential for phagocytic activity of macrophages. NOS does not directly affect phagocytosis, but stimulates NOX activity *via* nitric oxide-triggered ROS production of mitochondria. Treatment of macrophages with hemin results in intracellular accumulation of ferrous heme and an inhibition of phagocytosis. In contrast to NOS, HO products, including carbon monoxide, neither clearly affect NOX activity nor clearly affect phagocytosis, but phagocytosis is accelerated by HO-mediated degradation of heme.

Conclusion: Both enzymes contribute to the bactericidal activity of macrophages independently, by controlling different pathways.

Keywords: macrophage, phagocytosis, heme oxygenase, nitric oxide synthase, reactive oxygen species, ROS, mitochondria

INTRODUCTION

Macrophages are cells of the innate immune system that can be found in all tissues. They are required for maintenance of tissue homeostasis, defense against invading pathogens, tissue repair, and red blood cell recycling. Macrophages maintain homeostasis by receptor-mediated recognition and phagocytic uptake of pathogenic or microbial material and damaged or apoptotic host cells.

Degradation of the material taken up by phagocytosis is achieved *via* proteolytic enzymes and facilitated by the so-called oxidative burst. This involves the formation of reactive oxygen species (ROS) and nitric oxide (NO). Nicotinamide adenine dinucleotide phosphate (NADPH) oxidase (NOX) residing in the phagosomal membrane reduces oxygen (O_2) to superoxide anion ($O_2^{\bullet-}$). This leads to the formation of hydrogen peroxide (H_2O_2) and the subsequent generation of highly reactive hydroxyl radicals *via* the Fenton reaction or the synthesis of hypochlorite by myeloperoxidase. In addition, the reaction of ROS with NO yields peroxynitrite, which together with hypochlorite is very effective antimicrobial agent (1). Altogether these reactive species are termed as reactive oxygen and nitrogen species.

Also mitochondrial ROS (mtROS) plays an important role in various innate immune signaling pathways (2). They activate NOX (3–5), the NLRP3 inflammasome (6), and were shown to drive synthesis of inflammatory cytokines (7). Furthermore, mtROS are believed to increase the phagocytic activity of macrophages (8).

It is known that generation of mtROS is regulated by diatomic gaseous messengers such as NO (9) and carbon monoxide (CO) (10). NO is formed from arginine by nitric oxide synthases (NOSs) and is a ubiquitous signaling messenger involved in multiple pathophysiologic reactions (11). NO acts as a reversible inhibitor of mitochondrial respiration by competing with O_2 for binding to the heme moiety of cytochrome *c* oxidase (COX). NO also reacts with iron sulfur clusters in complex I and II of the mitochondrial electron transport chain (mETC) (12). However, this effect is more likely assigned to the formation of peroxynitrite. Peroxynitrite inhibits the complexes of the mETC irreversibly (13). Both reversible and irreversible inhibitions of the mETC were shown to enhance mtROS formation in different model systems (9).

CO is a product of heme degradation by heme oxygenase (HO). CO targets cellular heme-containing proteins, including soluble guanylate cyclase (14, 15), NOS (16, 17), and NOX (18). Similar to NO, CO also competes with O_2 for binding to COX. Higher levels of CO were shown to inhibit COX and to raise the production of mtROS, without decreasing mitochondrial potential (19).

Nitric oxide synthase and HO play an opposing role for the regulation of macrophage function, despite the similarity of the biological action of NO and CO. Macrophages with elevated NOS activity are considered to display a pro-inflammatory phenotype, associated with the generation of NO and peroxynitrite (20). In contrast, upregulated HO is associated with a tissue-protective phenotype (21, 22) and suppressed pro-inflammatory cytokine production. Obviously macrophages need to adapt their phenotype in accordance to the environment. Meanwhile it has become evident that the phenotype of macrophages displays a higher plasticity and a more dynamic functional repertoire than previously recognized (23).

Macrophages are particularly challenged under conditions of hemolysis, when they encounter increased levels of hemoglobin or free heme. Endocytosis of haptoglobin-bound hemoglobin *via* CD163 or uptake of the heme/hemopexin complex (24) lead to increased levels of intracellular heme (25) and initiate heme-mediated signaling cascades, among others upregulation of HO (26, 27). Recently, it was shown that the treatment of macrophages with hemin (ferric heme) inhibited phagocytosis (28). Currently, it is not clear whether the redox state of the central iron ion of the heme molecule is relevant for the inhibition of phagocytosis and thus for the regulation of macrophage function.

The iron ion in protoporphyrin can exist in a ferrous (Fe^{2+}, ferroprotoporphyrin, or heme) or in a ferric form (Fe^{3+}, ferriprotoporphyrin, or hemin), which can be further oxidized yielding ferryl species (29). The intracellular reactions mediated by either species are supposed to differ considerably. It is known that at least some heme-dependent processes critically depend on the redox state of heme. Ferrous heme acts as a potent catalyst of the Fenton reaction generating highly active ROS. However, as a regulator of protein function, heme appears to preferentially act in its ferric form within the cell. Ferric heme, and not ferrous heme, was shown to activate RNA-binding protein DGCR8 (30). Function of the heme-containing enzymes, NOS and cytochrome p450, requires binding of ferric heme (31). It further appears that an enhanced degradation of heme also requires ferric heme, as it mediates proteasomal degradation of the Bach repressor (32), which is required to induce HO-1 transcription. To shed light on the intracellular heme pool, we questioned whether the treatment of J774A.1 cells with ferric heme (hemin) would result in determinable amounts of ferrous heme.

Aims

The aim of this study is to investigate the contribution of NOS and HO to the regulation of NOX activity and phagocytosis. Particular attention was paid to the role of mtROS and hemin as modulators of ROS generation and phagocytic activity.

MATERIALS AND METHODS

Material

All chemicals used in this study were obtained from Sigma-Aldrich (St. Louis, MO, USA). HO inhibitors [tin protoporphyrin (SnPP), zinc protoporphyrin (ZnPP), and chromium mesoporphyrin (CrMP)] were obtained from Frontier Scientific (Logan, UT, USA). Fetal calf serum was purchased from Bio & Sell (Nürnberg, Germany).

Cell Culture

J774A.1 mouse macrophages (TIB-67™; ATCC®, Manassas, VA, USA) were grown in Dulbecco's modified Eagle's medium containing high glucose (glucose 25 mM, glutamine 4 mM, sodium

Abbreviations: CO, carbon monoxide; COX, cytochrome oxidase; CrMP, chromium mesoporphyrin; DEA/NO, diethylamine NONOate; DETA/NO, diethylenetriamine NONOate; DPI, diphenyleneiodonium chloride; ESR, electron spin resonance; HO, heme oxygenase; HRP, horseradish peroxidase; L-NAME, L-N^G-nitro-arginine methyl ester; mETC, mitochondrial electron transport chain; mtROS, mitochondrial ROS; NADPH, nicotinamide adenine dinucleotide phosphate; NO, nitric oxide; NOS, nitric oxide synthase; NOX, NADPH oxidase; NOX-ROS, NADPH oxidase-derived ROS; PMA, phorbol 12-myristate 13-acetate; RONS, reactive oxygen and nitrogen species; ROS, reactive oxygen species; SnPP, tin protoporphyrin; TC, *S*-methyl-L-thiocitrulline; ZnPP, zinc protoporphyrin.

bicarbonate 1.5 g/l, and sodium pyruvate 1 mM), supplemented with 10% fetal calf serum. They were grown either adherently in cell culture flasks or in suspension in roller culture. The cells were kept in a humid incubator with 95% of air and 5% of carbon dioxide at 37°C.

Inhibition of Underlying HO Activity of J774A.1 Cells

The presence of basal HO activity was confirmed in homogenates of J774A.1 cells using an optimized enzyme-coupled spectrophotometric assay detecting the final product bilirubin (33) (data not shown). Full inhibition of enzyme activity determined in the presence of hemin (20 μM) was found for the HO inhibitors ZnPP, SnPP, and CrMP at equimolar concentration (20 μM; data not shown). *In situ* HO activity was confirmed by the detection of bilirubin in the cell culture supernatant formed from hemin (20 μM) after incubation overnight as elsewhere described (33).

Inhibition of NOS Activity

The basal activity of NOS was confirmed indirectly by the acceleration of mitochondrial O_2 consumption rates by NOS inhibitors (data not shown). Effective concentrations of the inhibitors were determined by measuring nitrite (NO_2^-) formation from lipopolysaccharide-treated (1 μg/ml for 16 h) J774A.1 cells. NO_2^- formation was fully inhibited at concentrations of 10 mM L-N^G-Nitro-arginine methyl ester (L-NAME) and 50 μM S-methyl-thiocitrulline (TC; data not shown).

Determination of Total ROS, mtROS, and NADPH-Derived ROS (NOX-ROS)

Reactive oxygen species formation was quantified using Amplex® red (Molecular Probes, Eugene, Oregon, USA). Before the experiment (24 h), the cells were seeded in low-fluorescence 96-well plates at a density of 6×10^4 cells per well. Experiments were performed in 100 μl Krebs buffer [NaCl (135 mM), KCl (5 mM), $MgSO_4$ (1 mM), K_2HPO_4 (0.4 mM), $CaCl_2$ (1 mM), HEPES (15 mM), and glucose (25 mM); pH 7.4] containing Amplex® red (10 μM), horse radish peroxidase (HRP; 0.2 U/mL), and phorbol 12-myristate 13-acetate (PMA; 1 μM). Contribution of mitochondria, NOS, and HO to the determined ROS formation was investigated using mitoTEMPO (0.5 μM) or inhibitors of either NOS (L-NAME, 10 mM) or HO (SnPP, 20 μM). Each condition was measured in the presence and absence of the NOX inhibitor diphenyleneiodonium chloride (DPI, 0.05 μM). Plates were kept in the dark at 37°C for 35 min measuring fluorescence of the formed resorufin (excitation: 530 nm, emission: 590 nm) every 5 min. The fluorescence signals were corrected for background fluorescence determined in wells without cells. The slope of the regression lines calculated from the first 15 min of resorufin formation was taken as H_2O_2 release rate and was displayed as percentage of total H_2O_2 release rate in controls. Rates detected in the absence of DPI reflected total H_2O_2 production; rates in the presence of DPI were taken as a measure for the mitochondrial H_2O_2 production. The difference between total and mitochondrial H_2O_2 production was used as a measure for the H_2O_2 generation by NOX activity (**Figure 1**). Modulation of ROS formation by mtROS (mitoTEMPO) was determined in $n = 5$, by NOS (L-NAME) and HO (SnPP) in $n = 3$ independent experiments. Each condition was measured in technical replicates of $n = 6$.

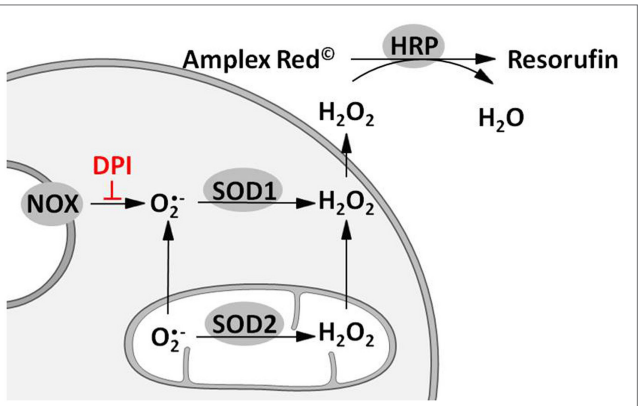

FIGURE 1 | Scheme illustrating the approach for measuring total, mitochondrial (mt) and nicotinamide adenine dinucleotide phosphate oxidase (NOX)-derived reactive oxygen species (ROS) formation. Superoxide radicals formed by either mitochondrial electron transport chain or NOX are converted to hydrogen peroxide (H_2O_2) by mitochondrial and cytoplasmic superoxide dismutase (SOD1 and SOD2). H_2O_2 capable of diffusing through membranes reacts with Amplex® red to resorufin on an equimolar basis in presence of horseradish peroxidase (HRP). Hence fluorescence of resorufin (excitation: 530–560 nm; emission: 590 nm) can be used as an indirect measure of ROS formation. Determination of mitochondrial ROS (mtROS) is achieved by inhibition of NOX using diphenyleneiodonium chloride (DPI). Difference of total and mtROS formation reflects NOX-ROS levels.

Determination of Phagocytosis

Phagocytic activity was assessed by using Phagotest™ (Glycotype Bioscience; Berlin, Germany) according to the following protocol. 1×10^6 cells were suspended in 200 μl Dulbecco's modified Eagle's medium buffered with 25 mM HEPES. The suspension was treated for 60 min with vehicle (dimethyl sulfoxide) or hemin (20 μM) with or without inhibitors of NOS (L-NAME, 10 mM; TC, 50 μM) or HO (ZnPP or CrMP, 20 μM). The viability of the cells after the initial 60 min of treatment (vehicle, hemin NOS/HO inhibitors) was analyzed by flow cytometry after propidium iodide staining (1 μg/ml) and was always higher than 90% (data not shown). Fluorescein isothiocyanate-labeled bacteria (20 μl diluted 1:2) were added, and the suspension was incubated at 37°C under shaking. After 30 min, phagocytosis was stopped by placing tubes on ice. Each sample was analyzed in duplicates. In addition, a control sample for each condition was kept on ice to prevent phagocytosis. After adding of 100 μl ice-cold quenching solution and incubation on ice for 3 min, cells were washed with ice-cold wash buffer (phosphate-buffered saline containing 0.3% fetal calf serum), fixed with 1% paraformaldehyde for 20 min at room temperature, washed again, and resuspended in 200 μl wash buffer. Uptake of bacteria was assessed on a FACScan (Becton Dickinson, Franklin Lakes, NJ, USA) flow cytometer and analyzed using Cell Quest 3.1 software (Becton Dickinson, Franklin Lakes, NJ, USA). A live gate was set in the scatter plot (forward scatter versus side scatter) to exclude debris. The green fluorescence

histogram (FL1, 530/30) was analyzed. Autofluorescence of J774A.1 cells was assessed in the respective control samples to set a marker for discrimination between non-phagocytosing and phagocytosing cells. Percentage of gated events above this marker equals the population of phagocytosing cells in the samples. The mean fluorescence in this population was taken as a measure for the number of bacteria taken up per individual cell. For each condition, $n = 4$ independent experiments were performed.

Determination of Ferrous Heme by Electron Spin Resonance (ESR) Spectroscopy

To determine the occurrence of intracellular ferrous heme, we analyzed the spectra of suspension cells treated for 24 h with vehicle, hemin, or hemin plus diethylenetriamine NONOate (DETA/NO). 5 min before collecting the cells or the supernatants, 1 mM diethylamine NONOate (DEA/NO; 1 mM) was added to convert all free ferrous heme into the nitrosylated form. The cell suspension was centrifuged (350 × g), the supernatant was harvested, and the pelleted cells were washed twice with PBS and resuspended in 300 µl phosphate-buffered saline. 300 µl of the samples were aspirated in standard 1 ml syringes and shock frozen in liquid nitrogen. ESR spectra were recorded at liquid nitrogen temperature (−196°C) with a Magnettech MiniScope MS 200 ESR spectrometer (Magnettech Ltd., Berlin, Germany). The general settings were as follows: modulation frequency, 100 kHz; microwave frequency, 9.425 GHz; microwave power, 8.3 mW; modulation amplitude, 5 G; gain, 200; range, 330 ± 20 mT. Two independent experiments were performed.

Data Analysis and Statistics

Data processing and visualization were performed using Excel or GraphPad Prism v6.01 (GraphPad Software Inc., La Jolla, CA, USA). Data are presented as means ± SEM. Differences between groups were assessed using paired *t*-test for ROS formation and for phagocytosis using matched two-way ANOVA followed by Sidak's multiple comparisons using GraphPad Prism. Differences were considered significant when $p < 0.05$.

RESULTS

Determination of Total ROS, mtROS, and NOX-ROS

The ROS formation from unstimulated cells was below the detection limit (data not shown). The application of PMA triggered ROS generation (**Figure 2A**) by activating both mitochondria- (**Figure 2B**) and NOX-dependent (**Figure 2C**) ROS formation. On treatment with the mitochondria-targeted antioxidant mitoTEMPO, total ROS formation was reduced by 30% (**Figure 2A**). MitoTEMPO at 0.5 µM was sufficient to scavenge about 25% of mtROS, corresponding to a portion of less than 5% of total ROS (**Figure 2B**). This in turn substantially reduced NOX-ROS formation (**Figure 2C**).

Effect of NOS Inhibition on Formation of mtROS and NOX-ROS

Inhibition of basal NOS activity reduced ROS formation by 30% (**Figure 3A**) in J774.A1 cells. NOS inhibitor attenuated mtROS

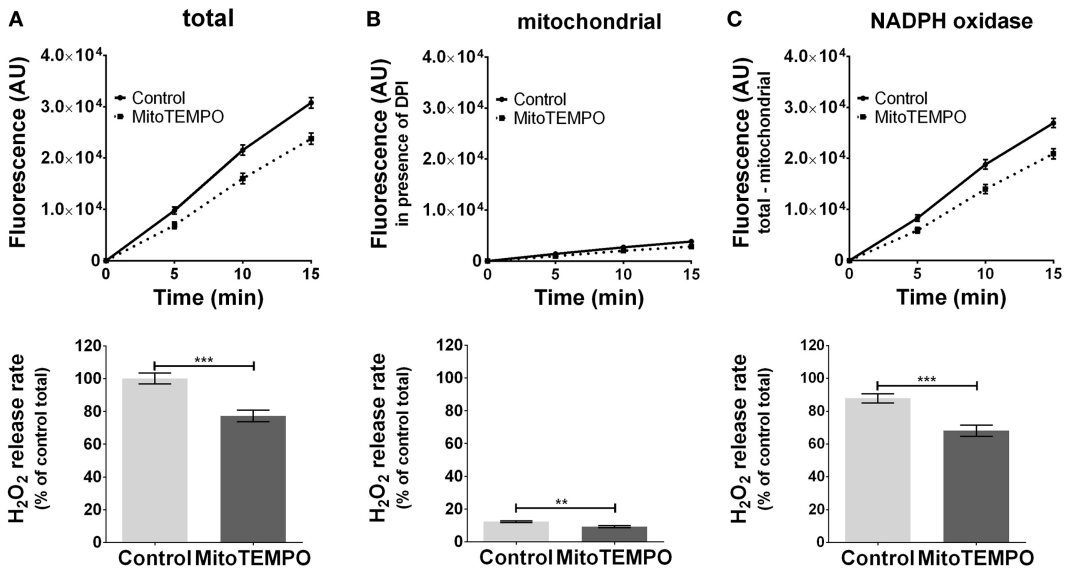

FIGURE 2 | Modulation of reactive oxygen species (ROS) formation in J774A.1 cells by mitochondria-targeted antioxidant MitoTEMPO. Hydrogen peroxide (H_2O_2) formation in J774A.1 cells treated with dimethyl sulfoxide (control) or MitoTEMPO (0.5 µM) was triggered by phorbol 12-myristate 13-acetate (1 µM). Formation of resorufin from Amplex® red was assessed over 15 min. H_2O_2 release rates correspond to slopes calculated from resorufin formation kinetics and are displayed as percentage of total H_2O_2 release rate of the controls **(A)**. Mitochondrial H_2O_2 release **(B)** was assessed by blocking nicotinamide adenine dinucleotide phosphate oxidase (NOX) using diphenyleneiodonium chloride (DPI; 0.05 µM). NOX H_2O_2 release **(C)** equals the difference of mitochondrial **(B)** from total H_2O_2 release **(A)**. Data are presented as mean ± SEM of five independent experiments. Significant differences ($p < 0.05$) are indicated (**$p < 0.01$ and ***$p < 0.005$).

formation (**Figure 3B**), which was accompanied by decreased ROS formation by NOX (**Figure 3C**) showing that NOS contributes to an enhanced NOX-ROS generation. These data suggest that NO activates NOX in a mtROS-dependent manner.

Effect of HO Inhibition on Formation of mtROS and NOX-ROS

In contrast to inhibitors of NOS, we did not observe a significant effect of HO inhibitors neither on total ROS (**Figure 4A**) nor on mtROS (**Figure 4B**) nor on NOX-ROS (**Figure 4C**) formation. However, there was a high tendency of an increased mtROS formation from mitochondria ($p = 0.0535$) when HO was inhibited. Simultaneously the inhibition of HO resulted in a decreased NOX-ROS formation by trend ($p = 0.0586$). Although the determined effects of HO inhibition were not strong enough to result in significant differences using a replicate number of 3, we cannot completely exclude a possible contribution of HO to ROS production. Thus, our data suggest that HO and NOS may affect mitochondrial ROS production in an opposite way.

Effect of NOS Inhibitors on Phagocytosis

Inhibition of NOS with L-NAME altered neither the percentage of phagocytosing cells (**Figure 5A**) nor the average number of bacteria ingested per cell (**Figure 5B**). We confirmed the results using TC, an alternate inhibitor of NOS. Considering that the action of HO and NOS at the level of phagocytosis can be synergistic, we repeated the experiment in the presence of hemin, the substrate of HO. Hemin strongly impaired phagocytic activity by reducing the number of phagocytosing cells (**Figures 5A** and **6A**) and even more the amount of bacteria ingested per cell (**Figures 5B** and **6B**). But even in the presence of hemin, NOS inhibitors had no effect on the rate of phagocytosis (**Figures 5A,B**).

Effect of HO Inhibitors on Hemin Modulated Phagocytosis

Since an inhibition of phagocytosis could be exerted either by hemin or by the products of HO reaction, we questioned whether the inhibition of basal HO activity would prevent the observed phagocytosis inhibition. Therefore, we studied phagocytosis in the presence of two different HO inhibitors, ZnPP and CrMP. Both HO inhibitors *per se* reduced phagocytosis (**Figures 6A,B**), especially the number of ingested bacteria per cell (**Figure 6B**), suggesting that the inhibition of phagocytosis is due to the accumulation of heme. This was confirmed by the further inhibition of phagocytic activity in presence of hemin (**Figures 6A,B**).

Occurrence of Ferrous Heme within Cells or Cell Supernatant

Phagocytosis was modulated by changes of HO activity, which affects the level of the intracellular heme pool. It is possible that the redox state of heme plays a role in this regulation. To understand whether treatment of the cells with ferric heme (hemin) would result in occurrence of intracellular ferrous heme, we additionally treated the cells with the NO-donor DEA/NO, which allows the detection of ferrous heme in its nitrosylated form by low-temperature ESR, due to its unique spectrum. Cells exposed to 1 mM NO-donor DEA/NO for 5 min did not display any NO-related signal (**Figure 7A**). Cells treated with hemin for 24 h

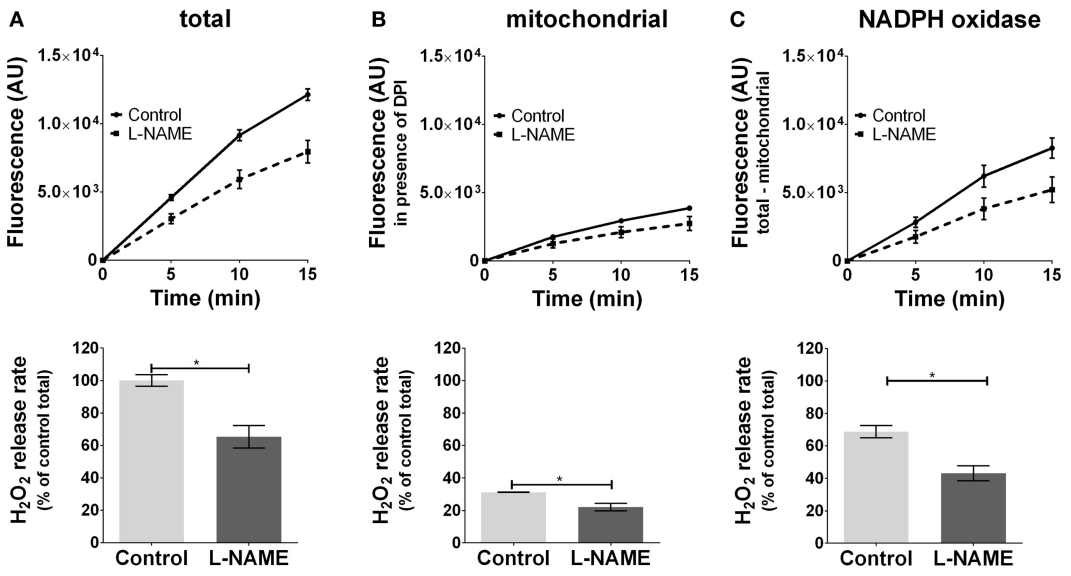

FIGURE 3 | Modulation of reactive oxygen species formation in J774A.1 cells by inhibition of nitric oxide synthase activity with L-N^G-nitro-arginine methyl ester (L-NAME). Hydrogen peroxide (H_2O_2) formation in J774A.1 cells in the absence (control) or presence of L-NAME (10 mM) was triggered by phorbol 12-myristate 13-acetate (1 μM). Formation of resorufin from Amplex® red was assessed over 15 min. H_2O_2 release rates correspond to slopes calculated from resorufin formation kinetics and are displayed as percentage of total H_2O_2 release rate of the controls **(A)**. Mitochondrial H_2O_2 release **(B)** was assessed by blocking nicotinamide adenine dinucleotide phosphate oxidase (NOX) using diphenyleneiodonium chloride (DPI; 0.05 μM). NOX H_2O_2 release **(C)** equals the difference of mitochondrial **(B)** from total H_2O_2 release **(A)**. Data are presented as mean ± SEM of three independent experiments. Significant differences ($p < 0.05$) are indicated (*$p < 0.05$).

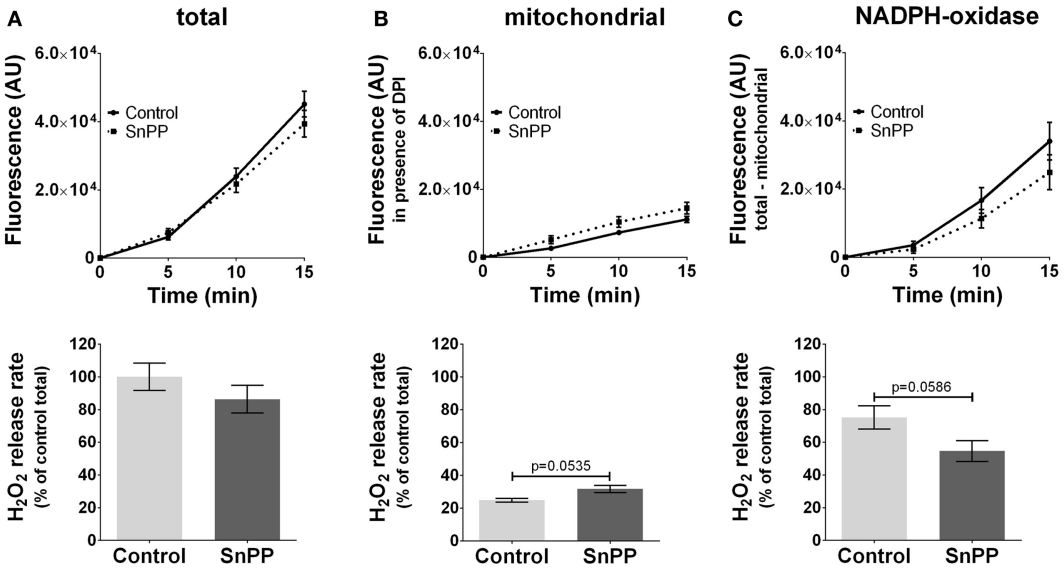

FIGURE 4 | Modulation of reactive oxygen species formation in J774A.1 cells by inhibition of heme oxygenase activity with tin protoporphyrin (SnPP). Hydrogen peroxide (H_2O_2) formation in J774A.1 cells treated with dimethyl sulfoxide (control) or with SnPP (20 mM) was triggered by phorbol 12-myristate 13-acetate (1 μM). Formation of resorufin from Amplex® red was assessed over 15 min. H_2O_2 release rates correspond to slopes calculated from resorufin formation kinetics and are displayed as percentage of total H_2O_2 release rates of the controls **(A)**. Mitochondrial H_2O_2 release **(B)** was assessed by blocking nicotinamide adenine dinucleotide phosphate oxidase (NOX) using diphenyleneiodonium chloride (DPI; 0.05 μM). NOX H_2O_2 release **(C)** equals the difference of mitochondrial **(B)** from total H_2O_2 release **(A)**. Data are presented as mean ± SEM of three independent experiments. *p* values obtained from the statistical analyses are indicated.

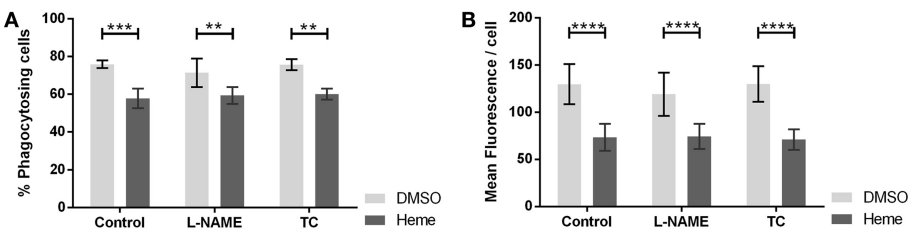

FIGURE 5 | Effect of nitric oxide synthase (NOS) inhibition on phagocytic activity of J774A.1 cells. The amount of phagocytosing cells from the entire population [in % **(A)**] and average amount of phagocytosed bacteria per cell **(B)** was determined. Macrophages were treated with dimethyl sulfoxide or hemin (20 μM) alone (control) or with additional NOS inhibitors L-N^G-nitro-arginine methyl ester (L-NAME; 10 mM) or *S*-methyl-L-thiocitrulline (TC; 50 μM). Phagocytic activity was assessed using Phagotest Kit (Glycotype Technology). Data are presented as mean ± SEM of four independent experiments. Significant differences are indicated as follows (**$p < 0.01$, ***$p < 0.005$, and ****$p < 0.001$).

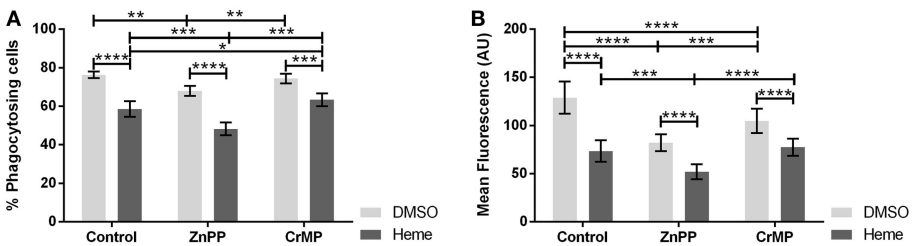

FIGURE 6 | Effect of heme oxygenase (HO) inhibition on phagocytic activity of J774A.1 cells. The amount of phagocytosing cells from the entire population [in % **(A)**] and average amount of phagocytosed bacteria per cell **(B)** was determined. Macrophages were treated with dimethyl sulfoxide (DMSO) or hemin (20 μM) alone (control) or with additional HO inhibitors zinc protoporphyrin (ZnPP; 20 μM) or chromium mesoporphyrin (CrMP; 20 μM). Phagocytic activity was assessed using Phagotest Kit (Glycotype Technology). Data are presented as mean ± SEM of four independent experiments. Significant differences are indicated as follows (*$p < 0.05$, **$p < 0.01$, ***$p < 0.005$, and ****$p < 0.001$).

and exposed to 1 mM NO-donor DEA/NO for the final 5 min showed the ESR signal typical for NO-heme centered at g = 2.009 and with the characteristic triplet splitting (**Figure 7A**). This signal indicates that at least a small portion of intracellular heme–iron occurs in a ferrous form. The signal was strongly increased after the simultaneous treatment with hemin and DETA/NO for 24 h (**Figure 7A**) and exposure to 1 mM NO-donor DEA/NO for the final 5 min, suggesting the accumulation of nitrosylated heme inside the cell. None of the supernatants showed a signal arising from nitrosyl–heme complexes. This indicates that exclusively ferric heme is present extracellularly in the supernatants (**Figure 7B**a–c) and that the reduction step required to form ferrous from ferric heme, allowing the formation of nitrosyl–heme complexes, occurred inside the cells.

DISCUSSION

We studied the role of HO and NOS on ROS generation and phagocytosis, two major tasks of macrophages. NOS and HO play an opposing role in the regulation of macrophages despite the similarity of the biological action of their products NO and CO. Macrophages with elevated NOS activity are considered to display a pro-inflammatory phenotype, which is associated with the generation of NO and peroxynitrite (20). In contrast, upregulated HO is associated with a tissue-protective phenotype and a suppressed pro-inflammatory cytokine production. The anti-inflammatory and tissue-protective effects are believed to be mediated mainly by the HO reaction products, CO (34, 35) and bilirubin (36). In addition, HO products were shown to inhibit inducible NOS expression and NO formation (37, 38). Macrophages activated by pro-inflammatory stimuli produce high levels of NO, by far exceeding the levels of CO that can be reached by active HO. We found that NOS product formation in LPS-stimulated J774A.1 cells was several 100-fold higher than the generation of HO products upon hemin stimulation within the same time (data not shown). Both NO and CO compete with oxygen for the binding to heme proteins of the mETC, such as COX. Therefore, the different binding affinities and the concentration ratios of all three ligands to each other determine the overall effects on the mETC. To avoid competition by excessively produced NO, we used macrophages without previous activation (resting macrophages), which display only basal NOS activity. To trigger ROS generation or phagocytosis, we used PMA stimulation or bacterial preparations, respectively.

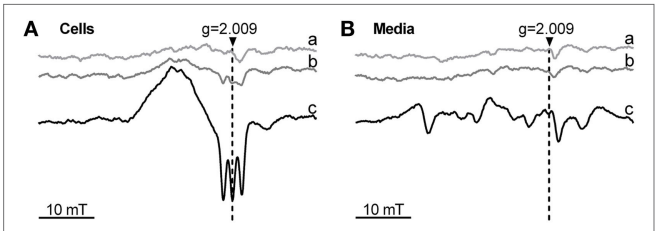

FIGURE 7 | Occurrence of ferrous heme determined by low-temperature electron paramagnetic resonance (ESR) spectra of J774A.1 cells **(A)** and incubation media **(B)** after treatment with hemin and nitric oxide (NO) donors. Cells were incubated for 24 h with medium alone (control; a) or in the presence of hemin (20 μM; b) or hemin (20 μM) and diethylenetriamine NONOate (100 μM; c). After incubation, cells were treated with diethylamine NONOate (1 mM) for 5 min. Released nitric oxide and ferrous heme form a nitrosyl-heme complex giving a triplet structured signal centered at g = 2.009. ESR parameters are described in Section "Materials and Methods." Representative spectra of two independent experiments are shown. g, g-factor; mT, millitesla.

mtROS Amplify NOX-ROS Formation

In J774A.1 cells, PMA induced ROS generation from both mitochondria and NOX. This is in line with the former report using human lymphoblasts (39). It was previously shown that mtROS may enhance the activity of NOX (3–5). Since we have found that the amount of ROS generated by mitochondria was about 10 times lower compared to that generated from NOX, we tested whether these levels would be sufficient for an enhancement of NOX activity in J774A1 cells, using the mitochondria-targeted ROS scavenger mitoTEMPO. As expected, mitoTEMPO attenuated mtROS generation, and in addition, it also attenuated generation of NOX-ROS, confirming previous findings in activated macrophages (5). This shows that mtROS contribute to NOX-ROS generation also in resting macrophages. In addition, these data show that mtROS operate as an amplifier of the NOX-ROS generation and underpin the role of mtROS as an essential regulator of the bactericidal activity of macrophages (5).

Formation of mtROS was shown to be modulated by NO and CO (9, 40). Therefore, both gaseous messengers are possible candidates for an indirect modulation of NOX-ROS generation in macrophages. In addition, it was suggested that NOX as a heme protein may be directly inhibited by NO or CO (41, 42). In resting macrophages, NOS- and HO-derived NO and CO are endogenously produced at low levels. To elucidate the potential of such basal enzyme activity to influence the activity of NOX *via* formed gaseous messengers, we applied specific NOS and HO inhibitors.

Basal NOS Contributes to NOX-ROS Formation *Via* mtROS in Resting Macrophages

Inhibition of NOS decreased mtROS formation and subsequently NOX-ROS generation. These findings confirm that the ROS-NOS cycle, which was previously described in hepatocytes (7), also exists in macrophages. In addition, the decrease of formation of NOX-ROS by NOS inhibition shows that mtROS formation is modulated by NO, possibly *via* inhibiting mETC. It should be noted that the macrophages were not activated and that NO production under these conditions is rather low. However, our data suggest that also in resting macrophages basal NOS activity is sufficient to activate NADPH oxidase in a mtROS-dependent manner.

No or Limited Contribution of Basal HO to ROS Formation in Resting Macrophages

While NOS inhibition affects only NO levels, HO inhibition not only leads to decreased CO levels but also simultaneously to decreased levels of ferrous iron and bilirubin. In addition,

the inhibition of HO leads to the accumulation of intracellular heme and may thereby promote other heme-mediated reactions as shown by others (43). Therefore, it is not possible to attribute effects in the HO inhibitor-treated cells solely to the absence of a single HO product. This and the comparably low concentrations of HO products formed by basal HO activity might explain that in our model ROS generation was not effected upon inhibition of HO, contrasting previous findings in RAW 264.A cells treated with HO-derived products (35, 36). However, there was a trend for a reduction of NOX-ROS generation when HO was inhibited. We found additionally that HO inhibition increased the mtROS formation by trend, which is in contrast to the findings obtained for the inhibition of NOS. Due to the limited number of replicates ($n = 3$), it is not possible to clearly exclude a modulatory effect of HO on NOX-ROS and mitochondrial ROS production and a possible contribution of HO on ROS generation in macrophages. Anyway, our data show that HO and NOS differ considerably regarding their contribution to mitochondrial ROS production. To find out whether these effects are of biological relevance, further studies have to be performed.

NOS Does Not Affect Phagocytosis in Resting J774A.1 Cells

An efficient phagocytosis is essential for macrophage bactericidal function, besides sufficient ROS formation. In pro-inflammatory macrophages, both NOS (44) and HO activities (45, 46) accelerate the process of phagocytosis. On the other hand, it was shown that knocking out HO-1 results in an increased expression of macrophage-specific scavenger receptor A (47), which is required for phagocytosis and inflammatory signal release (48). Therefore, we questioned whether NOS and HO activity contribute to the phagocytic activity in resting macrophages as well. NOS inhibitors did neither influence the number of phagocytosing cells nor influence the amount of phagocytosed bacteria. It is known that the substrate of HO, hemin, is an inhibitor of phagocytosis in macrophages (28). Since it is not clear whether NOS or HO products show additional modulating properties, we investigated phagocytosis in cells treated with hemin and simultaneously inhibited HO and NOS activity.

Hemin Impairs Phagocytosis in Resting J774A.1 Cells

We observed that hemin reduced phagocytic activity, which is in line with the study performed by Martins et al. (28). Both the number of phagocytosing cells and the amount of bacteria phagocytosed per cell were decreased by hemin treatment, and thus, we questioned whether this effect is mediated by the formation of HO products or by heme itself.

HO Partly Restores Phagocytosis by Degradation of Heme

Co-treatment of cells with hemin and an HO inhibitor further decreased the phagocytic activity, suggesting that hemin itself, rather than the HO products, modulate phagocytic activity. Since active HO degrades heme, these findings suggest that HO contributes indirectly to the efficiency of phagocytosis. This is supported by the findings that macrophages and neutrophils from HO-1 knockout animals showed an impaired bacterial clearance upon treatment with heme (28). In addition, we found that treatment with HO inhibitors alone also reduced phagocytic activity. HO inhibition is supposed to increase the levels of intracellular heme pool, even in the absence of an external heme supplementation. Thus, our findings indicate that the endogenous basal HO activity of J774A.1 cells is sufficient to accelerate phagocytosis. Our findings further suggest that it is not the treatment with hemin itself, but the change of the level of the intracellular heme pool, which is responsible for the modulation of phagocytosis.

Heme Exists as Ferrous Heme in the Intracellular Heme Pool

The reactions catalyzed by heme are dependent on its redox state. The availability of heme in the appropriate redox state appears to play an important role for its regulator function (49). For example, ferric heme, and not ferrous heme, was shown to activate RNA-binding protein DGCR8 (30). It is not known whether (i) the redox state of heme is relevant for the regulation of phagocytosis, (ii) heme within the heme pool exists predominately in its ferrous or ferric form in resting macrophages, and (iii) hemin, the ferric chloride salt of heme, increases the ferrous or ferric heme portion of the intracellular pool in these cells. Due to the reductive environment inside the cell, we expect the intracellular heme pool to contain iron predominantly in its ferrous form. Thus, we expected that treatment with hemin would result in discernable amounts of ferrous heme within J774A.1 cells. Our ESR analyses of heme-treated J774A.1 cells confirmed that a portion of heme exists in its ferrous form, since treatment with NO resulted in a clear nitrosylated heme ESR signal, which was absent in the cell supernatants. However, when cells were treated with NO throughout the incubation period, a stronger signal was determined, indicating an accumulation of the ferrous heme. This suggests that hemin treatment feeds the intracellular heme pool predominately with ferric heme. Our findings further indicate that NO may shift the balance between ferrous and the ferric heme toward the ferrous heme, thereby decreasing the portion of ferric heme. Upregulation of NOS under pro-inflammatory conditions yields higher levels of NO and is therefore supposed to favor the balance toward ferrous heme. Ferric heme, however, is the substrate of HO (50), which is supposed to predominantly decrease the portion of ferric heme. Thus, it is tempting to speculate that it is the balance between the ferrous and the ferric portion of the heme pool, which determines the predominant phenotype of the macrophage.

We admit as a limitation of our study that modulating effects of the essential enzymes NOS, HO, and NOX were obtained by indirect means, i.e., by using inhibitors of HO and NOS. Correspondingly, for impairing NOX activity, we used DPI, which is not a selective inhibitor of NADPH oxidases, but an inhibitor of all flavoproteins. For all inhibitors, we have chosen the lowest concentration that is possible to avoid excessive effects. However, further experiments are warranted to confirm our findings, ideally by using complementary methods.

CONCLUSION

We showed that both enzymes NOS and HO are essential for important functions of macrophages, namely ROS generation and phagocytosis. While NOS, *via* its product NO, enhances ROS production, HO indirectly, *via* decreasing intracellular heme levels, enhances phagocytosis. This indicates that both enzymes contribute to the bactericidal activity of macrophages independently by controlling different pathways.

AUTHOR CONTRIBUTIONS

CD, AK, and AM were responsible for conception and design of the study. AM and GD performed experiments and analyzed data. CD and AK interpreted data and supervised the study. AM, CD, and AK wrote the manuscript. All authors read and approved the final manuscript.

ACKNOWLEDGMENTS

We want to thank Stefan Puchner for his excellent technical assistance with performing the ESR analyses.

FUNDING

AM was supported by the Austrian Research Promotion Agency with a PhD grant: "Industrienahe Dissertation" (849090).

REFERENCES

1. Fang FC. Antimicrobial reactive oxygen and nitrogen species: concepts and controversies. *Nat Rev Microbiol* (2004) 2:820–32. doi:10.1038/nrmicro1004
2. Garaude J, cin-Perez R, Martinez-Cano S, Enamorado M, Ugolini M, Nistal-Villan E, et al. Mitochondrial respiratory-chain adaptations in macrophages contribute to antibacterial host defense. *Nat Immunol* (2016) 17:1037–45. doi:10.1038/ni.3509
3. Dikalov S. Cross talk between mitochondria and NADPH oxidases. *Free Radic Biol Med* (2011) 51:1289–301. doi:10.1016/j.freeradbiomed.2011.06.033
4. Daiber A. Redox signaling (cross-talk) from and to mitochondria involves mitochondrial pores and reactive oxygen species. *Biochim Biophys Acta* (2010) 1797:897–906. doi:10.1016/j.bbabio.2010.01.032
5. West AP, Brodsky IE, Rahner C, Woo DK, Erdjument-Bromage H, Tempst P, et al. TLR signalling augments macrophage bactericidal activity through mitochondrial ROS. *Nature* (2011) 472:476–80. doi:10.1038/nature09973
6. Zhou R, Yazdi AS, Menu P, Tschopp J. A role for mitochondria in NLRP3 inflammasome activation. *Nature* (2011) 469:221–5. doi:10.1038/nature09663
7. Weidinger A, Mullebner A, Paier-Pourani J, Banerjee A, Miller I, Lauterbock L, et al. Vicious inducible nitric oxide synthase-mitochondrial reactive oxygen species cycle accelerates inflammatory response and causes liver injury in rats. *Antioxid Redox Signal* (2015) 22:572–86. doi:10.1089/ars.2014.5996
8. Lo HM, Chen CL, Yang CM, Wu PH, Tsou CJ, Chiang KW, et al. The carotenoid lutein enhances matrix metalloproteinase-9 production and phagocytosis through intracellular ROS generation and ERK1/2, p38 MAPK, and RARbeta activation in murine macrophages. *J Leukoc Biol* (2013) 93:723–35. doi:10.1189/jlb.0512238
9. Kozlov AV, Lancaster JR Jr, Meszaros AT, Weidinger A. Mitochondria-meditated pathways of organ failure upon inflammation. *Redox Biol* (2017) 13:170–81. doi:10.1016/j.redox.2017.05.017
10. Piantadosi CA. Carbon monoxide, reactive oxygen signaling, and oxidative stress. *Free Radic Biol Med* (2008) 45:562–9. doi:10.1016/j.freeradbiomed.2008.05.013
11. Tuteja N, Chandra M, Tuteja R, Misra MK. Nitric oxide as a unique bioactive signaling messenger in physiology and pathophysiology. *J Biomed Biotechnol* (2004) 2004:227–37. doi:10.1155/S1110724304402034
12. Henry Y, Guissani A. Interactions of nitric oxide with hemoproteins: roles of nitric oxide in mitochondria. *Cell Mol Life Sci* (1999) 55:1003–14. doi:10.1007/s000180050351
13. Brown GC. Nitric oxide and mitochondrial respiration. *Biochim Biophys Acta* (1999) 1411:351–69. doi:10.1016/S0005-2728(99)00025-0
14. Schallner N, Romao CC, Biermann J, Lagreze WA, Otterbein LE, Buerkle H, et al. Carbon monoxide abrogates ischemic insult to neuronal cells via the soluble guanylate cyclase-cGMP pathway. *PLoS One* (2013) 8:e60672. doi:10.1371/journal.pone.0060672
15. Verma A, Hirsch DJ, Glatt CE, Ronnett GV, Snyder SH. Carbon monoxide: a putative neural messenger. *Science* (1993) 259:381–4. doi:10.1126/science.7678352
16. Marazioti A, Bucci M, Coletta C, Vellecco V, Baskaran P, Szabo C, et al. Inhibition of nitric oxide-stimulated vasorelaxation by carbon monoxide-releasing molecules. *Arterioscler Thromb Vasc Biol* (2011) 31:2570–6. doi:10.1161/ATVBAHA.111.229039
17. Zuckerbraun BS, Billiar TR, Otterbein SL, Kim PK, Liu F, Choi AM, et al. Carbon monoxide protects against liver failure through nitric oxide-induced heme oxygenase 1. *J Exp Med* (2003) 198:1707–16. doi:10.1084/jem.20031003
18. Taille C, El-Benna J, Lanone S, Boczkowski J, Motterlini R. Mitochondrial respiratory chain and NAD(P)H oxidase are targets for the antiproliferative effect of carbon monoxide in human airway smooth muscle. *J Biol Chem* (2005) 280:25350–60. doi:10.1074/jbc.M503512200
19. D'Amico G, Lam F, Hagen T, Moncada S. Inhibition of cellular respiration by endogenously produced carbon monoxide. *J Cell Sci* (2006) 119:2291–8. doi:10.1242/jcs.02914
20. Mustafa AK, Gadalla MM, Snyder SH. Signaling by gasotransmitters. *Sci Signal* (2009) 2:re2. doi:10.1126/scisignal.268re2
21. Naito Y, Takagi T, Higashimura Y. Heme oxygenase-1 and anti-inflammatory M2 macrophages. *Arch Biochem Biophys* (2014) 564:83–8. doi:10.1016/j.abb.2014.09.005
22. Schaer CA, Schoedon G, Imhof A, Kurrer MO, Schaer DJ. Constitutive endocytosis of CD163 mediates hemoglobin-heme uptake and determines the noninflammatory and protective transcriptional response of macrophages to hemoglobin. *Circ Res* (2006) 99:943–50. doi:10.1161/01.RES.0000247067.34173.1b
23. Martinez FO, Gordon S. The M1 and M2 paradigm of macrophage activation: time for reassessment. *F1000Prime Rep* (2014) 6:13. doi:10.12703/P6-13
24. Hvidberg V, Maniecki MB, Jacobsen C, Hojrup P, Moller HJ, Moestrup SK. Identification of the receptor scavenging hemopexin-heme complexes. *Blood* (2005) 106:2572–9. doi:10.1182/blood-2005-03-1185
25. Khan AA, Quigley JG. Control of intracellular heme levels: heme transporters and heme oxygenases. *Biochim Biophys Acta* (2011) 1813:668–82. doi:10.1016/j.bbamcr.2011.01.008
26. Abraham NG, Drummond G. CD163-Mediated hemoglobin-heme uptake activates macrophage HO-1, providing an antiinflammatory function. *Circ Res* (2006) 99:911–4. doi:10.1161/01.RES.0000249616.10603.d6
27. Alam MZ, Devalaraja S, Haldar M. The heme connection: linking erythrocytes and macrophage biology. *Front Immunol* (2017) 8:33. doi:10.3389/fimmu.2017.00033
28. Martins R, Maier J, Gorki AD, Huber KV, Sharif O, Starkl P, et al. Heme drives hemolysis-induced susceptibility to infection via disruption of phagocyte functions. *Nat Immunol* (2016) 17:1361–72. doi:10.1038/ni.3590
29. Kagan VE, Kozlov AV, Tyurina YY, Shvedova AA, Yalowich JC. Antioxidant mechanisms of nitric oxide against iron-catalyzed oxidative stress in cells. *Antioxid Redox Signal* (2001) 3:189–202. doi:10.1089/152308601300185160
30. Barr I, Smith AT, Chen Y, Senturia R, Burstyn JN, Guo F. Ferric, not ferrous, heme activates RNA-binding protein DGCR8 for primary microRNA processing. *Proc Natl Acad Sci U S A* (2012) 109:1919–24. doi:10.1073/pnas.1114514109

31. Shimizu T. Binding of cysteine thiolate to the Fe(III) heme complex is critical for the function of heme sensor proteins. *J Inorg Biochem* (2012) 108:171–7. doi:10.1016/j.jinorgbio.2011.08.018
32. Ogawa K, Sun J, Taketani S, Nakajima O, Nishitani C, Sassa S, et al. Heme mediates derepression of Maf recognition element through direct binding to transcription repressor Bach1. *EMBO J* (2001) 20:2835–43. doi:10.1093/emboj/20.11.2835
33. Mullebner A, Moldzio R, Redl H, Kozlov AV, Duvigneau JC. Heme degradation by heme oxygenase protects mitochondria but induces ER stress via formed bilirubin. *Biomolecules* (2015) 5:679–701. doi:10.3390/biom5020679
34. Ryter SW, Otterbein LE. Carbon monoxide in biology and medicine. *Bioessays* (2004) 26:270–80. doi:10.1002/bies.20005
35. Srisook K, Kim C, Cha YN. Role of NO in enhancing the expression of HO-1 in LPS-stimulated macrophages. *Methods Enzymol* (2005) 396:368–77. doi:10.1016/S0076-6879(05)96031-X
36. Lanone S, Bloc S, Foresti R, Almolki A, Taille C, Callebert J, et al. Bilirubin decreases nos2 expression via inhibition of NAD(P)H oxidase: implications for protection against endotoxic shock in rats. *FASEB J* (2005) 19:1890–2. doi:10.1096/fj.04-2368fje
37. Tsoyi K, Ha YM, Kim YM, Lee YS, Kim HJ, Kim HJ, et al. Activation of PPAR-gamma by carbon monoxide from CORM-2 leads to the inhibition of iNOS but not COX-2 expression in LPS-stimulated macrophages. *Inflammation* (2009) 32:364–71. doi:10.1007/s10753-009-9144-0
38. Wang WW, Smith DL, Zucker SD. Bilirubin inhibits iNOS expression and NO production in response to endotoxin in rats. *Hepatology* (2004) 40:424–33. doi:10.1002/hep.20334
39. Dikalov SI, Li W, Doughan AK, Blanco RR, Zafari AM. Mitochondrial reactive oxygen species and calcium uptake regulate activation of phagocytic NADPH oxidase. *Am J Physiol Regul Integr Comp Physiol* (2012) 302:R1134–42. doi:10.1152/ajpregu.00842.2010
40. Zuckerbraun BS, Chin BY, Bilban M, d'Avila JC, Rao J, Billiar TR, et al. Carbon monoxide signals via inhibition of cytochrome c oxidase and generation of mitochondrial reactive oxygen species. *FASEB J* (2007) 21:1099–106. doi:10.1096/fj.06-6644com
41. Srisook K, Han SS, Choi HS, Li MH, Ueda H, Kim C, et al. CO from enhanced HO activity or from CORM-2 inhibits both O2- and NO production and downregulates HO-1 expression in LPS-stimulated macrophages. *Biochem Pharmacol* (2006) 71:307–18. doi:10.1016/j.bcp.2005.10.042
42. Zollbrecht C, Persson AE, Lundberg JO, Weitzberg E, Carlstrom M. Nitrite-mediated reduction of macrophage NADPH oxidase activity is dependent on xanthine oxidoreductase-derived nitric oxide but independent of S-nitrosation. *Redox Biol* (2016) 10:119–27. doi:10.1016/j.redox.2016.09.015
43. Dutra FF, Bozza MT. Heme on innate immunity and inflammation. *Front Pharmacol* (2014) 5:115. doi:10.3389/fphar.2014.00115
44. Tumer C, Bilgin HM, Obay BD, Diken H, Atmaca M, Kelle M. Effect of nitric oxide on phagocytic activity of lipopolysaccharide-induced macrophages: possible role of exogenous L-arginine. *Cell Biol Int* (2007) 31:565–9. doi:10.1016/j.cellbi.2006.11.029
45. Chiang N, Shinohara M, Dalli J, Mirakaj V, Kibi M, Choi AM, et al. Inhaled carbon monoxide accelerates resolution of inflammation via unique proresolving mediator-heme oxygenase-1 circuits. *J Immunol* (2013) 190:6378–88. doi:10.4049/jimmunol.1202969
46. Hualin C, Wenli X, Dapeng L, Xijing L, Xiuhua P, Qingfeng P. The anti-inflammatory mechanism of heme oxygenase-1 induced by hemin in primary rat alveolar macrophages. *Inflammation* (2012) 35:1087–93. doi:10.1007/s10753-011-9415-4
47. Orozco LD, Kapturczak MH, Barajas B, Wang X, Weinstein MM, Wong J, et al. Heme oxygenase-1 expression in macrophages plays a beneficial role in atherosclerosis. *Circ Res* (2007) 100:1703–11. doi:10.1161/CIRCRESAHA.107.151720
48. Orr GA, Chrisler WB, Cassens KJ, Tan R, Tarasevich BJ, Markillie LM, et al. Cellular recognition and trafficking of amorphous silica nanoparticles by macrophage scavenger receptor A. *Nanotoxicology* (2011) 5:296–311. doi:10.3109/17435390.2010.513836
49. Kuhl T, Imhof D. Regulatory Fe(II/III) heme: the reconstruction of a molecule's biography. *Chembiochem* (2014) 15:2024–35. doi:10.1002/cbic.201402218
50. Yoshida T, Migita CT. Mechanism of heme degradation by heme oxygenase. *J Inorg Biochem* (2000) 82:33–41. doi:10.1016/S0162-0134(00)00156-2

Conflict of Interest Statement: The authors declare that the research was conducted in the absence of any commercial or financial relationships that could be construed as a potential conflict of interest.

3 Discussion

Despite intensive research for almost 50 years, the key regulatory mechanisms responsible for the development of MODS in critical care patients are still incompletely understood. Due to the important role of the liver for immune surveillance and the metabolism, hepatic dysfunction or failure in response to systemic inflammation increases the probability for MODS and associates with high mortality rates (reviewed in Yan et al. 2014).

We applied a clinically relevant model of sepsis to dissect the impact of infectious stimuli and tissue damage on the hepatic ER-stress and inflammatory response. Both conditions are associated with greatly increased enzymatic activities of HO and NOS. In order to elucidate their reciprocal association in the onset and shaping of the UPR and the inflammatory response, we performed *in vitro* studies with hepatocyte and macrophage cell lines.

3.1 Tissue damage and peritoneal infection constitute independent triggers of the hepatic UPR and the inflammatory response.

In this study, we examined a clinically relevant sepsis model (colon ascendens stent peritonitis, CASP) (Maier et al. 2004). The CASP model recapitulates polymicrobial abdominal sepsis and allows the control of the severity of SIRS via the diameter of the stent inserted into the colonic wall (Lustig et al. 2007). We defined the surgical procedure for placing the stent within the abdomen and the associated tissue damage as a trigger for releasing injury-associated signals. The leakage of fecal microorganisms into the peritoneal cavity via the stent, causing infection and peritonitis, was defined as a trigger for the release of infection-associated signals. In order to prevent excessive inflammation-associated tissue damage, which is seen in severe CASP models (Zhang et al. 2018) and superimposes the tissue damage induced by surgery, our samples were obtained from a sepsis model with moderate severity, capable of self-resolution (Herminghaus et al. 2019). This was confirmed by the De Ritis ratio, the quotient of aspartate aminotransferase (AST) and alanine aminotransferase (ALT), which has been described as an exquisite marker for hepatocellular damage (Botros and Sikaris 2013). We found that early after surgery (24 h) De Ritis ratio and AST levels were elevated in both groups undergoing surgery, sham and CASP animals. However, at later time points only (48 h and 96 h) De Ritis ratio was moderately higher in CASP compared to sham animals. This indicates that both, injury-associated signals and infection-associated signals contribute differently to liver cell damage.

In order to understand the association of liver cell damage with inflammatory response and ER stress in the liver, we analyzed markers for inflammation and UPR-signaling in response to CASP and sham surgery. The inflammatory response was clearly different in CASP groups compared to the sham animals. The pro-inflammatory cytokines IL-6 and TNF-α were significantly higher in the CASP group, reaching a maximum at 48 h after surgery with a subsequent decline. Interestingly, expression of iNOS and HO-1 revealed major and sustained differences between CASP and sham groups throughout the entire observation period. This indicates ongoing inflammation-associated stress in the liver, for which both enzymes are sensitive markers. Additionally this indicates an increased formation of the enzyme products in CASP livers later on.

In contrast, the expression profiles of UPR markers were similar in both, sham and CASP groups. XBP1s, indicating activation of the stress sentinel IRE1α, (van Schadewijk et al. 2012), as well as the downstream targets of XBP1s and cleaved ATF6, GRP78 and XBP1 were maximal at 24 h and thereafter declined until 72 h after surgery. Phosphorylated eIF2α, indicating activation of PERK pathway of UPR, continuously rose throughout the observation period to a similar extent in both groups. Markers associated with ER stress induced apoptosis increased by 48 h after surgery, with no differences between the groups. These findings indicate that injury-associated, not infectious signals are primary inducers of the hepatic UPR (**Figure 3A**). However, in the CASP group UPR markers, XBP1s, XBP1 and GRP78 showed stronger correlation with damage markers than in sham animals, suggesting a potential of inflammation-associated stimuli for shaping or fine-tuning the hepatic UPR.

The biatomic gas messengers NO and CO products of NOS and HO, respectively but also HO substrate heme, and heme degradation product BR have the potential to affect major intracellular functions, especially mitochondrial and ER function (Gáll et al. 2018, Higdon et al. 2012, Poderoso et al. 1996, Rodrigues et al. 2002, Zuckerbraun et al. 2007). Therefore, NOS and HO may modulate cellular UPR via their enzymatic reactions. Obviously, the impact of HO and NOS activities on subcellular structures depends on the cell type and its main functions. Considering macrophages' and hepatocytes' different role in inflammation and liver dysfunction, we studied the effect of HO and NOS enzymatic activities on their functions separately using *in vitro* studies.

3.2 HO protects mitochondrial integrity against damage mediated by free heme.

Tissue damage or hemolysis increase the levels of circulating hemoglobin and heme in sepsis (Adamzik et al. 2012, Larsen et al. 2010). Elevated levels of hemoglobin and heme are associated with an adverse effect on outcome in sepsis (Adamzik et al. 2012, Larsen et al. 2010), just as HO-1 deficiency (Larsen et al. 2010). Thus, HO's capacity to degrade heme, which increases in response to cell injury, contributes to cytoprotection, probably also in our CASP model. However, the mechanisms underlying the cytotoxicity of heme and the contribution of the generated HO products to cytoprotection incompletely understood.

Hepatocytes contain of large amounts of ER and abundant mitochondria to execute their secretory and detoxifying functions. We aimed at analyzing the effect of heme and HO degradation products on mitochondrial and ER function in hepatocytes. Long-term analyzes in *in vitro* studies require a stable gene expression profile. In primary liver cells relatively strong changes occur during the first 6 h after isolation, while the liver cell line BRL3A displays a relatively stable gene expression profile over several early passages. However, the gene expression profile from BRL3A cells clearly differs from whole liver (Boess et al. 2003). Therefore, we first tested their sensitivity to hemin and inducers of ER stress. We found them similarly responsive as has been described for primary hepatocytes (Borkham-Kamphorst et al. 2019, Silomon et al. 2007) or whole livers obtained from *in vivo* studies (Duvigneau et al. 2010, Luís et al. 2020).

In order to analyze the capacity of tissue or cell homogenate to convert heme, we applied our *in vitro* biochemical assay for the determination of HO activity based on spectrophotometric quantification of the stable product BR in organic extracts (Kozlov et al. 2010). Additionally, to assess the *in situ* HO activity of living cells, quantification of the formed BR from cell culture medium was performed. Both assays were adapted for taking into account the amount of BR that escapes from the extraction by adsorption to proteins. The capacity of rat liver homogenate and BRL3A cell homogenate degrading heme was similar, confirming suitability of BRL3A cells for analyzing the role of HO and investigating the effects of heme or HO products on subcellular function.

Treatment of BRL3A cells with hemin in combination with the heme analogue zinc protoporphyrin-IX (ZnPP), a competitive HO inhibitor, revealed that intracellular heme causes

a significant drop in mitochondrial membrane potential and increases mitochondrial fragmentation. Hemin, but not ZnPP, applied to isolated mitochondria compromised respiratory function demonstrating that heme itself, when accumulating within the cell, has the potential to compromise mitochondrial function. Since hemin treatment did not result in mitochondrial dysfunction in intact cells with operating HO, we questioned, whether the end product BR, which has previously been shown to protect the membrane interface against oxidant stress (Wu et al. 1991) would afford protection when added in physiological concentrations (Creeden et al. 2021) to hemin-challenged mitochondria. However, BR was not able to prevent heme-mediated decay of mitochondrial function. Instead, we observed that BR reduced the metabolic activity of BRL3A cells and decreased the proliferation rate. Already after 8 h, at concentrations between 4 µmol/l and 20 µmol/l, BR induced markers indicating activation of UPR. We found elevated levels of XBP1s, GRP78 and CHOP. Additionally, we determined increased levels of IL-6, suggesting onset of an inflammatory response, which is known to occur in conditions of ER stress (Zhang and Kaufman 2008). Thus, it appears that BR is capable to induce a similar UPR response as is triggered by pharmacological ER stress inducers (Oakes and Bend 2010, Zhang et al. 2006). BR was found to induce UPR also in other cell systems, such as hepatoma cells (Oakes and Bend 2010) and neurons (Qaisiya et al. 2017). Since BR is able to associate with calcium (van der Veere et al. 1995), it could deplete Ca^{2+}-levels in the ER lumen, and thereby directly contribute to ER stress. Metabolic gene expression networks directly respond to ER homeostasis (Kim et al. 2020). Therefore, the capacity of BR to sensitize ER likely results in the observed reduction in cell proliferation seen in BRL3A cells and a transiently decreased secretory activity of hepatocytes. A similar effect has been described in response to ER stressors in muscle cells, which lower anabolic processes (Deldicque et al. 2011). Further, liver specific depletion of GRP78 results in an exacerbation of liver damage due to an inappropriate UPR and a decreased resistance against ER challenging conditions (Ji et al. 2011). By sensitizing the ER, BR might induce an enhanced protein processing capacity and thereby contribute to stress relief later on, as has been described for the bile salt ER stress reliever TUDCA (Gani et al. 2015).

In conclusion, our data show that the heme-mediated increase in HO activity not only protects mitochondrial function, but may additionally enhance the ER stress response in hepatocytes (**Figure 3B**). Thus it is possible that up-regulation of HO in the livers of animal subjected to CASP, which we have determined (Müllebner et al. 2022), results in sufficient amounts of BR to interfere with UPR signaling. Whether the increased BR production supports the metabolic

function by up-regulating UPR, or limits the cytoprotective action of HO by enhancing ER stress in hepatocytes needs to be answered in subsequent studies.

Although heme is predominantly seen as a cytotoxic molecule, capable to induce pro-inflammatory reactions due to its pro-oxidant character (reviewed in Mendonça et al. 2016), its role for the immune response in the liver is under discussion. Heme and its degradation by HO play an important role for the polarization of macrophages. Acute hemolysis and erythrophagocytosis were shown to abrogate CD40-mediated macrophage activation and to decrease inflammatory cytokine secretion of liver macrophages (Pfefferlé et al. 2021). The anti-inflammatory heme-effect was mediated by increased intracellular heme levels (Pfefferlé et al. 2021), suggesting involvement of HO. Kupffer cells are the major site of expression of HO-1 in the liver under physiological conditions and HO-1 is further induced upon inflammatory stimuli (Immenschuh et al. 1999). Additionally, Kupffer cells mediate the hepatocellular induction of HO-1 in systemic inflammation (Rizzardini et al. 1998). Thus, we can assume that the increased HO-1 expression, which we have seen in our CASP model, can be attributed at least partially to the liver macrophages. Therefore, we next investigated the role of heme and HO on the functional activity of macrophages under resting and inflammatory conditions and its interplay with iNOS.

3.3 While NOS via NO directly contributes to the bactericidal activity of macrophages, HO contributes indirectly, by removing heme

Generation of ROS and NO is critical for the bactericidal function of macrophages. These highly reactive species are essential for killing microorganisms after phagocytic uptake (reviewed in Fang 2004). mtROS are needed for the activation of the NADPH-oxidase (NOX) activity (reviewed in Daiber 2010 and Dikalov 2011), the major source of ROS in macrophages. We have previously shown that NOS via the generated NO is capable to boost mitochondrial ROS-generation in livers and isolated hepatocytes of rats subjected to LPS (Weidinger et al. 2015). Increased mtROS generation may relate to the capability of biatomic gaseous messengers to inhibit heme-containing enzymes of the mitochondrial electron transport chain. This mechanism was shown for direct CO application, which moderately increased mtROS production by inhibiting cytochrome C (Zuckerbraun et al. 2007). This effect was associated with a decreased TNF-α production and should explain the anti-inflammatory action of CO application (Zuckerbraun et al. 2007). However, it is unclear whether a similar effect can be elicited by the endogenously formed products.

In order to understand contribution of the enzymatic activities of NOS and HO on ROS production in macrophages, we used the mouse macrophage cell line J774A.1. Initially, we validated the suitability of our system. Macrophages stimulated with LPS produce significant amounts of NO, as is exemplified in the kinetics of nitrite (an oxidation product of NO) accumulation in the medium of a rodent macrophage cell line, J774A.1 (**Unpublished data Figure 1**). Increased nitrite levels were determined already after 16 h, and further increased until 48 h of incubation. Addition of non-isoform selective inhibitors L-NAME or S-methyl-L-thiocitrulline to LPS-stimulated macrophages vastly blocked NO formation, indicating suitability of these compounds to inhibit NOS activity.

Stimulation of macrophages with 20 µmol/l heme resulted in a markedly increased HO activity. This was exemplified by the increased capacity of cell homogenate to degrade heme *in-vitro* assay (Duvigneau et al. 2020, Warenits et al. 2020) and by the many-fold higher amounts of BR extracted from the incubation medium of J774A.1 cells treated with heme (*in-situ* assay). The values obtained with both assays yield highly consistent results and correlate with HO-1 gene expression (**Unpublished data Figure 2**). Stimulation of cultured J774A.1 cells for 16 h with 2 µmol/l heme was already sufficient to increase *in-situ* HO activity by trend, but significantly higher levels of BR accumulated in medium upon stimulation with 20 µmol/l heme (**Unpublished data Figure 2A**). LPS stimulation prior to heme treatment further increased HO activity in J774A.1 cells, resulting in a nearly 5-fold higher capacity to convert heme compared to the untreated control cells (**Unpublished data Figure 2A**). Using ZnPP at a concentration of 20 µmol/l we found a substantial reduction of the *in situ* HO activity (**Unpublished data Figure 3A**). ZnPP at this concentration has previously been shown not to interact with NOS activity or with the activity of soluble guanylate cyclase (Appleton et al. 1999). Therefore, we considered these concentrations suitable for our experiments. However, incubation with ZnPP resulted in super-induction of HO-1 (**Unpublished data Figure 3B**). It can be assumed that this effect is mediated by two synergistically operating conditions, the increased intracellular heme levels due to the inhibition of heme degradation and the presence of ZnPP. Porphyrins are capable to bind to the Bach repressor, leading to recruitment of Nrf2, and thereby enhance HO-1 gene expression (reviewed in Schulz et al. 2012). In order to exclude an overcoming of HO activity inhibition by increased HO 1 protein abundance, we limited our investigations to an incubation time of maximal 16 h, where inhibition was confirmed.

In resting macrophages scavenging of mtROS using mitochondria targeted antioxidant mitoTEMPO reduced both, the rates of mitochondrial and NOX mediated ROS release in response to Phorbol 12-myristate 13-acetate treatment. These findings point towards the essential role of mitochondria in the regulation of NOX in our model. Inhibition of NOS caused a similar effect, a decrease of both mitochondrial and NOX mediated ROS generation, supporting the involvement of NOS in the regulation of ROS. In contrast, acute inhibition of HO did not substantially influence the release of ROS, neither from mitochondria nor from NOX. These findings are in contrast to what has been reported for direct application of CO to macrophages (Zuckerbraun et al. 2007), suggesting that the amount of CO generated by the HO reaction *in situ* doses not suffice to result in an inhibition of cytochrome c. Thus, NOS, but not HO, acutely regulates the release of ROS in macrophages. These data suggest that HO does not directly contribute to the biocidal activity of macrophages. This is also confirmed by our findings, that stimulation of HO using heme did not affect survival of bacteria phagocytosed by J774A.1 cells (**Unpublished data Figure 4A, B**). However, examination of phagocytosis rate revealed that while inhibition of NOS does not influence uptake of bacteria, inhibition of HO substantially reduces phagocytic activity. Acutely added hemin further reduced the phagocytic activity. Another study confirmed the inhibitory effect of hemin on phagocytosis of macrophages, suggesting a disruption of cytoskeletal dynamics as an underlying mechanism (Martins et al. 2016). This shows that heme itself, similarly to what we have found for hepatocytes, exerts an inhibitory effect on main cellular functions also in macrophages. This inhibition is abrogated by HO via removal of heme. We have shown that hemin (with iron in its ferric form), when taken up into the cells, is reduced into heme (with iron in its ferrous form), which acts as pro-oxidative species. The reduction of phagocytosis may represent a mechanism for protecting the cell against excessively increased intracellular heme levels and confirms that HO exerts its predominant protection by removal of its substrate

In LPS treated iNOS-expressing macrophages challenged with hemin the reactions of both enzymes, NOS and HO, are supposed to run in parallel, if sufficient substrates are available. NO leads to nitrosylation of intracellular ferrous heme (**Unpublished data Figure 5A**) and thus potentially inhibits enzymatic reactions at micromolar concentrations (Juckett et al. 1998). We questioned whether active NOS would affect simultaneous heme degradation of macrophages. Therefore, we tested the influence of inhibition of NOS enzymatic activity on the HO-1 expression and HO activity (**Unpublished data Figure 5B, C**). Inhibition of NOS activity did neither affect HO-1 expression nor heme degradation suggesting, that NOS does not regulate

HO activity in macrophages, at least under conditions used in our experimental models. In contrast, the HO substrate hemin greatly affected NOS as indicated by reduced iNOS gene expression and nitrite levels (**Unpublished data Figure 6A, B**). This is in line with reports of decreased iNOS expression and NO production via up-regulation of HO-1 in hemin-treated macrophages and astrocytes (Lin et al. 2003, Sheng et al. 2010). Reduction of nitrite levels was partly reverted upon adding the HO inhibitor chromium-mesoporphyrin to cultured J774A.1, suggesting that formation of an HO product is responsible for this effect. Indeed, our findings confirm that BR is able to inhibit NO production in LPS stimulated J774A.1 macrophages (**Unpublished data Figure 6C**), similarly to what has been found by others (Wang et al. 2004). Additionally, BR reduced the inflammatory response in an *in vivo* model of hind limb inflammation (Wang et al. 2004), indicating that the cellular HO enzymatic activity is capable to terminate an up-regulated biocidal activity of macrophages.

Our data suggest that heme degradation by HO influences macrophage function by two pathways; it supports phagocytosis by removing intracellular heme and it down-regulates iNOS and limits NO production by increased product generation due to the elevated HO activity. HO products, by down-modulating iNOS expression slow down and terminate the pro-inflammatory NOS/ROS/NOX pathway, which is required for the bactericidal activity. Thus, heme-induced formation of HO products contributes to a time-dependent shift of the macrophage function from pro-inflammatory to anti-inflammatory.

Additionally, UPR has an important role for the regulation of macrophage polarization. Knockdown of PERK by RNA silencing increased iNOS and inhibited expression of the anti-inflammatory marker protein arginase 1, suggesting a pro-inflammatory phenotype (Soto-Pantoja et al. 2017). Vice versa, LPS-activated macrophages decreased UPR signaling induced by pharmacological ER stressors. These macrophages displayed lower expression levels of pro-inflammatory cytokines, indicative for a shift of the macrophage polarity towards anti-inflammatory (Soto-Pantoja et al. 2017).

Since we found that HO via BR modulates UPR in hepatocytes, we next analyzed the potential of HO substrate and inhibitors to affect UPR in macrophages. We show that treatment with LPS up-regulated UPR (**Unpublished data Figure 7**). LPS-stimulated expression of XBP1 and GRP78 was completely blocked upon inhibition of endogenous heme degradation using ZnPP. However, additional heme, which leads to HO-1 super-induction and partially overcomes ZnPP inhibition, was able to restore XBP1 and GRP78 expression levels to some

extent (**Unpublished data Figure 7A, B**). In contrast, ZnPP could not down-modulate expression of CHOP, an upstream target of PERK, which increased in response to LPS. Hemin-mediated HO induction even further enhanced CHOP expression (**Unpublished data Figure 7C**). Thus, in macrophages heme and HO products both affect stress induced UPR signaling. Heme degradation is required to support LPS-induced IRE1α signaling, while CHOP expression seems to involve HO product formation, possibly BR, as shown for hepatocytes. Thus, our findings show that HO supports the LPS-triggered UPR either by heme removal or by accumulation of HO reaction products. Our data might be interpreted that HO by enhancing UPR in macrophages contributes to shift polarization of macrophages towards an anti-inflammatory phenotype (Soto-Pantoja et al. 2017). However this needs to be confirmed by additional experiments (**Figure 3C**).

Thus, the ER stress response, seen in the livers of our peritonitis rats, likely results from the cumulative responses of hepatocytes and macrophages. Both, heme removal and HO products generated by heme degradation are capable to sensitize ER and enhance UPR in both hepatocytes and macrophages. Although the enhanced UPR may transiently lower the secretory function of both, hepatocytes and macrophages, it may contribute to restore homeostasis and tissue remodeling and foster resolution of inflammation.

In conclusion, our findings using cell culture models indicate that HO has an important role in controlling central functions of hepatocytes and macrophages. Both cell types can contribute to the increased HO-1 expression, which we have found in the liver of CASP animals, and which is probably caused by elevated heme levels released during the inflammatory reaction. We suggest that both, the removal of heme and the generation of HO products constitute different aspects of cytoprotection exerted in a coordinated and time dependent fashion.

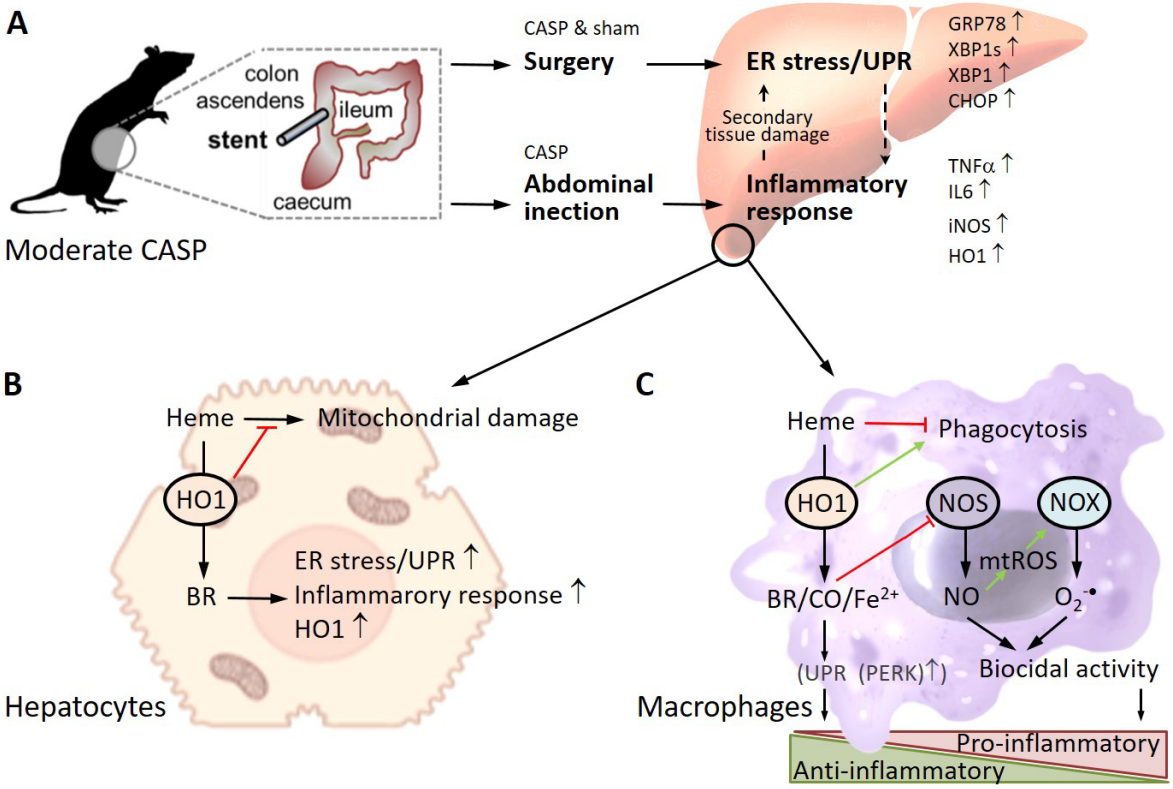

Figure 3: HO activity exerts a beneficial effect on liver ameliorating mitochondrial function and modulating macrophage activity. (A) In moderate colon ascendens stent peritonitis unfolded protein response (UPR) was primarily associated with surgery (tissue damage), while up-regulation of heme oxygenase (HO) -1 and inducible NO synthase (iNOS) observed in this model was primarily associated with abdominal infection (inflammatory response). **(B)** In hepatocytes an increased HO activity affects both, mitochondria and ER. Removal of heme protects mitochondria from heme induced oxidative damage, while the HO product bilirubin (BR) up-regulates UPR. **(C)** In macrophages NOS supports bactericidal activity by enhancing ROS production involving NADPH oxidase activation via increased mitochondrial ROS production. HO by heme removal supports phagocytosis. HO products (BR) dampen the inflammatory response of macrophages by down-modulating iNOS and possibly by up-regulating PERK-branch of UPR.

3.4 Conclusions

1. Here we show that ER-stress induced in clinically relevant sepsis model is not associated primarily with infection but with tissue damage. In contrast, up-regulation of HO-1 and iNOS observed in this model was primarily associated with the inflammatory response.
2. In hepatocytes an increased HO activity affects both, mitochondria and ER. Removal of heme protects mitochondria, while the HO product BR sensitizes ER and up-regulates UPR.
3. In macrophages NOS and HO regulate main macrophage functions distinctly. NOS supports bactericidal activity by enhancing ROS production involving NOX activation via increased mtROS production.
4. In contrast, heme removal by HO supports phagocytosis and IRE1α-mediated UPR signaling. HO products dampen the inflammatory response of macrophages by down-modulating iNOS and possibly by up-regulating PERK-branch of UPR.

Thus, inflammation mediated HO contributes to the restoration of liver homeostasis in moderate sepsis by multiple mechanisms. Our findings in hepatocytes and macrophages suggest that up-regulation of the cellular HO activity is capable to lower the inflammatory response contributes to liver homeostasis, is facilitated by elevated heme levels.

4 Summary

Liver dysfunction constitutes a serious complication in sepsis contributing to disease progression and death. It is supposed to result from a functional impairment of parenchymal cells induced by metabolic changes going along systemic inflammation. There exists evidence suggesting that disturbance of protein folding machinery, a condition called endoplasmic reticulum (ER) stress and subsequent induction of the unfolded protein response (UPR) are involved in these processes. Whether the initial triggers of hepatic ER stress and UPR are associated with tissue trauma or infection has not been addressed so far. Upon systemic inflammation heme oxygenase (HO) and nitric oxide synthase (NOS) activities are markedly increased due to up-regulation of stress inducible enzymes HO-1 and inducible NOS (iNOS). The activities of both enzymes are interactive and assumed to be involved in onset and shaping of the UPR and inflammatory response.

Thus, in the first part of this thesis, we aimed to dissect the role of infection and injury on the progression of HO-1 and iNOS gene expression in parallel with UPR markers in liver in a clinically relevant sepsis model. The aim of the second part of this thesis was to recapitulate the observed changes in hepatocytes and macrophages as they are considered key players in the development of liver dysfunction. In the hepatocyte cell line BRL3A we studied the protective role of the HO reaction and the HO product bilirubin against heme induced oxidative damage of mitochondria and ER. In macrophage cell line J774A.1 we studied the interplay of HO and NOS activity and their effects on the functional activity and stress response of macrophages under resting and inflammatory conditions.

Our results show, that ER-stress was not primarily associated with infection but with tissue damage in moderate sepsis. In contrast, HO-1 and iNOS were up-regulated in context with inflammatory response. Increased HO activity in hepatocytes directly protects mitochondria from heme induced oxidative damage by removal of heme, while bilirubin triggers UPR. In macrophages HO and NOS independently regulate main macrophage functions. NOS supports bactericidal activity by enhancing NADPH oxidase activity via increased mitochondrial reactive oxygen species production. HO supports phagocytosis by heme degradation, which is also involved in lipopolysaccharide induced UPR signaling. High levels of HO products dampen pro-inflammatory response in macrophages by down-modulating iNOS possibly in a UPR dependent manner.

To summarize, our data show that upon moderate sepsis HO activity exerts a beneficial effect on liver ameliorating mitochondrial function and modulating macrophage activity.

5 Zusammenfassung

Leberfunktionsstörungen stellen eine schwerwiegende Komplikation bei Sepsis dar, die zum Fortschreiten der Krankheit und zum Tod beiträgt. Die Ursache wird auf die durch systemische Entzündung hervorgerufenen Stoffwechselveränderungen und daraus resultierende Funktionsbeeinträchtigung parenchymaler Zellen zurückgeführt. Eine Störung der Proteinfaltungsmaschinerie, welche als endoplasmatischer Retikulums (ER) Stress bezeichnet wird und die dadurch eingeleitete „unfolded protein response“ (UPR) sollen an diesem Prozessen beteiligt sein. Ob die primären Auslöser von hepatischem ER-Stress und UPR mit einem Gewebetrauma oder einer Infektion zusammenhängen, wurde bisher nicht untersucht. Bei systemischen Entzündungen sind durch Hochregulierung der stressinduzierbaren Enzyme Hämoxygenase (HO)-1 und der induzierbaren Stickstoffmonoxid-Synthase (iNOS) die entsprechenden enzymatischen Aktivitäten deutlich erhöht. Diese wechselwirken miteinander und es wird angenommen, dass sie an der Einleitung und Regulation von UPR und Entzündungsreaktionen beteiligt sind.

Daher untersuchten wir im ersten Teil dieser Arbeit die Rolle von Entzündung und Verletzungen auf den Verlauf der Genexpression von HO-1 und iNOS parallel zu UPR-Markern in der Leber in einem klinisch relevanten Sepsis-Modell. Das Ziel des zweiten Teils dieser Arbeit war es, die beobachteten Veränderungen in Hepatozyten und Makrophagen nachzustellen, da diese als Schlüsselakteure bei der Entwicklung von Leberfunktionsstörungen gelten. In der Hepatozyten-Zelllinie BRL3A untersuchten wir die schützende Rolle der HO-Reaktion und des HO-Produkts Bilirubin gegen Häm-induzierte oxidative Schäden an Mitochondrien und ER. In der Makrophagen-Zelllinie J774A.1 untersuchten wir das Zusammenspiel von HO und NOS-Aktivität und ihre Auswirkungen auf Funktion und Stressreaktion von Makrophagen unter Ruhe- und Entzündungsbedingungen.

Unsere Ergebnisse zeigen, dass ER-Stress bei moderater Sepsis nicht primär mit Infektionen, sondern mit Gewebeschäden assoziiert war. Im Gegensatz dazu wurden HO-1 und iNOS im Zusammenhang mit der Entzündungsreaktion hochreguliert. Eine erhöhte HO-Aktivität in Hepatozyten schützt die Mitochondrien durch Abbau von Häm direkt vor oxidativen Schäden, während Bilirubin UPR auslöst. In Makrophagen regulieren HO und NOS unabhängig voneinander die wichtigsten Makrophagenfunktionen. NOS unterstützt die bakterizide Aktivität, indem es, über eine erhöhte Produktion mitochondrialer reaktiver Sauerstoffspezies, die Aktivität der NADPH-Oxidase steigert. HO unterstützt die Phagozytose durch Häm-Abbau,

der auch die Lipopolysaccharid-induzierten UPR-Signalübertragungswege beeinflusst. Hohe Mengen an HO-Produkten dämpfen eine proinflammatorische Reaktion in Makrophagen, indem sie iNOS, möglicherweise in einer UPR-abhängigen Weise, heruntermodulieren. Zusammenfassend zeigen unsere Daten, dass die HO-Aktivität bei moderater Sepsis eine positive Wirkung auf die Leber ausübt, indem sie die mitochondriale Funktion verbessert und die Makrophagenaktivität moduliert.

6 Abbreviations

ALT	alanine aminotransferase
AST	aspartate aminotransferase
ATF	activating transcription factor
BR	bilirubin
CASP	colon ascendens stent peritonitis
CHOP	CAAT/Enhancer binding protein (C/EBP) homolgous protein
CO	carbon monoxide
CrMP	chromium mesoporphyrin
EC	enzyme classification
eIF2α	eukaryotic translation initiation factor 2 alpha subunit
eNOS	endothelial nitric oxide synthase
ER	endoplasmic reticulum
ERAD	ER associated protein degradation
GRP78	glucose regulated protein 78
HO	heme oxygenase
HS	hydrogen sulfide
iNOS	inducible nitric oxide synthase
IRE1	inositol requiring enzyme 1
IL	interleukin

LPS	lipopolysaccharide
MAPK	p38 mitogen activated protein kinase
MODS	multiple organ dysfunction
mtROS	mitochondrial ROS
nNOS	neuronal nitric oxide synthase
NADPH	nicotinamide adenine dinucleotide phosphate
NO	nitric oxide
NOX	NADPH oxidase
Nrf2	nuclear factor-erythroid-derived 2 (NF-E2)-related factor 2
NF-κB	nuclear factor κ-light-chain-enhancer of activated B cells
NO	nitric oxide
NOS	nitric oxide synthase
PERK	protein kinase RNA-activated (PKR)-like ER kinase
ROS	reactive oxygen species
RONS	reactive oxygen and nitrogen species
S1P	site-1 protease
S2P	site-2 protease
SIRS	systemic inflammatory response syndrome
TNF-α	tumor necrosis factor alpha
UPR	unfolded protein response

XBP1	X-box binding protein
XBP1s	XBP1 spliced
ZnPP	zinc protoporphyrin-IX

7 References

Adamzik M, Hamburger T, Petrat F, Peters J, Groot H de, Hartmann M. 2012. Free hemoglobin concentration in severe sepsis: methods of measurement and prediction of outcome. Critical care (London, England), 16 (4): R125. DOI 10.1186/cc11425.

Almanza A, Carlesso A, Chintha C, Creedican S, Doultsinos D, Leuzzi B, Luís A, McCarthy N, Montibeller L, More S, Papaioannou A, Püschel F, Sassano ML, Skoko J, Agostinis P, Belleroche J de, Eriksson LA, Fulda S, Gorman AM, Healy S, Kozlov A, Muñoz-Pinedo C, Rehm M, Chevet E, Samali A. 2019. Endoplasmic reticulum stress signalling - from basic mechanisms to clinical applications. The FEBS journal, 286 (2): 241–278. DOI 10.1111/febs.14608.

Appleton SD, Chretien ML, McLaughlin BE, Vreman HJ, Stevenson DK, Brien JF, Nakatsu K, Maurice DH, Marks GS. 1999. Selective inhibition of heme oxygenase, without inhibition of nitric oxide synthase or soluble guanylyl cyclase, by metalloporphyrins at low concentrations. Drug metabolism and disposition: the biological fate of chemicals, 27 (10): 1214–1219.

Balla G, Jacob HS, Balla J, Rosenberg M, Nath K, Apple F, Eaton JW, Vercellotti GM. 1992. Ferritin: a cytoprotective antioxidant strategem of endothelium. Journal of Biological Chemistry, 267 (25): 18148–18153. DOI 10.1016/S0021-9258(19)37165-0.

Bertolotti A, Zhang Y, Hendershot LM, Harding HP, Ron D. 2000. Dynamic interaction of BiP and ER stress transducers in the unfolded-protein response. Nature cell biology, 2 (6): 326–332. DOI 10.1038/35014014.

Bilzer M, Roggel F, Gerbes AL. 2006. Role of Kupffer cells in host defense and liver disease. Liver international : official journal of the International Association for the Study of the Liver, 26 (10): 1175–1186. DOI 10.1111/j.1478-3231.2006.01342.x.

Boess F, Kamber M, Romer S, Gasser R, Muller D, Albertini S, Suter L. 2003. Gene expression in two hepatic cell lines, cultured primary hepatocytes, and liver slices compared to the in vivo liver gene expression in rats: possible implications for toxicogenomics use of in vitro systems. Toxicological sciences : an official journal of the Society of Toxicology, 73 (2): 386–402. DOI 10.1093/toxsci/kfg064.

Bone RC, Balk RA, Cerra FB, Dellinger RP, Fein AM, Knaus WA, Schein RM, Sibbald WJ. 1992. Definitions for sepsis and organ failure and guidelines for the use of innovative therapies in sepsis. The ACCP/SCCM Consensus Conference Committee. American College of Chest Physicians/Society of Critical Care Medicine. Chest, 101 (6): 1644–1655. DOI 10.1378/chest.101.6.1644.

Borkham-Kamphorst E, van de Leur E, Haas U, Weiskirchen R. 2019. Liver parenchymal cells lacking Lipocalin 2 (LCN2) are prone to endoplasmic reticulum stress and unfolded protein response. Cellular signalling, 55: 90–99. DOI 10.1016/j.cellsig.2019.01.001.

Botros M, Sikaris KA. 2013. The de ritis ratio: the test of time. The Clinical biochemist. Reviews, 34 (3): 117–130. DOI 10.1046/j.0013-0427.2003.00027.x.

Brüne B, Ullrich V. 1987. Inhibition of platelet aggregation by carbon monoxide is mediated by activation of guanylate cyclase. Molecular Pharmacology, 32 (4): 497–504.

Castell JV, Gómez-Lechón MJ, David M, Andus T, Geiger T, Trullenque R, Fabra R, Heinrich PC. 1989. Interleukin-6 is the major regulator of acute phase protein synthesis in adult human hepatocytes. FEBS letters, 242 (2): 237–239. DOI 10.1016/0014-5793(89)80476-4.

Chen X, Wang Y, Xie X, Chen H, Zhu Q, Ge Z, Wei H, Deng J, Xia Z, Lian Q. 2018. Heme Oxygenase-1 Reduces Sepsis-Induced Endoplasmic Reticulum Stress and Acute Lung Injury. Mediators of inflammation, 2018: 9413876. DOI 10.1155/2018/9413876.

Chuniaud L, Dessante M, Chantoux F, Blondeau JP, Francon J, Trivin F. 1996. Cytotoxicity of bilirubin for human fibroblasts and rat astrocytes in culture. Effect of the ratio of bilirubin to serum albumin. Clinica chimica acta; international journal of clinical chemistry, 256 (2): 103–114. DOI 10.1016/s0009-8981(96)06407-8.

Creeden JF, Gordon DM, Stec DE, Hinds TD. 2021. Bilirubin as a metabolic hormone: the physiological relevance of low levels. American journal of physiology. Endocrinology and metabolism, 320 (2): E191-E207. DOI 10.1152/ajpendo.00405.2020.

Cullinan SB, Zhang D, Hannink M, Arvisais E, Kaufman RJ, Diehl JA. 2003. Nrf2 is a direct PERK substrate and effector of PERK-dependent cell survival. Molecular and cellular biology, 23 (20): 7198–7209. DOI 10.1128/MCB.23.20.7198-7209.2003.

Daiber A. 2010. Redox signaling (cross-talk) from and to mitochondria involves mitochondrial pores and reactive oxygen species. Biochimica et biophysica acta, 1797 (6-7): 897–906. DOI 10.1016/j.bbabio.2010.01.032.

Deldicque L, Bertrand L, Patton A, Francaux M, Baar K. 2011. ER stress induces anabolic resistance in muscle cells through PKB-induced blockade of mTORC1. PloS one, 6 (6): e20993. DOI 10.1371/journal.pone.0020993.

Deng J, Lu PD, Zhang Y, Scheuner D, Kaufman RJ, Sonenberg N, Harding HP, Ron D. 2004. Translational repression mediates activation of nuclear factor kappa B by phosphorylated translation initiation factor 2. Molecular and cellular biology, 24 (23): 10161–10168. DOI 10.1128/MCB.24.23.10161-10168.2004.

Dhainaut JF, Marin N, Mignon A, Vinsonneau C. 2001. Hepatic response to sepsis: interaction between coagulation and inflammatory processes. Critical care medicine, 29 (7 Suppl): S42-7. DOI 10.1097/00003246-200107001-00016.

Dikalov S. 2011. Cross talk between mitochondria and NADPH oxidases. Free radical biology & medicine, 51 (7): 1289–1301. DOI 10.1016/j.freeradbiomed.2011.06.033.

Dizier S, Forel J-M, Ayzac L, Richard J-C, Hraiech S, Lehingue S, Loundou A, Roch A, Guerin C, Papazian L. 2015. Early Hepatic Dysfunction Is Associated with a Worse Outcome in Patients Presenting with Acute Respiratory Distress Syndrome: A Post-Hoc Analysis of the ACURASYS and PROSEVA Studies. PloS one, 10 (12): e0144278. DOI 10.1371/journal.pone.0144278.

Dubois V, Gheeraert C, Vankrunkelsven W, Dubois-Chevalier J, Dehondt H, Bobowski-Gerard M, Vinod M, Zummo FP, Güiza F, Ploton M, Dorchies E, Pineau L, Boulinguiez A, Vallez E, Woitrain E, Baugé E, Lalloyer F, Duhem C, Rabhi N, van Kesteren RE, Chiang C-M, Lancel S, Duez H, Annicotte J-S, Paumelle R, Vanhorebeek I, van den Berghe G, Staels B, Lefebvre P, Eeckhoute J. 2020. Endoplasmic reticulum stress actively suppresses hepatic molecular identity in damaged liver. Molecular systems biology, 16 (5): e9156. DOI 10.15252/msb.20199156.

Duvigneau JC, Kozlov AV, Zifko C, Postl A, Hartl RT, Miller I, Gille L, Staniek K, Moldzio R, Gregor W, Haindl S, Behling T, Redl H, Bahrami S. 2010. Reperfusion does not induce

oxidative stress but sustained endoplasmic reticulum stress in livers of rats subjected to traumatic-hemorrhagic shock. Shock (Augusta, Ga.), 33 (3): 289–298. DOI 10.1097/SHK.0b013e3181aef322.

Duvigneau JC, Trovato A, Müllebner A, Miller I, Krewenka C, Krenn K, Zich W, Moldzio R. 2020. Cannabidiol Protects Dopaminergic Neurons in Mesencephalic Cultures against the Complex I Inhibitor Rotenone Via Modulation of Heme Oxygenase Activity and Bilirubin. Antioxidants (Basel, Switzerland), 9 (2). DOI 10.3390/antiox9020135.

Eisenstein RS, Garcia-Mayol D, Pettingell W, Munro HN. 1991. Regulation of ferritin and heme oxygenase synthesis in rat fibroblasts by different forms of iron. Proceedings of the National Academy of Sciences of the United States of America, 88 (3): 688–692. DOI 10.1073/pnas.88.3.688.

Fang FC. 2004. Antimicrobial reactive oxygen and nitrogen species: concepts and controversies. Nature reviews. Microbiology, 2 (10): 820–832. DOI 10.1038/nrmicro1004.

Fribley A, Zhang K, Kaufman RJ. 2009. Regulation of apoptosis by the unfolded protein response. Methods in molecular biology (Clifton, N.J.), 559: 191–204. DOI 10.1007/978-1-60327-017-5_14.

Gáll T, Pethő D, Nagy A, Hendrik Z, Méhes G, Potor L, Gram M, Åkerström B, Smith A, Nagy P, Balla G, Balla J. 2018. Heme Induces Endoplasmic Reticulum Stress (HIER Stress) in Human Aortic Smooth Muscle Cells. Frontiers in physiology, 9: 1595. DOI 10.3389/fphys.2018.01595.

Gani AR, Uppala JK, Ramaiah KVA. 2015. Tauroursodeoxycholic acid prevents stress induced aggregation of proteins in vitro and promotes PERK activation in HepG2 cells. Archives of biochemistry and biophysics, 568: 8–15. DOI 10.1016/j.abb.2014.12.031.

Garaude J, Acín-Pérez R, Martínez-Cano S, Enamorado M, Ugolini M, Nistal-Villán E, Hervás-Stubbs S, Pelegrín P, Sander LE, Enríquez JA, Sancho D. 2016. Mitochondrial respiratory-chain adaptations in macrophages contribute to antibacterial host defense. Nature immunology, 17 (9): 1037–1045. DOI 10.1038/ni.3509.

Gozzelino R, Jeney V, Soares MP. 2010. Mechanisms of cell protection by heme oxygenase-1. Annual review of pharmacology and toxicology, 50: 323–354. DOI 10.1146/annurev.pharmtox.010909.105600.

Halliwell B, Gutteridge JM. 1984. HalliwellB_BiochemJ_1984_6326753 // Oxygen toxicity, oxygen radicals, transition metals and disease. The Biochemical journal, 219 (1): 1–14. DOI 10.1042/bj2190001.

Hartsfield CL. 2002. Cross talk between carbon monoxide and nitric oxide. Antioxidants and Redox Signaling, 4 (2): 301–307. DOI 10.1089/152308602753666352.

He CH, Gong P, Hu B, Stewart D, Choi ME, Choi AM, Alam J. 2001. Identification of activating transcription factor 4 (ATF4) as an Nrf2-interacting protein. Implication for heme oxygenase-1 gene regulation. The Journal of biological chemistry, 276 (24): 20858–20865. DOI 10.1074/jbc.M101198200.

Herminghaus A, Papenbrock H, Eberhardt R, Vollmer C, Truse R, Schulz J, Bauer I, Weidinger A, Kozlov AV, Stiban J, Picker O. 2019. Time-related changes in hepatic and colonic mitochondrial oxygen consumption after abdominal infection in rats. Intensive care medicine experimental, 7 (1): 4. DOI 10.1186/s40635-018-0219-9.

Higdon AN, Benavides GA, Chacko BK, Ouyang X, Johnson MS, Landar A, Zhang J, Darley-Usmar VM. 2012. Hemin causes mitochondrial dysfunction in endothelial cells through promoting lipid peroxidation: the protective role of autophagy. American journal of physiology. Heart and circulatory physiology, 302 (7): H1394-409. DOI 10.1152/ajpheart.00584.2011.

Hu F, Yu X, Wang H, Zuo D, Guo C, Yi H, Tirosh B, Subjeck JR, Qiu X, Wang X-Y. 2011. ER stress and its regulator X-box-binding protein-1 enhance polyIC-induced innate immune response in dendritic cells. European journal of immunology, 41 (4): 1086–1097. DOI 10.1002/eji.201040831.

Immenschuh S, Tan M, Ramadori G. 1999. Nitric oxide mediates the lipopolysaccharide dependent upregulation of the heme oxygenase-1 gene expression in cultured rat Kupffer cells. Journal of hepatology, 30 (1): 61–69. DOI 10.1016/s0168-8278(99)80008-7.

Jenne CN, Kubes P. 2013. Immune surveillance by the liver. Nature immunology, 14 (10): 996–1006. DOI 10.1038/ni.2691.

Ji C, Kaplowitz N, Lau MY, Kao E, Petrovic LM, Lee AS. 2011. Liver-specific loss of glucose-regulated protein 78 perturbs the unfolded protein response and exacerbates a spectrum of liver diseases in mice. Hepatology (Baltimore, Md.), 54 (1): 229–239. DOI 10.1002/hep.24368.

Juckett M, Zheng Y, Yuan H, Pastor T, Antholine W, Weber M, Vercellotti G. 1998. Heme and the endothelium. Effects of nitric oxide on catalytic iron and heme degradation by heme oxygenase. The Journal of biological chemistry, 273 (36): 23388–23397. DOI 10.1074/jbc.273.36.23388.

Kadl A, Pontiller J, Exner M, Leitinger N. 2007. Single bolus injection of bilirubin improves the clinical outcome in a mouse model of endotoxemia. Shock (Augusta, Ga.), 28 (5): 582–588. DOI 10.1097/shk.0b013e31804d41dd.

Kim JS, Hwang S in, Ryu JL, Hong HS, Lee J-M, Lee SM, Jin X, Han C, Kim J-H, Han J, Lee M-R, Woo D-H. 2020. ER stress reliever enhances functionalities of in vitro cultured hepatocytes. Stem cell research, 43: 101732. DOI 10.1016/j.scr.2020.101732.

Kirkby KA, Adin CA. 2006. Products of heme oxygenase and their potential therapeutic applications. American journal of physiology. Renal physiology, 290 (3): F563-71. DOI 10.1152/ajprenal.00220.2005.

Koch A, Horn A, Dückers H, Yagmur E, Sanson E, Bruensing J, Buendgens L, Voigt S, Trautwein C, Tacke F. 2011. Increased liver stiffness denotes hepatic dysfunction and mortality risk in critically ill non-cirrhotic patients at a medical ICU. Critical care (London, England), 15 (6): R266. DOI 10.1186/cc10543.

Kopp MC, Larburu N, Durairaj V, Adams CJ, Ali MMU. 2019. UPR proteins IRE1 and PERK switch BiP from chaperone to ER stress sensor. Nature structural & molecular biology, 26 (11): 1053–1062. DOI 10.1038/s41594-019-0324-9.

Koppenol WH. 2022. Ferryl for real. The Fenton reaction near neutral pH. Dalton transactions (Cambridge, England : 2003), 51 (45): 17496–17502. DOI 10.1039/d2dt03168j.

Kozlov AV, Grillari J. 2022. Pathogenesis of Multiple Organ Failure: The Impact of Systemic Damage to Plasma Membranes. Frontiers in medicine, 9: 806462. DOI 10.3389/fmed.2022.806462.

Kozlov AV, Lancaster JR, Meszaros AT, Weidinger A. 2017. Mitochondria-meditated pathways of organ failure upon inflammation. Redox biology, 13: 170–181. DOI 10.1016/j.redox.2017.05.017.

Kozlov AV, van Griensven M, Haindl S, Kehrer I, Duvigneau JC, Hartl RT, Ebel T, Jafarmadar M, Calzia E, Gnaiger E, Redl H, Radermacher P, Bahrami S. 2010. Peritoneal inflammation in pigs is associated with early mitochondrial dysfunction in liver and kidney. Inflammation, 33 (5): 295–305. DOI 10.1007/s10753-010-9185-4.

Kumar S, Bandyopadhyay U. 2005. Free heme toxicity and its detoxification systems in human. Toxicology letters, 157 (3): 175–188. DOI 10.1016/j.toxlet.2005.03.004.

Larsen R, Gozzelino R, Jeney V, Tokaji L, Bozza FA, Japiassú AM, Bonaparte D, Cavalcante MM, Chora A, Ferreira A, Marguti I, Cardoso S, Sepúlveda N, Smith A, Soares MP. 2010. A central role for free heme in the pathogenesis of severe sepsis. Science translational medicine, 2 (51): 51ra71. DOI 10.1126/scitranslmed.3001118.

Lerner AG, Upton J-P, Praveen PVK, Ghosh R, Nakagawa Y, Igbaria A, Shen S, Nguyen V, Backes BJ, Heiman M, Heintz N, Greengard P, Hui S, Tang Q, Trusina A, Oakes SA, Papa FR. 2012. IRE1α induces thioredoxin-interacting protein to activate the NLRP3 inflammasome and promote programmed cell death under irremediable ER stress. Cell metabolism, 16 (2): 250–264. DOI 10.1016/j.cmet.2012.07.007.

Li D, Zhao D, Du J, Dong S, Aldhamin Z, Yuan X, Li W, Du H, Zhao W, Cui L, Liu L, Fu N, Nan Y. 2020. Heme oxygenase-1 alleviated non-alcoholic fatty liver disease via suppressing ROS-dependent endoplasmic reticulum stress. Life sciences, 253: 117678. DOI 10.1016/j.lfs.2020.117678.

Li J, Ni M, Lee B, Barron E, Hinton DR, Lee AS. 2008. The unfolded protein response regulator GRP78/BiP is required for endoplasmic reticulum integrity and stress-induced autophagy in mammalian cells. Cell death and differentiation, 15 (9): 1460–1471. DOI 10.1038/cdd.2008.81.

Lin H-Y, Juan S-H, Shen S-C, Hsu F-L, Chen Y-C. 2003. Inhibition of lipopolysaccharide-induced nitric oxide production by flavonoids in RAW264.7 macrophages involves heme oxygenase-1. Biochemical pharmacology, 66 (9): 1821–1832. DOI 10.1016/s0006-2952(03)00422-2.

Lo H-M, Chen C-L, Yang C-M, Wu P-H, Tsou C-J, Chiang K-W, Wu W-B. 2013. The carotenoid lutein enhances matrix metalloproteinase-9 production and phagocytosis through intracellular ROS generation and ERK1/2, p38 MAPK, and RARβ activation in murine macrophages. Journal of leukocyte biology, 93 (5): 723–735. DOI 10.1189/jlb.0512238.

Luís A, Hackl M, Jafarmadar M, Keibl C, Jilge JM, Grillari J, Bahrami S, Kozlov AV. 2020. Circulating miRNAs Associated With ER Stress and Organ Damage in a Preclinical Model of Trauma Hemorrhagic Shock. Frontiers in medicine, 7: 568096. DOI 10.3389/fmed.2020.568096.

Lustig MK, Bac VH, Pavlovic D, Maier S, Gründling M, Grisk O, Wendt M, Heidecke C-D, Lehmann C. 2007. Colon ascendens stent peritonitis—a model of sepsis adopted to the rat: physiological, microcirculatory and laboratory changes. Shock (Augusta, Ga.), 28 (1): 59–64. DOI 10.1097/SHK.0b013e31802e454f.

Maier S, Traeger T, Entleutner M, Westerholt A, Kleist B, Hüser N, Holzmann B, Stier A, Pfeffer K, Heidecke C-D. 2004. Cecal ligation and puncture versus colon ascendens stent peritonitis: two distinct animal models for polymicrobial sepsis. Shock (Augusta, Ga.), 21 (6): 505–511. DOI 10.1097/01.shk.0000126906.52367.dd.

Mainali R, Zabalawi M, Long D, Buechler N, Quillen E, Key C-C, Zhu X, Parks JS, Furdui C, Stacpoole PW, Martinez J, McCall CE, Quinn MA. 2021. Dichloroacetate reverses sepsis-induced hepatic metabolic dysfunction. eLife, 10. DOI 10.7554/eLife.64611.

Maines MD, Gibbs PEM. 2005. 30 some years of heme oxygenase: from a “molecular wrecking ball” to a “mesmerizing” trigger of cellular events. Biochemical and biophysical research communications, 338 (1): 568–577. DOI 10.1016/j.bbrc.2005.08.121.

Martinon F, Chen X, Lee A-H, Glimcher LH. 2010. TLR activation of the transcription factor XBP1 regulates innate immune responses in macrophages. Nature immunology, 11 (5): 411–418. DOI 10.1038/ni.1857.

Martins R, Maier J, Gorki A-D, Huber KVM, Sharif O, Starkl P, Saluzzo S, Quattrone F, Gawish R, Lakovits K, Aichinger MC, Radic-Sarikas B, Lardeau C-H, Hladik A, Korosec A, Brown M, Vaahtomeri K, Duggan M, Kerjaschki D, Esterbauer H, Colinge J, Eisenbarth SC, Decker T, Bennett KL, Kubicek S, Sixt M, Superti-Furga G, Knapp S. 2016. Heme drives hemolysis-induced susceptibility to infection via disruption of phagocyte functions. Nature immunology, 17 (12): 1361–1372. DOI 10.1038/ni.3590.

McNeill E, Crabtree MJ, Sahgal N, Patel J, Chuaiphichai S, Iqbal AJ, Hale AB, Greaves DR, Channon KM. 2015. Regulation of iNOS function and cellular redox state by macrophage Gch1 reveals specific requirements for tetrahydrobiopterin in NRF2 activation. Free radical biology & medicine, 79: 206–216. DOI 10.1016/j.freeradbiomed.2014.10.575.

Medina MV, Sapochnik D, Garcia Solá M, Coso O. 2020. Regulation of the Expression of Heme Oxygenase-1: Signal Transduction, Gene Promoter Activation, and Beyond. Antioxidants & redox signaling, 32 (14): 1033–1044. DOI 10.1089/ars.2019.7991.

Mendonça R, Silveira AAA, Conran N. 2016. Red cell DAMPs and inflammation. Inflammation research : official journal of the European Histamine Research Society … [et al.], 65 (9): 665–678. DOI 10.1007/s00011-016-0955-9.

Morishima N, Nakanishi K, Nakano A. 2011. Activating transcription factor-6 (ATF6) mediates apoptosis with reduction of myeloid cell leukemia sequence 1 (Mcl-1) protein via induction of WW domain binding protein 1. The Journal of biological chemistry, 286 (40): 35227–35235. DOI 10.1074/jbc.M111.233502.

Müllebner A, Herminghaus A, Miller I, Kames M, Luís A, Picker O, Bauer I, Kozlov AV, Duvigneau JC. 2022. Tissue Damage, Not Infection, Triggers Hepatic Unfolded Protein Response in an Experimental Rat Peritonitis Model. Frontiers in medicine, 9: 785285. DOI 10.3389/fmed.2022.785285.

Muñoz-Sánchez J, Chánez-Cárdenas ME. 2014. A review on hemeoxygenase-2: focus on cellular protection and oxygen response. Oxidative medicine and cellular longevity, 2014: 604981. DOI 10.1155/2014/604981.

Naito Y, Takagi T, Higashimura Y. 2014. Heme oxygenase-1 and anti-inflammatory M2 macrophages. Archives of biochemistry and biophysics, 564: 83–88. DOI 10.1016/j.abb.2014.09.005.

Nemeth E, Rivera S, Gabayan V, Keller C, Taudorf S, Pedersen BK, Ganz T. 2004. IL-6 mediates hypoferremia of inflammation by inducing the synthesis of the iron regulatory hormone hepcidin. The Journal of clinical investigation, 113 (9): 1271–1276. DOI 10.1172/JCI20945.

Nürnberger S, Miller I, Duvigneau JC, Kavanagh ET, Gupta S, Hartl RT, Hori O, Gesslbauer B, Samali A, Kungl A, Redl H, Kozlov AV. 2012. Impairment of endoplasmic reticulum in liver as an early consequence of the systemic inflammatory response in rats. American journal of physiology. Gastrointestinal and liver physiology, 303 (12): G1373-83. DOI 10.1152/ajpgi.00056.2012.

Oakes GH, Bend JR. 2010. Global changes in gene regulation demonstrate that unconjugated bilirubin is able to upregulate and activate select components of the endoplasmic reticulum stress response pathway. Journal of biochemical and molecular toxicology, 24 (2): 73–88. DOI 10.1002/jbt.20313.

Otterbein LE, Bach FH, Alam J, Soares M, Tao Lu H, Wysk M, Davis RJ, Flavell RA, Choi AM. 2000. Carbon monoxide has anti-inflammatory effects involving the mitogen-activated protein kinase pathway. Nature medicine, 6 (4): 422–428. DOI 10.1038/74680.

Pahl HL. 1999. Signal transduction from the endoplasmic reticulum to the cell nucleus. Physiological reviews, 79 (3): 683–701. DOI 10.1152/physrev.1999.79.3.683.

Perl M, Chung C-S, Garber M, Huang X, Ayala A. 2006. Contribution of anti-inflammatory/immune suppressive processes to the pathology of sepsis. Frontiers in bioscience : a journal and virtual library, 11: 272–299. DOI 10.2741/1797.

Pfefferlé M, Ingoglia G, Schaer CA, Hansen K, Schulthess N, Humar R, Schaer DJ, Vallelian F. 2021. Acute Hemolysis and Heme Suppress Anti-CD40 Antibody-Induced Necro-Inflammatory Liver Disease. Frontiers in immunology, 12: 680855. DOI 10.3389/fimmu.2021.680855.

Poderoso JJ, Carreras MC, Lisdero C, Riobó N, Schöpfer F, Boveris A. 1996. Nitric oxide inhibits electron transfer and increases superoxide radical production in rat heart mitochondria and submitochondrial particles. Archives of biochemistry and biophysics, 328 (1): 85–92. DOI 10.1006/abbi.1996.0146.

Qaisiya M, Brischetto C, Jašprová J, Vitek L, Tiribelli C, Bellarosa C. 2017. Bilirubin-induced ER stress contributes to the inflammatory response and apoptosis in neuronal cells. Archives of toxicology, 91 (4): 1847–1858. DOI 10.1007/s00204-016-1835-3.

Rizzardini M, Zappone M, Villa P, Gnocchi P, Sironi M, Diomede L, Meazza C, Monshouwer M, Cantoni L. 1998. Kupffer cell depletion partially prevents hepatic heme oxygenase 1 messenger RNA accumulation in systemic inflammation in mice: role of interleukin 1beta. Hepatology (Baltimore, Md.), 27 (3): 703–710. DOI 10.1002/hep.510270311.

Robbins RA, Grisham MB. 1997. Nitric oxide. The international journal of biochemistry & cell biology, 29 (6): 857–860. DOI 10.1016/s1357-2725(96)00167-7.

Rodrigues CMP, Solá S, Brito MA, Brites D, Moura JJG. 2002. Bilirubin directly disrupts membrane lipid polarity and fluidity, protein order, and redox status in rat mitochondria. Journal of hepatology, 36 (3): 335–341. DOI 10.1016/s0168-8278(01)00279-3.

Ron D. 2002. Translational control in the endoplasmic reticulum stress response. The Journal of clinical investigation, 110 (10): 1383–1388. DOI 10.1172/JCI16784.

Rudd KE, Johnson SC, Agesa KM, Shackelford KA, Tsoi D, Kievlan DR, Colombara DV, Ikuta KS, Kissoon N, Finfer S, Fleischmann-Struzek C, Machado FR, Reinhart KK, Rowan K, Seymour CW, Watson RS, West TE, Marinho F, Hay SI, Lozano R, Lopez AD, Angus DC, Murray CJL, Naghavi M. 2020. Global, regional, and national sepsis incidence and mortality, 1990-2017: analysis for the Global Burden of Disease Study. Lancet (London, England), 395 (10219): 200–211. DOI 10.1016/S0140-6736(19)32989-7.

Ryter SW. 2021. Significance of Heme and Heme Degradation in the Pathogenesis of Acute Lung and Inflammatory Disorders. International journal of molecular sciences, 22 (11). DOI 10.3390/ijms22115509.

Ryter SW, Alam J, Choi AMK. 2006. Heme oxygenase-1/carbon monoxide: from basic science to therapeutic applications. Physiological reviews, 86 (2): 583–650. DOI 10.1152/physrev.00011.2005.

Sakr Y, Lobo SM, Moreno RP, Gerlach H, Ranieri VM, Michalopoulos A, Vincent J-L. 2012. Patterns and early evolution of organ failure in the intensive care unit and their relation to outcome. Critical care (London, England), 16 (6): R222. DOI 10.1186/cc11868.

Schulz S, Wong RJ, Vreman HJ, Stevenson DK. 2012. Metalloporphyrins - an update. Frontiers in pharmacology, 3: 68. DOI 10.3389/fphar.2012.00068.

Sheng WS, Hu S, Nettles AR, Lokensgard JR, Vercellotti GM, Rock RB. 2010. Hemin inhibits NO production by IL-1β-stimulated human astrocytes through induction of heme oxygenase-1 and reduction of p38 MAPK activation. Journal of neuroinflammation, 7: 51. DOI 10.1186/1742-2094-7-51.

Silomon M, Bauer I, Bauer M, Nolting J, Paxian M, Rensing H. 2007. Induction of heme oxygenase-1 and heat shock protein 70 in rat hepatocytes: the role of calcium signaling. Cellular & molecular biology letters, 12 (1): 25–38. DOI 10.2478/s11658-006-0052-0.

Singer M, Deutschman CS, Seymour CW, Shankar-Hari M, Annane D, Bauer M, Bellomo R, Bernard GR, Chiche J-D, Coopersmith CM, Hotchkiss RS, Levy MM, Marshall JC, Martin GS, Opal SM, Rubenfeld GD, van der Poll T, Vincent J-L, Angus DC. 2016. The Third International Consensus Definitions for Sepsis and Septic Shock (Sepsis-3). JAMA, 315 (8): 801–810. DOI 10.1001/jama.2016.0287.

Singer M, Santis V de, Vitale D, Jeffcoate W. 2004. Multiorgan failure is an adaptive, endocrine-mediated, metabolic response to overwhelming systemic inflammation. Lancet (London, England), 364 (9433): 545–548. DOI 10.1016/S0140-6736(04)16815-3.

Siore AM, Parker RE, Stecenko AA, Cuppels C, McKean M, Christman BW, Cruz-Gervis R, Brigham KL. 2005. Endotoxin-induced acute lung injury requires interaction with the liver. American journal of physiology. Lung cellular and molecular physiology, 289 (5): L769-76. DOI 10.1152/ajplung.00137.2005.

Soares MP, Bozza MT. 2016. Red alert: labile heme is an alarmin. Current opinion in immunology, 38: 94–100. DOI 10.1016/j.coi.2015.11.006.

Soto-Pantoja DR, Wilson AS, Clear KY, Westwood B, Triozzi PL, Cook KL. 2017. Unfolded protein response signaling impacts macrophage polarity to modulate breast cancer cell clearance and melanoma immune checkpoint therapy responsiveness. Oncotarget, 8 (46): 80545–80559. DOI 10.18632/oncotarget.19849.

Stocker R, Yamamoto Y, McDonagh AF, Glazer AN, Ames BN. 1987. Bilirubin is an antioxidant of possible physiological importance. Science (New York, N.Y.), 235 (4792): 1043–1046. DOI 10.1126/science.3029864.

Takasu O, Gaut JP, Watanabe E, To K, Fagley RE, Sato B, Jarman S, Efimov IR, Janks DL, Srivastava A, Bhayani SB, Drewry A, Swanson PE, Hotchkiss RS. 2013. Mechanisms of cardiac and renal dysfunction in patients dying of sepsis. American journal of respiratory and critical care medicine, 187 (5): 509–517. DOI 10.1164/rccm.201211-1983OC.

Tenhunen R, Marver HS, Schmid R. 1968. The enzymatic conversion of heme to bilirubin by microsomal heme oxygenase. Proceedings of the National Academy of Sciences of the United States of America, 61 (2): 748–755. DOI 10.1073/pnas.61.2.748.

Thiemermann C. 2000. Nitric oxide and septic shock. In: . Nitric Oxide. : Elsevier, 159–166.

Tran DT, Jeong YY, Kim JM, Bae HB, Son SK, Kwak SH. 2020. The Anti-Inflammatory Role of Bilirubin on “Two-Hit” Sepsis Animal Model. International journal of molecular sciences, 21 (22). DOI 10.3390/ijms21228650.

Travers KJ, Patil CK, Wodicka L, Lockhart DJ, Weissman JS, Walter P. 2000. Functional and genomic analyses reveal an essential coordination between the unfolded protein response and ER-associated degradation. Cell, 101 (3): 249–258. DOI 10.1016/s0092-8674(00)80835-1.

Uemura A, Oku M, Mori K, Yoshida H. 2009. Unconventional splicing of XBP1 mRNA occurs in the cytoplasm during the mammalian unfolded protein response. Journal of cell science, 122 (Pt 16): 2877–2886. DOI 10.1242/jcs.040584.

Urano F, Wang X, Bertolotti A, Zhang Y, Chung P, Harding HP, Ron D. 2000. Coupling of stress in the ER to activation of JNK protein kinases by transmembrane protein kinase IRE1. Science (New York, N.Y.), 287 (5453): 664–666. DOI 10.1126/science.287.5453.664.

van der Veere CN, Schoemaker B, van der Meer R, Groen AK, Jansen PL, Oude Elferink RP. 1995. Rapid association of unconjugated bilirubin with amorphous calcium phosphate. Journal of Lipid Research, 36 (8): 1697–1707. DOI 10.1016/S0022-2275(20)41489-0.

van Schadewijk A, van't Wout EFA, Stolk J, Hiemstra PS. 2012. A quantitative method for detection of spliced X-box binding protein-1 (XBP1) mRNA as a measure of endoplasmic reticulum (ER) stress. Cell stress & chaperones, 17 (2): 275–279. DOI 10.1007/s12192-011-0306-2.

Wang WW, Smith DLH, Zucker SD. 2004. Bilirubin inhibits iNOS expression and NO production in response to endotoxin in rats. Hepatology (Baltimore, Md.), 40 (2): 424–433. DOI 10.1002/hep.20334.

Warenits A-M, Hatami J, Müllebner A, Ettl F, Teubenbacher U, Magnet IAM, Bauder B, Janata A, Miller I, Moldzio R, Kramer A-M, Sterz F, Holzer M, Högler S, Weihs W, Duvigneau JC. 2020. Motor Cortex and Hippocampus Display Decreased Heme Oxygenase Activity 2 Weeks After Ventricular Fibrillation Cardiac Arrest in Rats. Frontiers in medicine, 7: 513. DOI 10.3389/fmed.2020.00513.

Watanabe E, Muenzer JT, Hawkins WG, Davis CG, Dixon DJ, McDunn JE, Brackett DJ, Lerner MR, Swanson PE, Hotchkiss RS. 2009. Sepsis induces extensive autophagic vacuolization in hepatocytes: a clinical and laboratory-based study. Laboratory investigation; a journal of technical methods and pathology, 89 (5): 549–561. DOI 10.1038/labinvest.2009.8.

Weidinger A, Müllebner A, Paier-Pourani J, Banerjee A, Miller I, Lauterböck L, Duvigneau JC, Skulachev VP, Redl H, Kozlov AV. 2015. Vicious inducible nitric oxide synthase-mitochondrial reactive oxygen species cycle accelerates inflammatory response and causes liver injury in rats. Antioxidants & redox signaling, 22 (7): 572–586. DOI 10.1089/ars.2014.5996.

West AP, Brodsky IE, Rahner C, Woo DK, Erdjument-Bromage H, Tempst P, Walsh MC, Choi Y, Shadel GS, Ghosh S. 2011. TLR signalling augments macrophage bactericidal activity through mitochondrial ROS. Nature, 472 (7344): 476–480. DOI 10.1038/nature09973.

Wu TW, Carey D, Wu J, Sugiyama H. 1991. The cytoprotective effects of bilirubin and biliverdin on rat hepatocytes and human erythrocytes and the impact of albumin. Biochemistry and cell biology = Biochimie et biologie cellulaire, 69 (12): 828–834. DOI 10.1139/o91-123.

Yan J, Li S, Li S. 2014. The role of the liver in sepsis. International reviews of immunology, 33 (6): 498–510. DOI 10.3109/08830185.2014.889129.

Ye J, Rawson RB, Komuro R, Chen X, Davé UP, Prywes R, Brown MS, Goldstein JL. 2000. ER stress induces cleavage of membrane-bound ATF6 by the same proteases that process SREBPs. Molecular cell, 6 (6): 1355–1364. DOI 10.1016/s1097-2765(00)00133-7.

Yoshida H, Matsui T, Yamamoto A, Okada T, Mori K. 2001. XBP1 mRNA is induced by ATF6 and spliced by IRE1 in response to ER stress to produce a highly active transcription factor. Cell, 107 (7): 881–891. DOI 10.1016/s0092-8674(01)00611-0.

Zhang K, Kaufman RJ. 2008. From endoplasmic-reticulum stress to the inflammatory response. Nature, 454 (7203): 455–462. DOI 10.1038/nature07203.

Zhang K, Shen X, Wu J, Sakaki K, Saunders T, Rutkowski DT, Back SH, Kaufman RJ. 2006. Endoplasmic reticulum stress activates cleavage of CREBH to induce a systemic inflammatory response. Cell, 124 (3): 587–599. DOI 10.1016/j.cell.2005.11.040.

Zhang L, Tian Y, Yang J, Li J, Tang H, Wang Y. 2018. Colon Ascendens Stent Peritonitis (CASP) Induces Excessive Inflammation and Systemic Metabolic Dysfunction in a Septic Rat Model. Journal of proteome research, 17 (1): 680–688. DOI 10.1021/acs.jproteome.7b00730.

Zuckerbraun BS, Chin BY, Bilban M, d'Avila JdC, Rao J, Billiar TR, Otterbein LE. 2007. Carbon monoxide signals via inhibition of cytochrome c oxidase and generation of mitochondrial reactive oxygen species. FASEB journal : official publication of the Federation of American Societies for Experimental Biology, 21 (4): 1099–1106. DOI 10.1096/fj.06-6644com.

8 Appendix

8.1 Unpublished Data

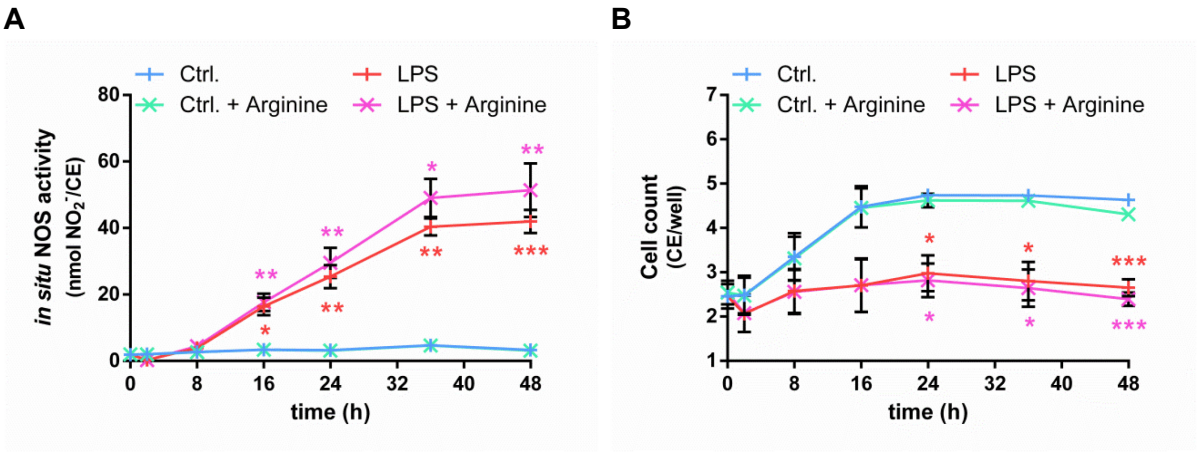

Unpublished data Figure 1. LPS induces nitric oxide (NO) formation by NO synthase (NOS) in J774A.1 cells. Cells were treated with 1µg/ml LPS for 2, 8, 16, 24, 36 or 48 h in DMEM with 10% FCS or DMEM with 10% FCS supplemented L-arginine (2 mmol/L). **(A)** To assess *in situ* NOS activity, amounts of NO oxidation product nitrite (NO_2^-) in the cell culture supernatants were measured using Grieß-method and normalized for the underlying cell counts. **(B)** Cell counts were determined using crystal violet assay (Müllebner et al. 2015) and expressed as cell equivalents (CE; 1 CE corresponds to 10^6 cells). Three independent experiments were performed (*n=3*). Data are shown as mean +/-SEM. Statistical differences between control and LPS groups were calculated using homoscedastic two-sided Students t-test and are indicated by **p<0.05*, ***p<0.01*, ****p<0.001*. **(A)(B)** A preliminary version of these data has been published in (Michenthaler 2016).

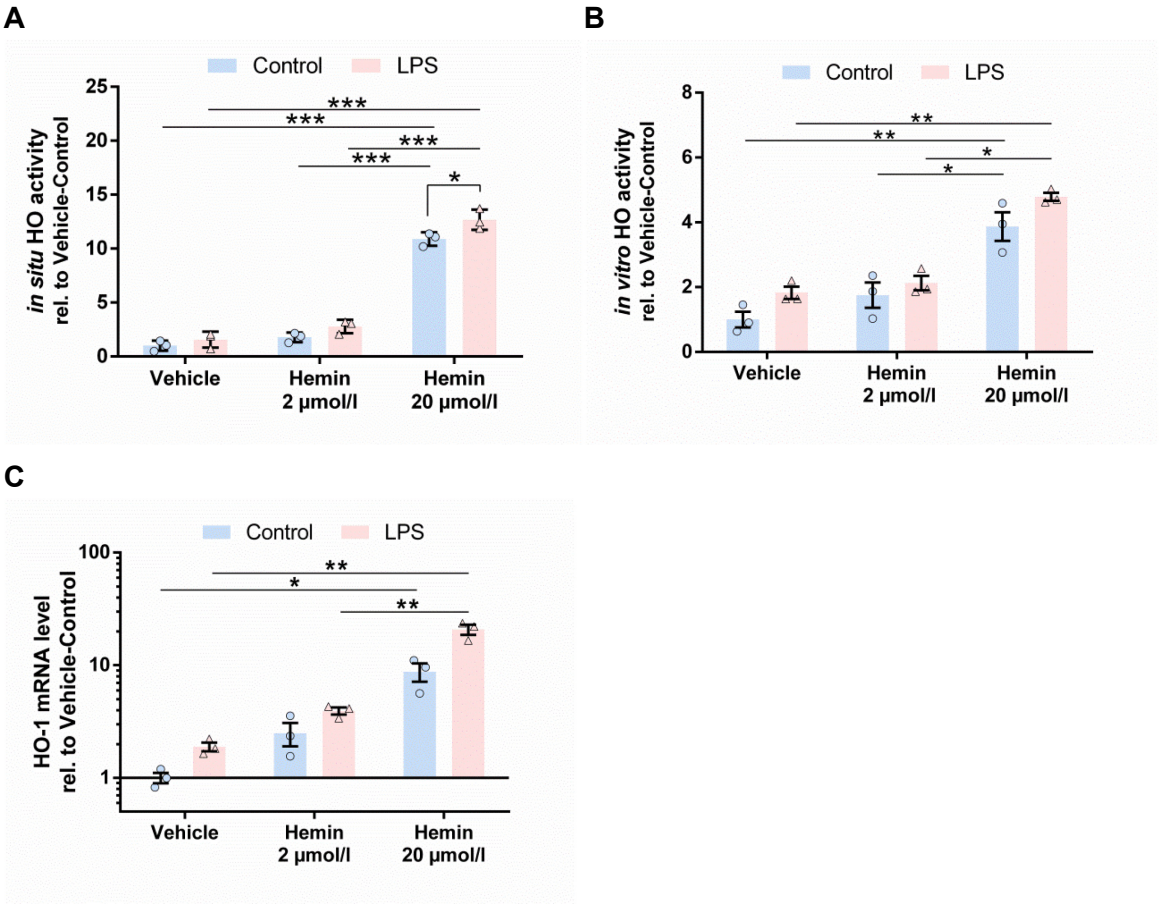

Unpublished data Figure 2. Hemin augments HO activity by induction heme oxygenase (HO) 1 expression. Two sets of J774A.1 cells were either left untreated (control) or pretreated with LPS (1µg/mL). After 2 h each group was split into three subgroups and treated with additional vehicle (DMSO), hemin (2 µmol/L) or hemin (20 µmol/L) for another 16 h. **(A)** The *in situ* HO activity was determined by extraction and spectrophotometric quantification of bilirubin (BR) accumulating in the cell culture medium in 16 h. It was normalized for underlying cell count assessed by crystal violet assay (see legend Fig. X). Data are presented relative to vehicle control (*n=3*). **(B)** The *in vitro* HO activity was determined in homogenates of J774A.1 cells using a biochemical assay. Amount of BR (nmol) formed in 30 min per mg cell-protein was determined (Duvigneau et al. 2020). Data are presented relative to vehicle-control (*n=2*). **(C)** HO-1 mRNA levels were determined by reverse transcription qPCR. Data were normalized for internal reference genes cyclophilin A and hypoxanthine phosphoribosyltransferase and are displayed relative to vehicle-control (*n=3*). Data are shown as mean +/- SEM. Statistical differences were calculated using matched two way ANOVA followed by Bonferroni multiple comparison test and are indicated by **p<0.05*, ***p<0.01 ***p<0.001*. **(A)(B)** A preliminary version of these data has been published in (Michenthaler 2016)

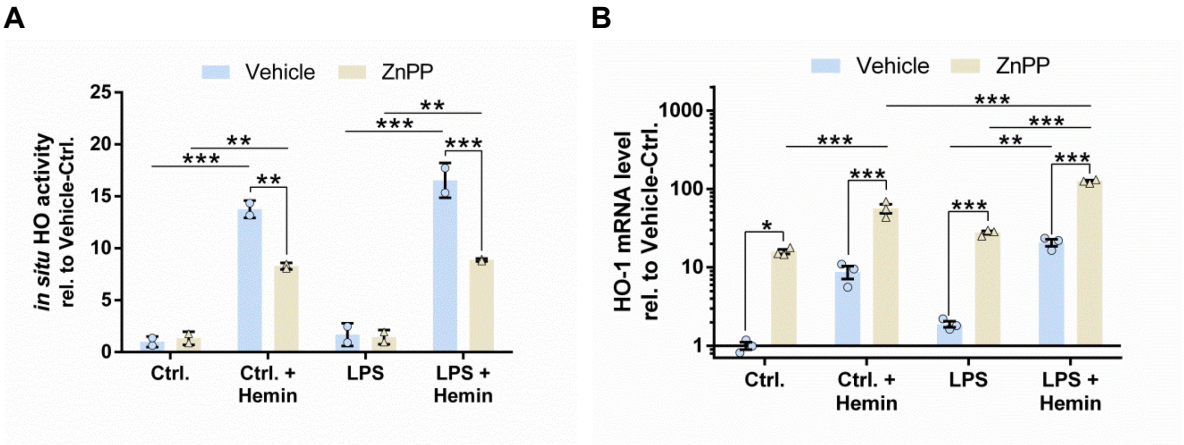

Unpublished data Figure 3. Heme oxygenase (HO) inhibitor zinc protoporphyrin (ZnPP) leads to super-induction of HO-1 gene expression. Two sets of J774A.1 cells were either left untreated (control) or pretreated with LPS (1µg/mL). After 2 h each set was split into 4 subsets and treated with additional vehicle (DMSO), hemin (20 µmol/L), ZnPP (20 µmol/L) or the combination of hemin (20 µmol/l) and ZnPP (20 µmol/L) for another 16 h. **(A)** *In situ* HO activity was determined by extraction and spectrophotometric quantification of bilirubin (BR) formed *in situ* (see legend of Fig. XI) and is presented relative to vehicle-control (*n=2*). **(B)** Gene expression of HO-1 was determined as described (see legend of Fig. XI) and is given relative to vehicle-control (*n=3*). Data are shown as mean +/- SEM. Statistical differences were calculated using matched one way ANOVA followed by Bonferroni multiple comparison test and are indicated by **p<0.05*, ***p<0.01*, ****p<0.001*. . **(A)(B)** A preliminary version of these data has been published in (Michenthaler 2016)

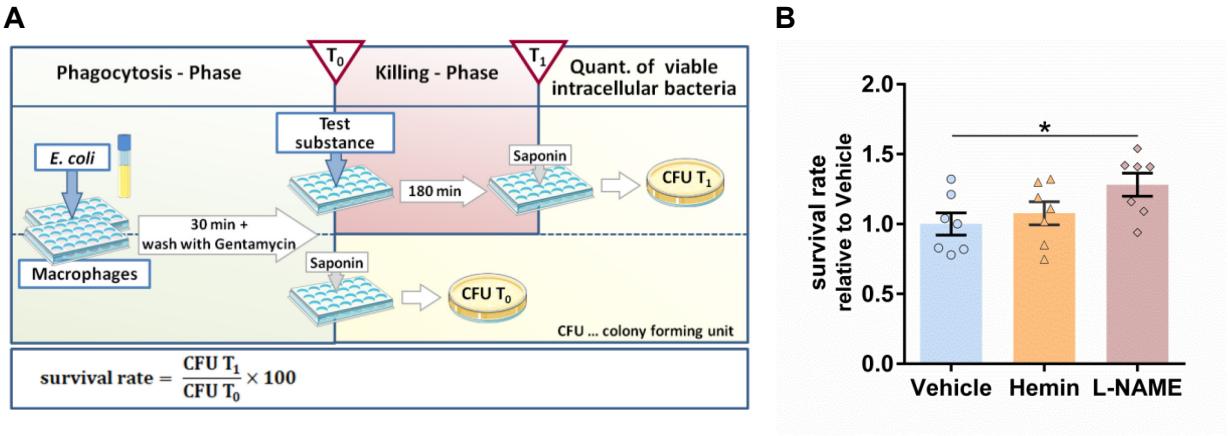

Unpublished data Figure 4. Activity of nitric oxide synthase (NOS) but not heme oxygenase (HO) supports bactericidal activity of J774A.1 macrophages. (A) Schematic overview of the method for analyzing bactericidal activity adapted from Subashchandrabose et al. (2013). In two 24 well plates J774A.1 cells (0,5 x 10^6 cells/well) were incubated with *E. coli* for 30 min at 37°C (phagocytosis phase). Thereafter, cells were washed with PBS (supplemented with Ca^{2+} and Mg^{2+} and gentamicin 200 µg/mL) to eliminate extracellular bacteria and stop phagocytosis. At this point (T_0) cells in one plate were lysed by saponin (1 %) and plated on agar (Luria Bertani agar plates) for determining the number of colony forming units (CFU) which equals number of viable phagocytosed bacteria. The cells on the second plate were incubated with the test substances or vehicle for another 180 min (killing phase). At the consecutive time point (T_1) number of viable phagocytosed bacteria was assessed by lysing cells with saponin (1%) and determination of CFU. CFU were quantified by counting colonies grown over night at 37°C on LB-plates inoculated with 1/500th of lysed cells. Survival rate was calculated in % of viable bacteria at T_1 (CFU T_1) from the total amount of phagocytosed bacteria (CFU T_0). **(B)** Survival rates in presence of HO substrate hemin (20 µmol/L) and NOS inhibitor L-NAME (10 mmol/L) are displayed relative to mean of vehicle (DMSO) control (*n=7*). Data are shown as mean +/- SEM. Statistical differences to vehicle-control were calculated using matched two way ANOVA and are indicated by **p<0.05*.

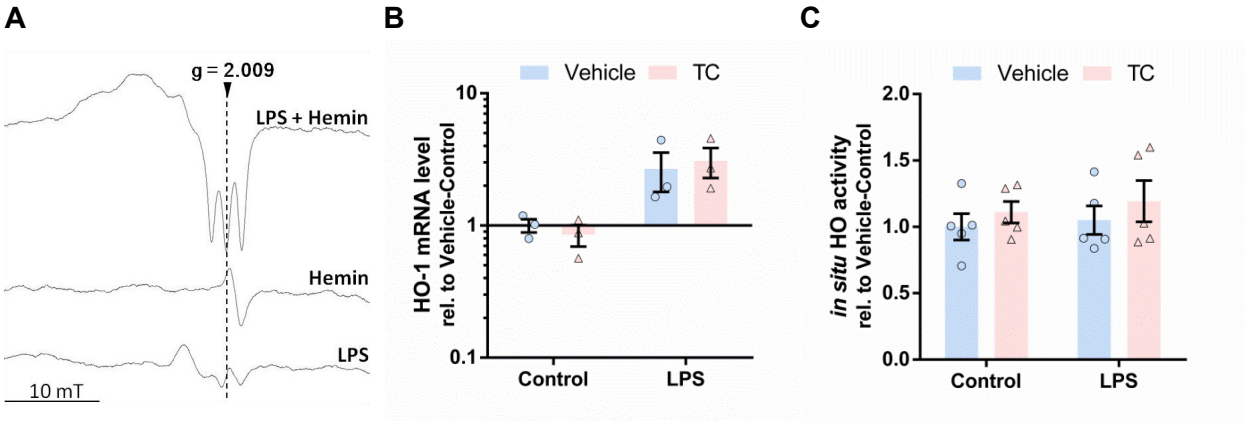

Unpublished data Figure 5. NO derived by nitric oxide synthase (NOS) activity does not affect heme oxygenase (HO) 1 expression and HO activity in macrophages. (A) Two sets of J774A.1 cells were either left untreated (control) or treated with LPS (1µg/mL). After 8 h LPS treated cells were split in two groups. One LPS group was treated with additional vehicle (DMSO), the other LPS and the control group with additional hemin (20 µmol/l) for 60 min. Accumulation of nitrosyl-heme complex formed from released NO and ferrous heme was determined in the cells by low-temperature electron paramagnetic resonance (ESR). Nitrosyl-heme complex gives a triplet structured signal centered at g = 2.009. ESR parameters were as follows: modulation frequency, 100 kHz; microwave frequency, 9.425 GHz; microwave power, 8.3 mW; modulation amplitude, 5 G; gain, 50; range, 330 ± 30 mT. Spectrum of one representative experiment is shown. g, g-factor; mT, millitesla. **(B)(C)** J774A.1 cells were treated with vehicle (PBS) or NOS inhibitor S-methyl-L-thiocitruline (TC, 50 µmol/L) alone or in combination with LPS (1 µg/mL) for 8 h **(B)** or 16 h **(C)**. **(B)** HO-1 mRNA levels were determined by reverse transcription qPCR (see legend Fig XI). Data are displayed relative to mean of vehicle-control (*n=3*). **(C)** *In situ* HO activity was determined as described (see figure legend XI). Data are presented relative to vehicle control (*n=5*). Data are shown as mean +/- SEM. No statistical differences were found using matched two way ANOVA.

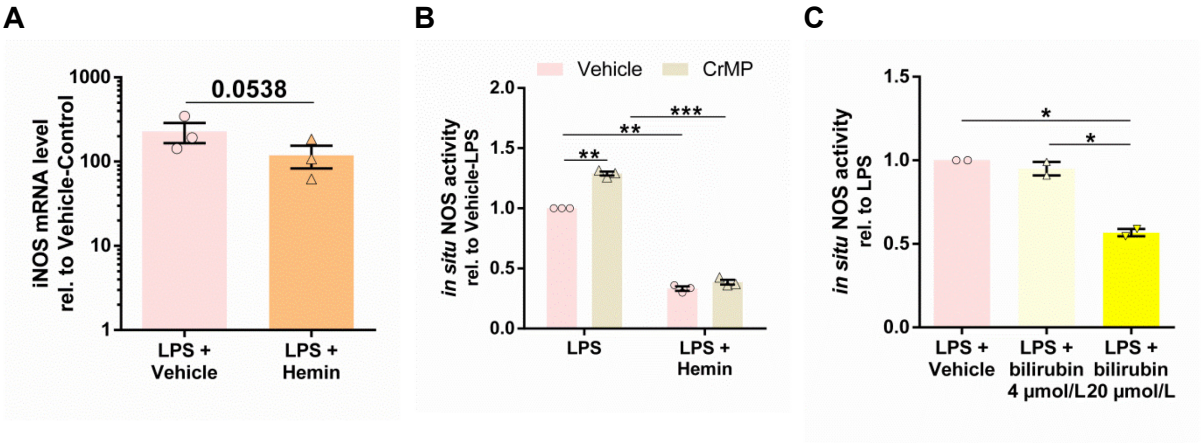

Unpublished data Figure 6. Heme oxygenase (HO) substrate hemin diminishes inducible nitric oxide synthase (iNOS) expression and NOS activity. (A) A set of J774A.1 cells was pretreated with LPS (1µg/mL). After 2 h they were split in two groups treated with additional vehicle (DMSO) or hemin (20 µmol/L). Vehicle treated control was run in parallel. Gene expression levels of iNOS were determined by reverse transcription qPCR (see legend Fig XI). Data are displayed relative to vehicle-control (*n=3*). **(B)** A set of J774A.1 cells was pretreated with LPS (1 µg/mL). After 2 h they were split into 4 subgroups and treated with additional vehicle (DMSO), hemin (20 µmol/L), HO inhibitor chromium mesoporphyrin (CrMP, 20 µmol/L) or the combination of hemin (20 µmol/l) and CrMP (20 µmol/L) for another 16 h. *In situ* NOS activity was assessed as described (see legend of Fig. X) and presented relative to LPS-vehicle controls (*n=3*). **(C)** A set of J774A.1 cells was pretreated with LPS (1µg/mL). After 2 h they were split in three groups treated with additional vehicle (DMSO), bilirubin (4 µmol/L) or bilirubin (20 µmol/L). *In situ* NOS activity was assessed as described (see legend of Fig. X) and presented relative to LPS-vehicle controls (*n=2*). Data are shown as mean +/- SEM. Statistical differences were calculated using **(A)** two sided paired students t-test, **(B)** matched two way ANOVA or **(C)** matched one way ANOVA followed by Bonferroni multiple comparison test and are indicated by **p<0.05*, ***p<0.01*, ****p<0.001*. **(B)** A preliminary version of these data from has been published in (Michenthaler 2016)

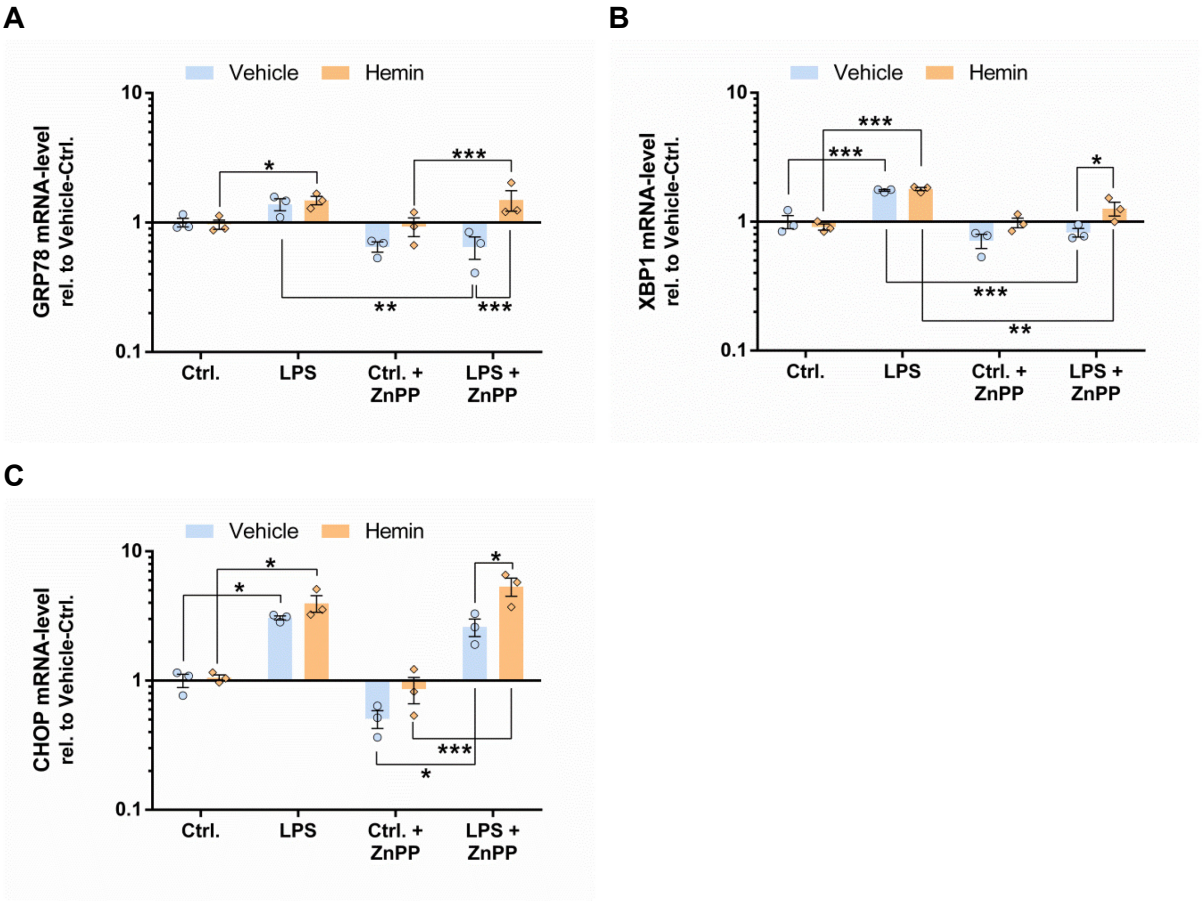

Unpublished data Figure 7. Inhibition of heme oxygenase (HO) activity alleviates LPS triggered unfolded protein response (UPR). Two sets of J774A.1 cells were either left untreated (control) or pretreated with LPS (1µg/mL). After 2 h either group was split into 4 subgroups and treated with additional vehicle (DMSO), hemin (20 µmol/L), zinc protoporphyrin (ZnPP, 20 µmol/L) or the combination of hemin (20 µmol/l) and ZnPP (20 µmol/L) for another 16 h. Expression levels of UPR genes **(A)** glucose regulated protein 78 (GRP78), **(B)** X-box binding protein (XBP1) and **(C)** CAAT/enhancer binding protein (C/EBP) homologous protein (CHOP) were determined by reverse transcription qPCR as described (see legend of Fig. XI). Data are displayed relative to mean of vehicle-control (*n=3*). Data are shown as mean +/- SEM. Statistical differences were calculated using matched one way ANOVA followed by Bonferroni multiple comparison test and are indicated by **p<0.05*, ***p<0.01*, ****p<0.001*.

8.2 References to Unpublished Data

Duvigneau JC, Trovato A, Müllebner A, Miller I, Krewenka C, Krenn K, Zich W, Moldzio R. 2020. Cannabidiol Protects Dopaminergic Neurons in Mesencephalic Cultures against the Complex I Inhibitor Rotenone Via Modulation of Heme Oxygenase Activity and Bilirubin. Antioxidants (Basel, Switzerland), 9 (2). DOI 10.3390/antiox9020135.

Michenthaler H. 2016. Cross talk between heme oxygenase and nitric oxide synthase in macrophages. Vienna: University of veterinary medicine.

Müllebner A, Moldzio R, Redl H, Kozlov AV, Duvigneau JC. 2015. Heme Degradation by Heme Oxygenase Protects Mitochondria but Induces ER Stress via Formed Bilirubin. Biomolecules, 5 (2): 679–701. DOI 10.3390/biom5020679.

Subashchandrabose S, Smith SN, Spurbeck RR, Kole MM, Mobley HLT. 2013. Genome-wide detection of fitness genes in uropathogenic Escherichia coli during systemic infection. PLoS pathogens, 9 (12): e1003788. DOI 10.1371/journal.ppat.1003788.

9 Curriculum vitae

Personal data

Name	Andrea Müllebner
Date of birth	February 14, 1984
Nationality	Austrian

Work experience

2009-now	Research associate with teaching appointment Institute of Medical Biochemistry, University of Veterinary Medicine, Vienna
2015-2018	Research associate Ludwig Boltzmann Institute for Experimental and Clinical Traumatology
2011-2012	Research associate Ludwig Boltzmann Institute for Experimental and Clinical Traumatology

Education

2015 - present	PhD Thesis University of Veterinary Medicine, Vienna
2006 - 2008	Master's Degree Biomedicine and Biotechnology University of Veterinary Medicine, Vienna
2003 - 2006	Bachelor's degree in Biomedicine and Biotechnology University of Veterinary Medicine, Vienna
1998 - 2003	Secondary college for Chemical Technology, Specialisation on Biochemistry and Biochemical Technology HBLVA Rosensteingasse, Vienna

Publications

2) Müllebner A, Herminghaus A, Miller I, Kames M, Luís A, Picker O, Bauer I, Kozlov AV, Duvigneau JC. 2022. Tissue Damage, Not Infection, Triggers Hepatic Unfolded Protein Response in an Experimental Rat Peritonitis Model. Frontiers in medicine, 9: 785285. DOI 10.3389/fmed.2022.785285.
3) Weidinger A, Birgisdóttir L, Schäffer J, Meszaros AT, Zavadskis S, Müllebner A, Hecker M, Duvigneau JC, Sommer N, Kozlov AV. 2022. Systemic Effects of mitoTEMPO upon Lipopolysaccharide Challenge Are Due to Its Antioxidant Part, While Local Effects in the Lung Are Due to Triphenylphosphonium. Antioxidants (Basel, Switzerland), 11 (2). DOI 10.3390/antiox11020323.
4) Warenits A-M, Hatami J, Müllebner A, Ettl F, Teubenbacher U, Magnet IAM, Bauder B, Janata A, Miller I, Moldzio R, Kramer A-M, Sterz F, Holzer M, Högler S, Weihs W, Duvigneau JC. 2020. Motor Cortex and Hippocampus Display Decreased Heme Oxygenase Activity 2 Weeks After Ventricular Fibrillation Cardiac Arrest in Rats. Frontiers in medicine, 7: 513. DOI 10.3389/fmed.2020.00513.
5) Duvigneau JC, Trovato A, Müllebner A, Miller I, Krewenka C, Krenn K, Zich W, Moldzio R. 2020. Cannabidiol Protects Dopaminergic Neurons in Mesencephalic Cultures against the Complex I Inhibitor Rotenone Via Modulation of Heme Oxygenase Activity and Bilirubin. Antioxidants (Basel, Switzerland), 9 (2). DOI 10.3390/antiox9020135.
6) Müllebner A, Sassu EL, Ladinig A, Frömbling J, Miller I, Ehling-Schulz M, Hennig-Pauka I, Duvigneau JC. 2018. Actinobacillus pleuropneumoniae triggers IL-10 expression in tonsils to mediate colonisation and persistence of infection in pigs. Veterinary immunology and immunopathology, 205: 17–23. DOI 10.1016/j.vetimm.2018.10.008.
7) Mkrtchyan GV, Üçal M, Müllebner A, Dumitrescu S, Kames M, Moldzio R, Molcanyi M, Schaefer S, Weidinger A, Schaefer U, Hescheler J, Duvigneau JC, Redl H, Bunik VI, Kozlov AV. 2018. Thiamine preserves mitochondrial function in a rat model of traumatic brain injury, preventing inactivation of the 2-oxoglutarate dehydrogenase complex. Biochimica et biophysica acta. Bioenergetics, 1859 (9): 925–931. DOI 10.1016/j.bbabio.2018.05.005.
8) Müllebner A, Dorighello GG, Kozlov AV, Duvigneau JC. 2017. Interaction between Mitochondrial Reactive Oxygen Species, Heme Oxygenase, and Nitric Oxide Synthase Stimulates Phagocytosis in Macrophages. Frontiers in medicine, 4: 252. DOI 10.3389/fmed.2017.00252.

9) Sassu EL, Frömbling J, Duvigneau JC, Miller I, Müllebner A, Gutiérrez AM, Grunert T, Patzl M, Saalmüller A, Altrock A von, Menzel A, Ganter M, Spergser J, Hewicker-Trautwein M, Verspohl J, Ehling-Schulz M, Hennig-Pauka I. 2016. Host-pathogen interplay at primary infection sites in pigs challenged with Actinobacillus pleuropneumoniae. BMC Veterinary Research, 13 (1). DOI 10.1186/s12917-017-0979-6.

10) Mair KH, Stadler M, Talker SC, Forberg H, Storset AK, Müllebner A, Duvigneau JC, Hammer SE, Saalmüller A, Gerner W. 2016. Porcine CD3(+)NKp46(+) Lymphocytes Have NK-Cell Characteristics and Are Present in Increased Frequencies in the Lungs of Influenza-Infected Animals. Frontiers in immunology, 7: 263. DOI 10.3389/fimmu.2016.00263.

11) Müllebner A, Moldzio R, Redl H, Kozlov AV, Duvigneau JC. 2015. Heme Degradation by Heme Oxygenase Protects Mitochondria but Induces ER Stress via Formed Bilirubin. Biomolecules, 5 (2): 679–701. DOI 10.3390/biom5020679.

12) Weidinger A, Müllebner A, Paier-Pourani J, Banerjee A, Miller I, Lauterböck L, Duvigneau JC, Skulachev VP, Redl H, Kozlov AV. 2015. Vicious inducible nitric oxide synthase-mitochondrial reactive oxygen species cycle accelerates inflammatory response and causes liver injury in rats. Antioxidants & redox signaling, 22 (7): 572–586. DOI 10.1089/ars.2014.5996.

13) Soler L, Gutiérrez A, Müllebner A, Cerón JJ, Duvigneau JC. 2013. Towards a better understanding of salivary and meat juice acute phase proteins determination in pigs: an expression study. Veterinary immunology and immunopathology, 156 (1-2): 91–98. DOI 10.1016/j.vetimm.2013.09.018.

14) Weidinger A, Dungel P, Perlinger M, Singer K, Ghebes C, Duvigneau JC, Müllebner A, Schäfer U, Redl H, Kozlov AV. 2013. Experimental data suggesting that inflammation mediated rat liver mitochondrial dysfunction results from secondary hypoxia rather than from direct effects of inflammatory mediators. Frontiers in physiology, 4: 138. DOI 10.3389/fphys.2013.00138.

15) Reutner K, Leitner J, Müllebner A, Ladinig A, Essler SE, Duvigneau JC, Ritzmann M, Steinberger P, Saalmüller A, Gerner W. 2013. CD27 expression discriminates porcine T helper cells with functionally distinct properties. Veterinary research, 44: 18. DOI 10.1186/1297-9716-44-18.

16) Mair KH, Müllebner A, Essler SE, Duvigneau JC, Storset AK, Saalmüller A, Gerner W. 2013. Porcine CD8αdim/-NKp46high NK cells are in a highly activated state. Veterinary research, 44: 13. DOI 10.1186/1297-9716-44-13.

17) Käser T, Müllebner A, Hartl RT, Essler SE, Saalmüller A, Catharina Duvigneau J. 2012. Porcine T-helper and regulatory T cells exhibit versatile mRNA expression capabilities for cytokines and co-stimulatory molecules. Cytokine, 60 (2): 400–409. DOI 10.1016/j.cyto.2012.07.007.
18) Müllebner A, Patel A, Stamberg W, Staniek K, Rosenau T, Netscher T, Gille L. 2010. Modulation of the mitochondrial cytochrome bc1 complex activity by chromanols and related compounds. Chemical research in toxicology, 23 (1): 193–202. DOI 10.1021/tx900333f.

Conferences and scientific meeting abstracts

---

1) Müllebner A, Dorighello G, Michenthaler H, Kames M, Meszaros A, Kozlov AV, Duvigneau JC. 2016. Crosstalk between Nitric Oxide Synthase, Heme Oxygenase and NADPH oxidase in macrophages. 7th congress on Targeting Mitochondria, Berlin, Germany, October 24-26 2016 (Poster)
2) Müllebner A, Dorighello G, Michenthaler H, Duvigneau JC, Kozlov AV, 2016, Crosstalk between Heme Oxygenase, Nitric Oxide Synthase and NADPH Oxidase in macrophages, a possible mechanism regulating their function. LBG Meeting for Health Sciences, Vienna, Austria, November 28-29 2016 (Poster)
3) Müllebner A, Hartl RT, Kehrer I, Kozlov AV, Duvigneau JC. 2017. Interplay between mitochondrial ROS and UPR upon systemic inflammation. VIB Conference “ER-Stress, Autophagy & Immune System”, Bruges, Belgium January 26-27 2017 (Poster)
4) Müllebner A, Dorighello G, Michenthaler H, Rupprecht A, Kozlov AV, Duvigneau JC. 2017. Distinct effects of HO and NOS derived products on mitochondrial function of resting macrophages. 17th Congress of the European Shock Society, Paris, France, September 13-15 2017 (Poster)
5) Müllebner A, Hartl R, Kehrer I, Kozlov A, Duvigneau JC. 2018. Interplay between mitochondrial ROS and UPR upon systemic inflammation. 19-19.-23. Tagung der Fachgruppe Physiologie und Biochemie der Deutschen Veterinärmedizinischen Gesellschaft; Feb 21-23, 2018; Vienna, Austria. (Poster)
6) Müllebner A, Dorighello G, Michenthaler H, Kames M, Rupprecht A, Kozlov AV, Duvigneau JC. 2018. Mitochondrial Reactive Oxygen Species, Heme Oxygenase and Nitric Oxide Synthase in the regulation of phagocytosis in macrophages. 14th YSA PhD-Symposium, Vienna, Austria, June 7-8 2018 (Poster)

7) Müllebner A, Dorighello G, Michenthaler H, Kames M, Rupprecht A, Kozlov AV, Duvigneau JC. 2018. Regulatory Role of Heme Oxygenase and Nitric Oxide Synthase in macrophages. 20th European Bioenergetics Conference; Budapest, Hungary, August 25-30 2018 (Poster)
8) Müllebner A, Warenits AM, Hatami J, Ettl F, Magnet IAM, Högler S, Weihs W, Duvigneau JC. 2018. Decreased activity of Heme Oxygenase in Cerebral Cortex and Hippocampus two weeks after experimental cardiac arrest. Short oral presentation at LBG Meeting for Health Sciences, Vienna, Austria, November 29-30 2018 (Short oral communication)